九州大学学術情報リポジトリ
Kyushu University Institutional Repository

Studies on cholesterol metabolism in non-alcoholic fatty liver disease

蔡, 瑋庭

https://hdl.handle.net/2324/5068276

出版情報：Kyushu University, 2022, 博士（農学）, 課程博士
バージョン：
権利関係：

KYUSHU UNIVERSITY

Studies on cholesterol metabolism in non-alcoholic fatty liver disease

Tsai Wei Ting

2022

Study on cholesterol metabolism in non-alcoholic fatty liver disease

Contents

CHAPTER I Introduction 1

CHAPTER II Effect of diet induced NAFLD in animal models 26

High cholesterol-containing sucrose diet lowers cholesterol content and promotes triacylglycerol deposition in the liver of rats 26

Soyasaponin ameliorates fatty liver and increases hepatic cholesterol accumulation in high-fat diet-fed male C57BL/6J mice 57

CHAPTER III Effect of free fatty acid induced NAFLD in cell model..... 90

D-Psicose improves palmitic acid induced cholesterol accumulation and cellular senescence in HepG2 cells 90

Summary and Conclusions 118

Acknowledgments 120

Literature cited 121

CHAPTER I Introduction

Cholesterol ($C_{27}H_{46}O$) is a hydrophobic molecule consisting of cholestane with a double bond at the carbon 5,6-position and a 3 beta-hydroxy groups at carbon 17. As an important lipid, cholesterol plays an essential role in diversely biological processes. The majority of cellular cholesterol is distributed in the plasma membrane to engage in the regulation of membrane fluidity and signal transduction [1]. Cholesterol is the source of the synthesis of steroid hormone precursor, pregnenolone [2]. In addition, cholesterol via oxidation reaction generates various oxysterols, some of which are synthesized into bile acid [3]. Consumption of dietary cholesterol is the primary source to obtain of cholesterol in vitro. According to dietary recommendations from the Ministry of Health, Labor, and Welfare in Japan, daily cholesterol intake should low than 200 mg/day (50 g egg roughly containing 186 mg cholesterol) for individuals [4]. Several human studies have shown that the amount of cholesterol intake is associated with the development of non-alcoholic fatty liver disease [5-6]. Dietary intake of cholesterol in patients with nonalcoholic steatohepatitis (NASH) (> 500 mg/day) is richer than those of healthy subjects (400 mg/day) [5]. Another cross-sectional study reported that increased daily cholesterol consumption is correlated with the severity of fatty liver (290 mg/day) and NASH (360 mg/day) [6]. Thus, high amounts of cholesterol intake are regarded as the risk factor for the progression from non-alcoholic fatty liver (NAFL) to NASH.

Non-alcoholic fatty liver disease (NAFLD) is a series of liver histological diseases starting from fatty liver (or called steatosis) to further develop into NASH, cirrhosis, and hepatocellular carcinoma. The histological definition of fatty liver is accumulated over 5% lipids in the liver and includes various forms

of small and large droplet macrovesicular steatosis, with or without lobular and portal inflammation. Excessive deposition of lipotoxic lipids (free cholesterol (FC), free fatty acids (FFA), diacylglycerol, and ceramides) causes hepatocyte abnormalities [7-8]. In particular, contents of hepatic non-esterified FC with slightly increased are still highly toxic to multiple cellular processes and organelles and result in steatohepatitis, ie NASH. Histological characteristics of NASH include steatosis, hepatocyte injury (ballooning, apoptosis, or lytic necrosis), and lobular inflammation. Reportedly, dietary, genetic, and lifestyle co-factors either lead to the accumulation of hepatic cholesterol or interact with hepatic cholesterol to promote the progression of NASH. Human clinical trials indicated that statins, a cholesterol-lowering drug, lower the risk of NASH and hepatic fibrosis [9-10]. Therefore, inhibition of cholesterol accumulation during the fatty liver stage may effectively prevent the progression of NASH.

Liver cholesterol metabolism

The liver is the central organ in controlling cholesterol homeostasis. In healthy mice, liver has a relatively low content of cholesterol (132 mg/kg body weight), however, it has large flow of sterols (143 mg/day/kg body weight) through the liver from extrahepatic tissue daily [11]. This means that liver cholesterol pool is in the statute of dynamic equilibrium which is the rate of uptake and synthesis of cholesterol consistent with excretion and secretion of cholesterol. When disrupting the dynamic equilibrium, liver cholesterol homeostasis is dysregulated causing liver cholesterol accumulation.

It has been known that dietary cholesterol and hepatic *de novo* cholesterol synthesis are two major sources of hepatic cholesterol. Dietary cholesterol is absorbed in the small intestine through Niemann–Pick type C1 (NPC1)-like 1 (NPC1L1) protein and is combined together in enterocytes with triacylglycerides (TAGs) and apolipoprotein B48 into chylomicrons, then releases into circulation [12]. Thereby, dietary cholesterol is taken up by the liver as chylomicrons. In addition, *de novo* cholesterol synthesis in the liver is a multi-enzymatic pathway that starts from acetate and is upregulated by activated sterol regulatory element binding protein-2 (SREBP-2).

SREBP-2 is a membrane-bound transcription factor involved in cholesterol metabolism [13]. When cellular sterols depletion, SREBP-2/ SREBP cleavage-activating protein (Scap) complex in the endoplasmic reticulum (ER) disassociate [14], SREBP-2 transport to the Golgi where it is activated and enters the nucleus to promote the transcription of genes related to cholesterol uptake (low-density lipoprotein receptor, *Ldlr*) and synthesis (3-hydroxy-3-methylglutaryl coenzyme A reductase, *Hmgcr*) [15].

Cholesterol uptake

The main receptors mediated cholesterol uptake in the liver are LDLR and scavenger receptor class B1 (SR-B1), the former is responsible for carrying LDL and chylomicron remnants into cell, whereas the latter is in charge of uptake of high-density lipoprotein (HDL) into cell.

LDLR is a 160 kDa glycoprotein widely expressed on cell membranes of hepatocytes or other cells. Precursor LDLR (120 kDa) is synthesized in rough ER and matured by glycosylation in the Golgi followed by translocating to cell surface [16]. LDLR recognizes particles which are containing apolipoprotein B100 (Apo B100) or apolipoprotein E (Apo E), such as LDL and chylomicron remnants, and binds to those ligands for transporting LDLR-ligands complex into cell by endocytosis [16]. LDLR-ligands complexes are separated in the endosomes, LDLR backs to cell membranes for reuse, while ligands are transported to lysosomes for releasing cholesterol [17]. The amount of LDLR distribution on the cell surface is changed by intracellular cholesterol content. When intracellular low level of cholesterol, *LDLR* gene expression is upregulated by SREBP-2, conversely [18], when intracellular high level of cholesterol, the degradation of LDLR is increased by combining with proprotein convertase subtilisin/kexin type 9 (PCSK9) [19]. The amount of LDLR on the cell surface is the majority regulated by PCSK9, although LDLR gene expression is transcriptional regulated by SREBP-2. PCSK9 is primarily synthesized and secreted by the liver that combines with LDLR after secretion to guide the LDLR into lysosomes for degradation [19]. Thus, PCSK9 is the post-translation regulator for LDLR. Moreover, the translational level of PCSK9 is directly upregulated by SREBP-2 [20].

The SR-B1 is a membrane receptor protein that plays an important role in the regulation of lipid metabolism. SR-B1 mediates cholesterol esters in HDL particles influx to the liver by selective uptake [21]. After that, cholesterol-depleted HDL particles are released back into the circulation to intake cholesterol from peripheral tissues. Contrary to LDLR-mediated endocytosis of LDL, SR-B1-mediated HDL-derived cholesterol esters (CE) influx is not through the internalization of lipoprotein particles [22]. In addition, hepatic SR-B1 expression is regulated by numerous transcription factors. The transcriptional synergy of farnesoid X receptor (FXR) with liver X receptor (LXR) upregulates the expression of hepatic SR-B1 [23].

Cholesterol *de novo* synthesis

Cholesterol is synthesized from acetate via a series of multistep enzymatic processes which occurred in the cytoplasm and in the ER [24]. According to enzymatic reactions, it can be divided into four primary steps: (1) acetate condenses to isoprene; (2) isoprene polymerizes to squalene; (3) squalene cyclizes to lanosterol; (4) lanosterol converts to cholesterol.

HMGCR and squalene monooxygenase (SM) are two well-known rate-limiting enzymes in cholesterol synthesis, and the expression of both is tightly regulated by SREBP-2 [25-26]. When ER sterol levels are sufficient, SREBP precursors bind to Scap and remain inactive in the ER. When ER cholesterol is depleted, the Scap-SREBP complex translocate from the ER to the Golgi where forms activated SREBP [27]. So that, activated SREBP-2 moves into the nucleus to bind the sterol regulatory element (SRE) in the promoter of HMGCR and SM for upregulating their transcription. When the hepatic levels of

cholesterol or its derivatives (lanosterol, 25-hydroxycholesterol and 27-hydroxycholesteroland) are increased, they would induce the degradation of HMGCR and SM [28].

There are two intersecting pathways for the conversion of lanosterol to cholesterol, which are the Bloch pathway and the Kandutsch-Russell pathway (Figure 1). The two pathways are determined by the phase of the reduction of the double bond at C24 in the side chain. In the Kandutsch–Russell pathway (K-R pathway), lanosterol is first reduced by the 24-dehydrocholesterol reductase (DHCR24), and then 7-dehydrocholesterol, as a terminal intermediate, is catalyzed by 7-dehydrocholesterol reductase (DHCR7) to form cholesterol. In the Bloch pathway, the last biosynthetic precursor desmosterol is synthesized into cholesterol by DHCR24. Besides performing as the end and the start of each pathway, DHCR24 also can control any intermediates in the Bloch pathway to shift them into the Kandutsch-Russell pathway. Like other cholesterol synthesis enzymes, the transcriptional level of DHCR7 and DHCR24 are regulated via SREBP-2. Also, protein levels of DHCR7 and DHCR24 are negative feedback controlled by its products, including 7-dehydrocholesterol, desmosterol, and cholesterol. It is noteworthy that DHCR24 activity influences DHCR7 activity, with overexpression and knockdown of DHCR24 enhancing and suppressing the activity of DHCR7. Moreover, the relative contribution of these two pathways displays age, tissue, and cell-type dependence. Mitsche et al. (2015) revealed that in both human hepatoma cells and mice livers, cholesterol synthesis is achieved primarily by utilization of the Bloch pathway [29]. The concentration of serum cholesterol precursors (lathosterol, desmosterol, and 7-dehydrocholesterol) which can

reflect the content of hepatic cholesterol precursors, are usually regarded as markers of cholesterol synthesis [30].

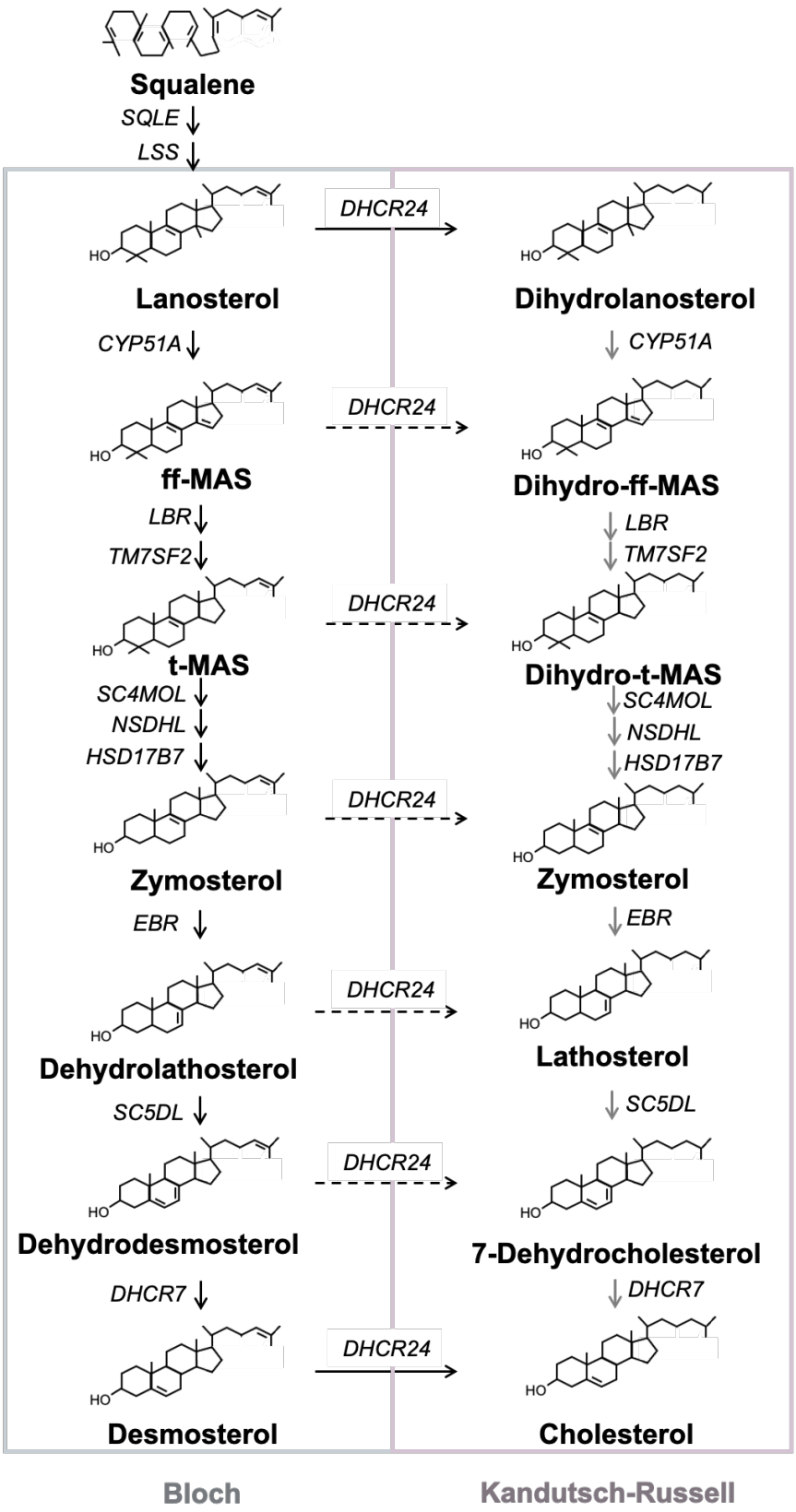

Figure 1. The Bloch and Kandutsch-Russell pathways in cholesterol synthesis. This figure is made from ref. 29.

Esterification of cholesterol

FC is a lipotoxic lipid that its excessive accumulation results in hepatotoxicity. Thus, FC is transformed into non-lipotoxic form by acyl-CoA: cholesterol acyltransferase enzyme 2 (ACAT2) and storage in lipid droplets [31]. ACAT2 is the cross-membrane protein in hepatic ER that catalyzes the synthesis of CE from FC and is potently activated by cholesterol. Contrary to the function of ACAT2, neutral CE hydrolase (nCEH) hydrolyzes CE to FC. When FC is needed by the liver, nCEH is upregulated to hydrolyze CE, whereas ACAT2 is downregulated [32].

Bile acid synthesis and excretion

Bile acid synthesis is a process that removes hepatic FC as neutral sterols. The classical and alternative pathways are two ways to mediate the conversion of cholesterol to bile acids. In the classical pathway, two primary bile acids, cholic acid (CA) and chenodeoxycholic acid (CDCA) are produced by cytochrome P450 family 7 subfamily A member 1 (CYP7A1), which is the rate-limiting enzyme in bile acid synthesis. The alternative pathway begins with cytochrome P450 family 27 subfamily A1 (CYP27A1) to synthesize CDCA. The progression of cholesterol converting to bile acids is accompanied by the production of oxysterols [33-34] **(Figure 2)**.

CYP7A1 is the first enzyme in the bile acids synthesis pathway, that mediates FC conversion to neutral sterol, i.e., bile acids [35]. The expression of CYP7A1 is a positive correlation with hepatic generation of bile acids. Moreover, when hepatic bile acid level is high, CYP7A1 activity is suppressed by bile acids

through negative feedback [36]. Additionally, several nuclear receptors also tightly downregulate CYP7A1 expressions, such as FXR and LXR [37].

The heterodimer of ATP binding cassette subfamily G member 5/8 (ABCG5/ABCG8) is the major receptor for cholesterol excretion in the liver, responsible for 70% to 90% of hepatic biliary cholesterol efflux [38]. The transcriptional level of ABCG5/ABCG8 is directly regulated by LXR [39]. LXRα is heterodimerization with retinoid X receptor (RXR) after activation by several oxysterols, followed by binding to the LXR response elements (LXREs) in ABCG5/ABCG8 promoter to upregulate their gene expression [40].

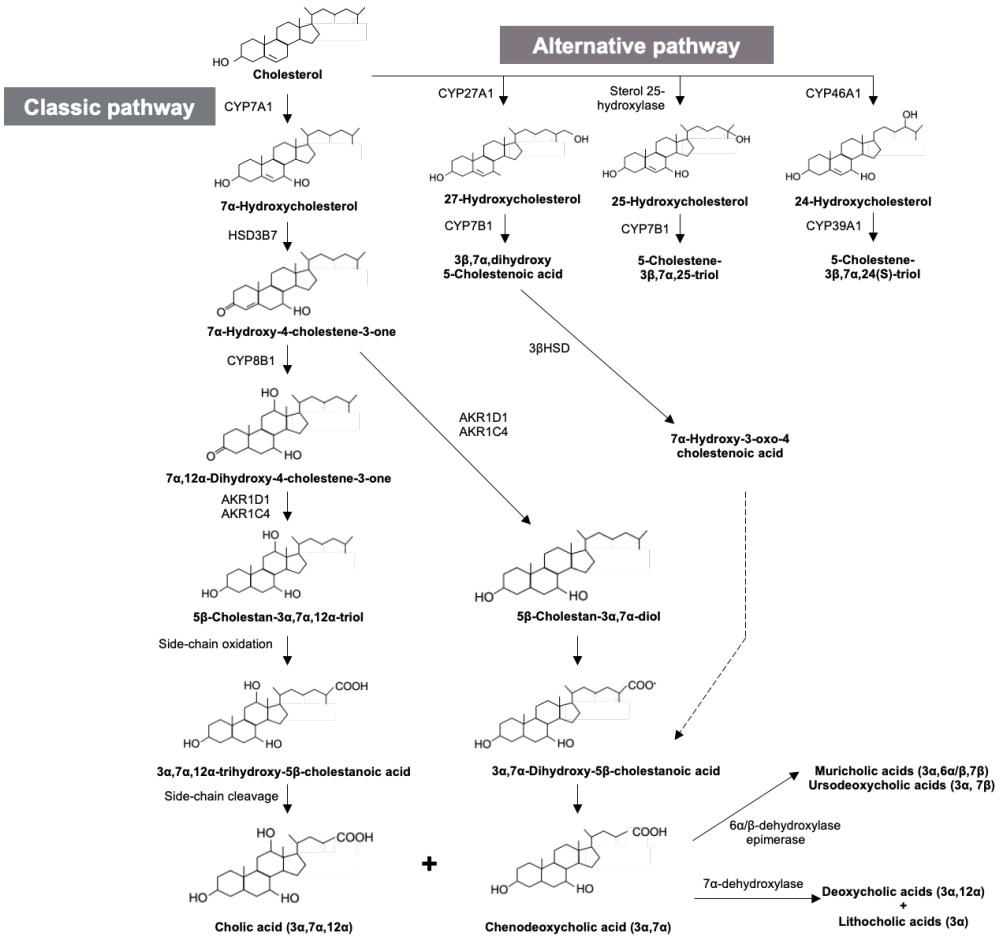

Figure 2. Bile acid biosynthetic pathways. This figure is made from ref. 34.

Cholesterol secretion into circulation

Another way to flux cholesterol out of the liver is transported by ATP binding cassette subfamily A member 1 (ABCA1). Hepatic ABCA1-mediated cholesterol efflux to the production of nascent HDL particles has been described by two mechanisms [33]. One is that apolipoprotein A-I (apoA-I) binds to ABCA1 at the plasma membrane to form a complex that picks up cholesterol and phospholipid to formation of nascent HDL particles [33]. The other is that ABCA1 promotes cholesterol efflux to apoA-I by the retroendocytosis pathway which from the cell surface to late endosomes and lysosomes and then to resecure from the cells [41]. The gene expression of ABCA1 is upregulated by LXR/RXR heterodimer, causing an increase in cholesterol efflux from the liver [42].

Liver dysregulated cholesterol metabolism in NAFLD

Abnormal hepatic cholesterol metabolism has been determined in the case of NAFLD, which caused the accumulation of liver cholesterol. A human liver lipidomic analysis demonstrated that the content of liver FC increases by 1.7-folds only in NASH, while not in nonalcoholic fatty liver (NAFL). Also, the level of liver CE in NAFL and NASH is no different in comparison with healthy control [43]. Another report of assessment of the molecular pathways of hepatic cholesterol metabolism in NAFLD patients points out that the protein expression of SREBP-2 increases roughly 2-folds, and HMGCR elevates 4-folds, which is a positive correlation with liver FC accumulation [44]. The serum LDL-c levels in NASH patients had proved to be positively related to HMGCR expression and negatively related to LDLR expression [44]. The liver mRNA level of nCEH is 6-folds higher in NAFLD patients than in healthy subjects [44]. In addition, hepatic cholesterol export and uptake and bile acid synthesis are also reduced in NASH patients, with a decrease in protein levels of ABCG8, ABCG1, LDLR, CYP7A1, and CYP27A1 by 60%, 50%, 70%, 67%, and 50%, respectively, compared to those in healthy subjects [44]. Moreover, a shift from the classical to the alternative BA synthesis pathway and increased levels of conjugated BAs (taurocholic acid and taurodeoxycholic acid) were observed in the liver of patients with NASH [45]. An increase in hepatic bile acids synthesis and levels of several liver oxysterols (7α-hydroxycholesterol, 7α-hydroxycholest-4-en-3-one, 7α,27-dihydroxycholesterol, 7β-hydroxycholesterol, 24S-hydroxycholesterol, and 24R-hydroxycholesterol) also have been previously demonstrated in patients with NASH [46]. The above

evidence showed that hepatic imbalanced cholesterol homeostasis occurred in the development of NAFLD.

Liver cholesterol metabolism in diet-induced NAFLD animal model and in free-fatty acid-induced NAFLD cell model

Diet-induced NAFLD animal model

Numbers of overnutrition-foundation models have sought to mimic the hepatic histological features and the metabolic disorder similar to human NAFLD. In animal studies, dietary ingredients induced NAFLD have been widely examined, but the mechanism of liver cholesterol metabolism in those studies is still rarely investigated. In the **Table 1**, we have summarized studies on the effects of dietary ingredients on liver cholesterol metabolism in the NAFLD.

Dietary carbohydrates

Overconsumption of carbohydrates leads to unfavorable metabolic effects has been confirmed [47]. Several epidemiological studies have presented that added sugars (e.g., sucrose and fructose) have found a positive association with the risk of NAFLD [45-46]. Fructose stimulates liver *de novo* lipogenesis, oxidative stress, and insulin resistance resulting in greater liver lipids accumulation than in comparison to glucose [48]. Therefore, high-fructose diet or high-sucrose diet are usually used to mimic the etiology of human NAFLD.

As shown in **Table 1**, animals fed high-carbohydrate diets revealed a change in liver histology [51-57]. Despite feeding periods being different, mice fed high sucrose diet (32% energy from sucrose or 60% sucrose (w/w)) result in a 1.5-

to 2-fold increase in the levels of hepatic TAG, and a significant increase in macrovesicular and microvesicular steatosis [51-52.54-57]. In addition to the change in hepatic TAG metabolism, the change in hepatic cholesterol metabolism has been observed under the condition of high sucrose diet feeding. Flister et al. and Fernandes-Lima et al. fed mice a high-sucrose diet (32% energy from sucrose) for 90 days and 4 weeks, respectively, then these mice showed an increase in cholesterol content in the liver by 1.3-folds and 2-folds, respectively [51-52]. The research of Apro et al. indicated that rats consumed a high-sucrose diet (60% sucrose (w/w)) with 10% fructose beverage for 10 days caused liver cholesterol accumulation, which results from decreasing bile acid synthesis-related gene expressions of CYP7A1, ABCG5, and ABCG8 by 60%, 88%, and 93%, respectively [53]. Mice-fed high-sucrose diet (60% sucrose (w/w)) for 20 days from Berger et al. study pointed out that the liver retained more cholesterol as a result of decreased excretion of bile acids and decreased excretion of cholesterol into feces [54]. Also, the liver also obtained more cholesterol from plasma LDL and HDL [54]. However, Oliveira et al. study observed that the high-sucrose (32% energy from sucrose) diet did not significantly change the liver content of cholesterol in mice [55]. It can be seen that dietary high sucrose results in TAG metabolism disorder but does not certainly affect cholesterol metabolism in the liver [51-55]. Furthermore, in a high-fructose diet (35% energy from fructose) fed for 15 weeks of C57BL/6 mice, the liver cholesterol content and protein expression of HMGCR, acetyl-coenzyme A acetyltransferase 1 (ACAT1), and cluster of differentiation 36 (CD36) were increased by 3.8-folds, 3.6-folds, and 2-folds [56]. In the study by Ichigo et al., a high-fructose diet (65% fructose (w/w)) significantly increased

hepatic levels of cholesterol and ACAT2 protein expression by 1.7-folds, whereas lowered hepatic mRNA levels of ABCG5 by 60% in Wistar rats [57]. The hepatic gene expression of *Hmgcr, Ldlr, Acat1*, microsomal triglyceride transfer protein (*Mttp*), and *Cyp7a1* did not change with a high-fructose diet in comparison to the control diet (glucose diet) [57]. Consequently, there are different mechanisms affecting liver cholesterol metabolism in different feeding conditions of dietary fructose. It is worth noting that the hepatic phenotype of NASH cannot be produced by using a high sucrose diet or high fructose diet alone.

Dietary fats

Excessive consumption of fat increases the development of obesity, due to it being the highest energy density nutrient in human nutrition. High-fat diet (HFD), especially saturated fatty acid, is strongly associated with an increase in liver lipids, due to an increase in lipolysis of adipose tissue and an increase in liver *de novo* lipogenesis. It has been known that HFD (fat content varying between 45 and 75 kcal%)-fed animals for long period can be used as a useful tool to reproduce the etiology of NAFLD in humans.

As represented in **Table 1**, animals fed HFD caused a 4.3-fold increase in liver TAG content and developed steatosis [58-59]. C57BL/6 mice fed with HFD (60 % energy from fat) for 12 weeks developed obesity, hyperlipidemia, and liver steatosis [58]. Under this diet feeding, mice also developed liver cholesterol accumulation, which is related to an increase in protein expression of Hmgcr by 1.5-folds. Conversely, a decrease in mRNA level of hepatic HMGCR by 50% was observed in the study by Kant et al. when C57BL/6 mice

were fed with a 60 % fat diet for 8 weeks [59]. Also, 60 % of HFD suppressed gene expressions of *Cyp7a1* and *Mttp* by 10% and 60%, respectively, and enhanced the mRNA level of *Abca1* by 1.6-folds in the liver of mice [59]. Another study of Sprague–Dawley rats fed 12 weeks of HFD (45 % energy from fat) showed that protein expressions of HMGCR and LDLR were enhanced by 4-folds and 1.5-folds, separately, and the protein level of CYP7A1 was suppressed by 60% [60].

Despite HFD-induced liver cholesterol metabolism disorder, the HFD is not a favored model for researchers to investigate NASH in NAFLD. Due to the strong association between cholesterol intake and the development of NASH, thus cholesterol diets are widely used to observe the mechanism of dysregulated cholesterol metabolism in NAFLD. The HFD containing 1.25% or 2.5% cholesterol induces higher serum aminotransferase levels, severe steatosis, moderate lobular inflammation, and ballooning degeneration in Sprague-Dawley (SD) rats over 9 weeks of feeding. Liver cholesterol deposition had also occurred in rats fed the HFD in combination with 2.5% cholesterol, and hepatic gene expressions of *Srebp-2*, *Abcg5*, *Hmgcr*, and *Ldlr* were decreased [61]. Ioannou et al. reported that the different content of dietary cholesterol (0.25%, 0.5%, 0.75%, and 1%) have different effects on liver cholesterol levels. After 24 weeks of the feeding of C57BL/6J mice, the content of liver cholesterol in feeding dietary 1% cholesterol is roughly 5-fold higher than in feeding dietary 0.25% cholesterol [62]. Although pronounced liver histological changes by dietary cholesterol, in fact, the level of dietary cholesterol content (>0.5%) in those high cholesterol diets is not applicable to humans due to being toxic and far over human consumption.

Free-fatty acid-induced NAFLD cell model

An elevated serum level of free fatty acids has been observed in patients with NAFLD, particularly lipotoxic fatty acid palmitate acid (PA) [63]. In the hepatocyte model to induce NAFLD, PA is a largely utilized inducer. Under the case of treatment with PA, hepatocytes develop abnormal lipid metabolism, which leads to hepatic steatosis. Derangement of hepatic cholesterol metabolism is also noticed in this model (**Table 1**). The research of Mayer et al. [64] showed that, in HepG2 cells, 250 μM PA greatly increased the content of TAG by 1.4-folds and the expression of lipogenic enzyme genes (sterol regulatory element-binding protein-1c (*SREBF1*), stearoyl-CoA desaturase (*SCD*), carnitine palmitoyltransferase 1A (*CPT1A*), and carnitine palmitoyltransferase 2 (*CPT2*)). In addition, cellular levels of total cholesterol and cholesterol esters were elevated by 2-folds and 2.8-folds under this condition [64]. Another hepatocyte study showed that 250 μM of PA had an increase in hepatic lipid and TAG accumulation through the enhancement of lipogenesis-related gene and protein expression, including SREBP1-c, fatty acid synthesis (FAS), and SCD-1 [65]. Also, protein levels of *de novo* cholesterol synthesis-associated enzymes, such as SREBP-2 and HMGCR increased by 1.6-folds and 6-folds, respectively, in 250 μM of PA treatment [65]. Similarly, a higher mRNA level of SREBF-2 and lipid accumulation were observed in HepG2 cells treated with 300 μM of PA [66]. Interestingly, an increase in hepatic secretion PCSK9 ability and a decrease in uptake of LDL ability by hepatocytes were proved in a high PA environment, which may result from PA-induced ER stress [66]. According to the above studies, PA induces higher intracellular cholesterol, probably because of stimulating *de novo*

cholesterol synthesis [64-66]. However, other mechanisms of cholesterol metabolism, such as utilization, excretion, and uptake have rarely been reported in this cell model.

Table 1. Influence of dietary ingredients on hepatic cholesterol metabolism.

Animal	Diet	Period	Energy intake	Liver cholesterol metabolism	Liver Histology	Cites
High sucrose diet						
Male Swiss mice	Control diet (10% energy from sucrose, without cholesterol) High-sucrose diet (32% energy from sucrose, without cholesterol)	90 days	Control: about 7 kcal/day/10 g BW High-sucrose: about 5 kcal/day/10 g BW	TAG level ↑ (1.5-folds) Total cholesterol ↑(1.3-folds)	Microvesicular steatosis	51
Swiss Webster mice	Control diet (8% energy from sucrose, without cholesterol) High-sucrose diet (32% energy from sucrose, without cholesterol)	4 weeks	Control: 187.3 ± 2 kcal/day/100 g BM High-sucrose: 178.3 ± 6 kcal/day/100 g BM	TAG level ↑ (2-folds) Cholesterol level ↑(2-folds)	Macrovesicular and microvesicular steatosis	52
Male Sprague Dawley rats	Control diet (2% sucrose (w/w), without cholesterol) High-sucrose diet (60 sucrose (w/w), without cholesterol & 10% fructose in the drinking water)	10 days	ND	Cholesterol level ↑(1.6-folds) *Cyp7a1* mRNA level ↓ (60%) *Abcg5* mRNA level ↓ (88%) *Abcg8* mRNA level ↓ (93%)	ND	53
Males C57BL/6J mice	High-sucrose diet (60% sucrose (w/w))	20 days	ND	TAG level ↑ (1.75-folds) Cholesterol level ↑(1.2-folds) HMGCR protein level ↓ Cholesterol synthesis ↓ (67%) ^{3}H-Cholesterol from LDL↑ (1.2-folds) SR-B1 protein level ↑ VLDL secretion ↑ (1.7-folds) *Bile acid level in the bile ↓ (8%) *Fecal cholesterol ↓ (72%)	Macrovesicular and microvesicular steatosis	54
Male C57BL/6 mice	Control diet (8% energy from sucrose, without cholesterol) High-sucrose diet (32% energy from sucrose, without cholesterol)	8 weeks	Control: 10.4 ± 0.2 kcal/day High-sucrose: 11.1 ± 0.1 kcal/day	TAG level ↑ (1.8-folds) Cholesterol level -	Macrovesicular and microvesicular steatosis	55

High fructose diet						
C57BL/6 mice	Control diet (0 % energy from fructose, without cholesterol) High-fructose diet (35 % energy from fructose, without cholesterol)	15 weeks	ND (ad libitum)	Cholesterol level ↑ (1.5-folds) HMGCR protein level↑(3.8-folds) ACAT1 protein level↑ (3.6-folds) CD36 protein level↑(2-folds)	ND	56
Male Wistar rats	Control diet (65% glucose (w/w), without cholesterol) High-fructose diet (65% fructose (w/w), without cholesterol)	12 days	Control: 12.9 ± 0.4 kcal/day High-fructose: 12.0 ± 0.3 kcal/day	TAG level ↑ (2.6-folds) Cholesterol level ↑(1.4-folds) *Soat2* mRNA level ↑ (2.1-folds) ACAT2 protein level ↑ (1.7-folds) *Abcg5* mRNA level ↓ (60%)	ND	57
High fat diet						
Male C57BL/6J mice	Control diet (13.5 % kcal fat) High fat diet (60 % kcal fat)	12 weeks	Control: 13.6 kcal/day HFD: 15.7-16.6 kcal/day	TAG level ↑ (4.3-folds) Cholesterol level ↑(2.4-folds) HMGCR protein level ↑(1.5-folds)	Fatty liver	58
Male C57BL/6 mice	Control diet (10 % kcal fat) High fat diet (60 % kcal fat)	8 weeks	ND	TAG level ↑ (4.3-folds) *Hmgcr* mRNA level ↓ (50%) *Abca1* mRNA level ↑ (1.6-folds) *Mttp* mRNA level ↓ (60%) *Cyp7a1* mRNA level ↓ (10%)	steatosis	59
Male Sprague Dawley rats	Control diet (10 % kcal fat) High fat diet (45 % kcal fat)	12 weeks	ND (ad libitum)	HMGCR protein level ↑(4-folds) LDLR protein level ↑(1.5-folds) CYP7A1 protein level ↓ (60%)	steatosis	60
High cholesterol diet						
Sprague–Dawley rats	High fat diet (68% MF, 30% palm oil, 2% cholic acid) without cholesterol High fat diet with 1.25% cholesterol High fat diet with 2.5% cholesterol	9 weeks	HFD: 5840 ± 303 kcal HFD with 1.25: 6301 ± 109 kcal HFD with 2.5: 5840 ± 328 kcal	TAG level ↑ (6; 4-folds) Cholesterol level ↑ (1.3; 1.5-folds) HFD with 1.25 *Cyp7a1* mRNA level ↑(5.3-folds) *Abcb11* mRNA level ↓ (50%) HFD with 2.5 *Abab11* mRNA level ↓ (75%) *Mttp* mRNA level ↓ (60%)	Severe micromacrovesicular steatosis Mild to moderate inflammation Ballooning degeneration	61

C57BL/6J mice	High fat diet (15 % (w/w)) with 0%, 0.25%, 0.5%, 0.75%, or 1% cholesterol	24 weeks	0%: 3.2 ± 0.3 g/d 0.25%: 3.3 ± 0.3 g/d 0.5%: 3.0 ± 0.3 g/d 0.75%: 2.9 ± 0.3 g/d 1%: 2.9 ± 0.3 g/d	Cholesterol ester 0.25%: ↑ (13-folds) 0.5%: ↑ (37.5-folds) 0.75%: ↑ (60-folds) 1%: ↑ (61.5-folds)	Steatosis Lobular inflammation Fibrosis (over 0.5%)	62

Cell	Treatment	Period		Cites
HepG2 cells	Palmitic acid 250 μM	24 h	Intracellular TAG level ↑ (1.4-folds) Intracellular total cholesterol ↑ (2-folds) Intracellular cholesterol ester ↑ (2.8-folds)	64
HepG2 cells	Palmitic acid 250 μM	24 h	Lipid accumulation ↑ (2-folds) Intracellular TAG level ↑ (2.5-folds) SREBP-2 protein level ↑ (1.6-folds) Activated SREBP-2 level ↑ (3.6-folds) *HMGCR* mRNA level ↑ (1.8-folds) HMGCR protein level ↑ (6-folds)	65
HepG2 cells	Palmitic acid 300 μM	24 h	Intracellular TAG accumulation ↑ *SREBF-2* mRNA level ↑(3-folds) SREBP2 transcriptional activity ↑ PCSK9 mRNA level ↑(3.2-folds) Secreted PCSK9 level ↑(1.4-folds) *LDLR* mRNA level↑ (2.8-folds) LDL uptake ↓ (15%)	66

Aim of this study

Liver cholesterol deposition is a risk factor to accelerate the development of NAFL to NASH and fibrosis. Early prevention of dysregulated cholesterol metabolism may effectively arrest the development of NASH. But current studies on the change of liver cholesterol metabolism in NAFLD are still incomplete. Therefore, we used three different models to induce NAFLD. The purpose of this study is to investigate the effect of natural compounds derived from food ingredients on cholesterol metabolism with animal or cell models in NAFLD.

Excessive carbohydrate intake is known to favor the progression of NAFLD. However, the effect of dietary cholesterol on dietary carbohydrate consumption in animals was not considered in many previous studies. Therefore, rats were fed with cholesterol-containing high sucrose or starch diets for 4 weeks by pair feeding. In CHAPTER II, PART1, the effect of high carbohydrate diets on the mechanism of cholesterol metabolism in the liver, serum, and feces in rats would be explained in detail.

In CHAPTER II, PART 2, we fed C57BL/6 mice HFD for 9-weeks to cause abnormal liver lipid metabolism. The effect of anti-obesity and improvement of hyperlipidemia by soyasaponin have been proved in HFD-fed animals. Based on previous researches, we predicted that soyasaponin can ameliorate dysregulated liver cholesterol metabolism in mice that resulted from HFD. Therefore, the CHAPTER III, PART 2, of this study focuses on the effects of soyasaponin on liver cholesterol metabolism and further investigates this mechanism of action.

In CHAPTER III, we used toxicity fatty acid PA to treat HepG2 cells for the establishment of the NAFLD cell model. In our previous studies, we demonstrated that rare sugar, D-psicose, contributed to reducing atherosclerosis risk in hamsters and enhancing cholesterol uptake of HDL in primary rat hepatocytes. According to these evidence, we speculated that D-psicose play a role in hepatic cholesterol metabolism. However, the regulation of D-psicose on cholesterol metabolism in the progression of NAFLD is still not been proven. Thus, this chapter focuses on clarifying the mechanism of D-psicose on cholesterol metabolism in the NAFLD cell model.

Abbreviations used in this thesis

ATP binding cassette subfamily A member 1, ABCA1; ATP binding cassette subfamily G member 5/8, ABCG5/ABCG8; Acetyl-coenzyme A acetyltransferase 1, ACAT1; Acyl-CoA: cholesterol acyltransferase enzyme 2, ACAT2; acetyl-CoA carboxylase, ACC; Acyl-CoA oxidase, ACO; Alanine aminotransferase, ALT; AMP-activated protein kinase, AMPK; adipocyte protein 2, aP2; apolipoprotein A-I, apoA-I; apolipoprotein B100 ,Apo B100; apolipoprotein E, Apo E; α-tocopherol, α-Toc; Activation transcription factor 4, ATF4; Activation transcription factor 6, ATF6; Bile acids, BAs; Beta-actin, β-actin; Bovine serum albumin, BSA; Cholic acid, CA; Cluster of differentiation 36, CD36; Complementary DNA, cDNA; Chenodeoxycholic acid, CDCA; cholesterol esters, CE; CCAAT/enhancer-binding protein α, C/EBPα; C/EBP-homologous protein, CHOP; Carnitine palmitoyltransferase 1A, CPT1A; Carnitine palmitoyltransferase 2, CPT2; Cytochrome P450 family 7 subfamily A member 1, CYP7A1; Cytochrome P450 family 27 subfamily A1, CYP27A1; Dulbecco's modified Eagle medium, DMEM; 7-dehydrocholesterol reductase, DHCR7; 24-dehydrocholesterol reductase, DHCR24; Diacylglycerol O-acyltransferase 1, Dgat1; esterified cholesterol, EC; Ethylenediaminetetraacetic acid, EDTA; Endoplasmic reticulum, ER; Fatty acids, FAs; Fatty acid synthesis, FAS; Δ5-desaturase, FADS1; Δ6-desaturase, FADS2; Fetal bovine serum, FBS; Free cholesterol, FC; Free fatty acids, FFA; farnesoid X receptor, FXR; Gas chromatography-flame ionization detection, GC-FID; Gas chromatography-mass spectroscopy, GC-MS; glucose-6-phosphatase, G6p; Glyceraldehyde-3-phosphate-dehydrogenase, GAPDH; Glucose-6 phosphate dehydrogenase, G6PDH; 3-hydroxy-3-methylglutaryl coenzyme A reductase, HMGCR; High density lipoprotein, HDL; High density lipoprotein cholesterol, HDL-c; High-fat diet, HFD; Inositol requiring enzyme 1α/β, IRE1; Kandutsch–Russell pathway, K-R pathway; Low-density lipoprotein receptor, LDLR; Low-density lipoprotein cholesterol, LDL-c; Liver X receptor, LXR; LXR response elements, LXREs; Cytosolic malic

enzyme, ME1; Microsomal triglyceride transfer protein, MTTP; Monounsaturated fatty acids, MUFAs; Disodium hydrogen phosphate, Na2HPO4; Monosodium phosphate, NaH2PO4; Sodium chloride, NaCl; Nicotinamide adenine dinucleotide phosphate, NADPH; nonalcoholic fatty liver, NAFL; Nonalcoholic steatohepatitis, NASH; Non-alcoholic fatty liver disease, NAFLD; neutral CE hydrolase, nCEH; Niemann–Pick type C1 (NPC1)-like 1, NPC1L1; cyclin-dependent kinase inhibitor 1A, p21; cyclin-dependent kinase inhibitor 2A, p16; Palmitate acid, PA; Phosphoenolpyruvate carboxykinase-1, Pck-1; Proprotein convertase subtilisin/kexin type 9, PCSK9; PKR-like ER kinase, PERK; pancreatic lipase, PL (Study II); phospholipids, PL; 2,2,5,7,8-penta-methyl 6-hydroxycromane, PMC; Peroxisome proliferator-activated receptor-α, PPAR-α; Peroxisome proliferator-activated receptor-γ, PPAR-γ; Pentose phosphate pathway, PPP; Polyunsaturated fatty acids, PUFAs; polyvinylidene fluoride, PVDF; quantitative real-time reverse transcription-polymerase chain reaction, qRT-PCR; Retinoid X receptor, RXR; Soyasaponin sample, SAP; Senescence-associated β-galactosidase, SA-β-gal; SREBP cleavage-activating protein, Scap; Stearoyl-CoA desaturase, SCD; Standard error of the mean, SEM; Saturated fatty acids, SFAs; Scavenger receptor class B1, SR-B1; Sterol regulatory element-binding protein-1c, SREBP-1c; Sterol regulatory element binding protein-2, SREBP-2; Squalene monooxygenase, SM; Sterol regulatory element, SRE; Triacylglycerol, TAG; total cholesterol, TC; Very-low-density lipoprotein, VLDL; White adipose tissues, WATs; Unfolded protein response, UPR; X-box-binding protein 1, XBP1.

CHAPTER II Effect of diet induced NAFLD in animal models

PART1

High cholesterol-containing sucrose diet lowers cholesterol content and promotes triacylglycerol deposition in the liver of rats

Introduction

Metabolic disorders induced by excessive carbohydrate intake are mainly due to excessive sucrose that is added to processed foods as a sweetener or preservative [67-69]. Excessive consumption of sucrose is associated with weight gain [67], fatty liver development [68], hyperglycemia, and insulin resistance [69]. When consumed within the range of appropriate calorie intake, sucrose is not detrimental to human health [70] Sucrose is a disaccharide composed of glucose and fructose. The effects of isocaloric intake of dietary glucose or fructose do not differ in terms of body weight, liver TAG levels, and serum insulin levels in mice [71]. Fructose has been shown to contribute to hepatic disorders of lipid and carbohydrate metabolism. Habitual drinking of fructose-containing water results in fatty liver by increasing fatty acid synthesis via activation of SREBP-1c in mice [72]. Excessive glucose and fructose consumption activate cholesterol synthesis by increasing SREBP-2 expression, resulting in the accumulation of cholesterol in the liver [73]. Additionally, high fructose consumption leads to hyperglycemia by promoting hepatic gluconeogenesis [74]. Intake of different ratios of carbohydrates leads to different metabolic consequences in the liver. For instance, a high-sucrose diet (a diet containing 40% sucrose and 32% starch) can induce fatty liver compared

with a normal diet (a diet containing 10% sucrose and 62% starch) in mice [55]. However, the effect of dietary cholesterol on dietary carbohydrate consumption in animals was not considered in these studies [55, 71-74]. In humans, high dietary cholesterol (>500 mg/day) is regarded as a risk factor for the development of fatty liver [75-76]. Ichimura et al. reported that dietary cholesterol >1.25% accelerated steatosis in rats [77]. The major types of dietary carbohydrates are starch and sucrose [78]. The physiological effects of dietary intake of cholesterol along with sucrose or starch remain unclear. In this study, under pair-feeding conditions to ensure iso-energy intake, rats were fed equivalent carbohydrate diets (sucrose or starch, 67% of total calories) containing 0.2% cholesterol. We used this rat model to evaluate the effects of dietary sucrose and starch on liver lipid and carbohydrate metabolism.

Methods

Reagents

The chemicals used in the experiments were purchased from Nacalai Tesque (Kyoto, Japan). *N*, *O*-bis (trimethylsilyl)trifluoroacetamide with 1% trimethylchlorosilane, *N*-methyl-*N*-trimethylsilyl-trifluoroacetamide, and trimethylchlorosilane were purchased from TCI Chemicals (Kyoto, Japan). The purified oxidized cholesterol compounds, 5α-cholestane and 19-hydroxycholesterol (19-OH), were purchased from Steraloids Inc. (Newport, RI, USA).

Animal studies

Four-week-old male SD rats (total of 12) were purchased from CLEA Japan, Inc. (Shiga, Japan) via Kyudo (Saga, Japan). Rats were housed at 21–24 °C with a 12-h light-dark cycle and free access to a commercial chow diet (NMF; Oriental Yeast Co., Ltd., Tokyo, Japan) and autoclaved deionized water. After one week of adaptation, rats with a similar amount of food intake were distributed to the different groups. Rats were fed a sucrose diet (sucrose group) or starch diet (starch group) for 4 weeks by pair-feeding (n = 6 for each group). Pair feeding was executed by two rats with similar food intake in two different groups as a subgroup, controlling the amount of food provided daily, so as to match the quantity of food consumption in each subgroup. The diets provided were formulated based on AIN-76 formula, which contained 0.2% cholesterol with 64.8% starch or sucrose. The detailed composition of the diet and dietary fatty acids are shown in **Table 2**. Food intake and body weight were monitored daily. After the feeding period, the rats were fasted for 9 h and sacrificed by decapitation under anesthesia with isoflurane (FUJIFILM Wako Chemicals Co., Osaka, Japan). The blood samples were kept at room temperature for 30 min and centrifuged at 1,500 × g, 4 °C, 20 min to obtain serum samples. The liver, white adipose tissue, and femoral muscle tissues were harvested, weighed, and snap frozen in liquid nitrogen. All samples were stored at -30 °C until further analysis. All experimental animals were handled and euthanized in accordance with national guidelines, and ethical approval for the experiments was granted by the Animal Care and Use Committee of Kyushu University (authorization number: A30-312-0).

Table 2. Composition of experimental diets

	Starch diet	Sucrose diet
	(g/100 g)	
Cellulose	5.0	5.0
Casein	20.0	20.0
Corn oil	5.0	5.0
Corn starch	64.8	-
Sucrose	-	64.8
Vitamin Mix (AIN-76)	1.0	1.0
Mineral Mix (AIN-76)	3.5	3.5
DL-Methionine	0.3	0.3
Choline bitatrate	0.2	0.2
Cholesterol	0.2	0.2
Fatty acid	mol%	
C10:0	0.03	
C14:0	0.06	
C15:0	0.01	
C16:0	12.6	
C16:1 (n-9)	0.07	
C16:1 (n-7)	0.22	
C17:0	0.15	
C18:0	3.65	
C18:1 (n-9)	32.0	
C18:2 (n-6)	45.7	
C20:0	0.90	
C20:1	1.00	
C18:3 (n-3)	2.40	
C20:2	0.22	
C22:0	0.43	
C24:0	0.41	

Blood analysis

Serum levels of alanine aminotransferase (ALT), FFA, TAG, phospholipids (PL), glucose, and insulin were determined using commercial enzyme assay kits (Transaminase C II-test, NEFA C-Test, Triglyceride E-Test, Phospholipid C-test, Glucose C-II-test, FUJIFILM Wako Chemicals Co., Osaka, Japan; LBIS Mouse Insulin ELISA Kit, FUJIFILM Wako Shibayagi Co., Gunma, Japan). Serum HDL fractions were separated as described previously [79]. Serum levels of cholesterol and HDL-cholesterol (HDL-c) were determined using a Cholesterol E-test kit (FUJIFILM Wako Chemicals Co., Osaka, Japan).

Liver TAG, PL, and glycogen

Liver lipids were extracted using Folch's chloroform/methanol (2:1, v/v) method [80]. Liver TAG contents in the extracted lipids were measured with the modified method using the triglyceride E-test as described previously [81]. Liver PL content of the extracted lipids was measured using the method described by Rouser et al. [82]. The liver glycogen content was measured using the method described by Lo et al. [83].

Fatty acid composition in liver TAG and PL

Liver lipid extracts were separated by thin-layer chromatography on silica gel G (20 × 20 cm; Merck, Darmstadt, Germany) using a solvent mixture of petroleum ether: diethyl ether: acetate (82:18:1, v/v/v). The fractions corresponding to TAG and PL were scraped and methylated with sulfuric acid solvent: methanol (2:115, v/v) at 80 °C for 2 h. Methylated samples were extracted using sodium hydroxide solution: hexane (1:1, v/v). The separated

hexane layer was transferred to a tube, evaporated to dryness under nitrogen, and redissolved in a lower volume of hexane. The samples were analyzed by gas chromatography-flame ionization detection (GC-FID) (GC-17A and GC-2014) (Shimadzu Co., Kyoto, Japan) equipped with a CP-Sil 88 for FAME column (100 m × 0.25 mm i.d., 0.25-μm) (Agilent, CA, USA). The temperature of the injection port and detection was set to 250 °C. The column temperature was 140–240 °C. The flow rate of helium as a carrier gas was 40 cm/s.

Sterol content analysis in rats

Serum lipids were extracted using Folch's method [80]. Fecal lipids were extracted using a previously described method [84]. The levels of total cholesterol (TC), FC, esterified cholesterol (EC), fecal cholesterol, and coprostanol were measured according to a previous report [81]. The conversion rate of cholesterol to coprostanol was calculated by dividing fecal cholesterol content by coprostanol content. Phytosterols in the serum, liver, and feces, and cholesterol precursors in the liver were analyzed as previously described [85]. Briefly, using 5α-cholestane as an internal standard, lipid samples were saponified in 0.71 M ethanolic KOH at 65 °C for 1 h. Unsaponified lipids were extracted using hexane and derivatized to trimethylsilyl esters by *N, N, O*-bis (trimethylsilyl)trifluoroacetamide with 1% trimethylchlorosilane. Samples were detected by GC-FID (GC-2014) (Shimadzu Co.) equipped with an SPB-1 capillary column (60 m x 0.25 mm x 0.25 μm) (Sigma-Aldrich, MO, USA). The temperature of the injection port and detection was set to 300 °C. The column temperature was 275 °C. The flow rate of helium as the carrier gas was 32.5 cm/s. Liver oxidized cholesterol levels were analyzed as previously

described [85]. Briefly, liver lipid samples containing 19-OH as the internal standard were saponified using 1 M ethanolic KOH at 25 °C overnight. Saponified lipids were extracted using hexane and applied to a Sep-Pak Silica Vac Cartridge (Nihon Waters, Tokyo, Japan) to separate the oxidized cholesterol from cholesterol. The cartridge was washed with hexane before use. Saponified lipid samples were added to the cartridge and eluted with hexane: 2-propanol (1:200, v/v) and hexane: 2-propanol (3:7, v/v), which allowed for the sequential elution of cholesterol and 19-OH plus oxidized cholesterols, respectively. Eluted samples were dried under nitrogen gas and then derivatized into trimethylsilyl ethers in a mixture solution of dried pyridine, hexamethyldisilazane, and trimethylchlorosilane (9:3:1, v/v/v) at 25 °C for 30 min. Each sample was dried under nitrogen gas and dissolved in hexane for gas chromatography-mass spectroscopy (GC-MS) analysis. Oxidized cholesterol levels were measured by GC-MS (Shimadzu GC-17A version 3) coupled with a SPB-1 fused silica capillary column (60 m × 0.25 mm, 0.25 μm thickness) (Spelco Inc., PA, USA) according to the method described by Shirouchi et al. [86].

Liver gene expression

Total liver RNA was extracted using phenol/chloroform solution [87]. cDNA was synthesized from 1 μg RNA using the Transcriptor First Strand cDNA Synthesis Kit (Roche, Switzerland). Gene expression was measured by quantitative real-time reverse transcription-polymerase chain reaction with a SYBR Premix Ex TaqPerfect Real-time kit (Takara Bio., Shiga, Japan) on

Mx3000P Real-Time PCR System (Stratagene, CA, USA). *Actb* mRNA was used as an internal control. The primer sequences used are listed in **Table 3.**

Table 3. Rat primers for qRT-PCR.

Gene	Forward primer	Reverse primer
Actb	TCA GGT CAT CAC TAT CGG CA	TCA TGG ATG CCA CAG GAT TC
CD36	GAA GCA CTG AAG AAT CTG AAG AG	TCC AAC ACC AAG TAA GAC CAT C
MTP	CGA CGG TGA CGA TGA TCA ACT	TGA CCC GCA TTT TCG ACA TT
DGAT1	GAT GCT CTT TTT CAC CCA GC	GAG ACG CTC AAT GAT TCG TG
G6PC	CTA CCT TGC GGC TCA CTT TC	ATC CAA GTG CGA AAC CAA AC
PCK1	GGG GAG TTT ATC AAG TGC CTC	CAC CGT ATC CGC TTC CGA A
SCD1	GAG ATA CAC TCT GGT GCT C	AAG GCG TGA TGG TAG TTG TGG
SREBP-1c	ATG CCA TGG GCA AGT ACA CA	ACG TGT CAA GAA GTG CAA GG
SREBP-2	GAT CAT CCA GCA GCC TTT GA	TGT GGT GTA GCG ACT GTC TG

Liver FAS activity

Details of the liver FAS activity analysis were described in our previous study [88]. Briefly, the liver (0.5 g) was homogenized in an ice-cold homogenization buffer (sucrose 250 mM, Tris-HCl 10 mM, EDTA 1 mM). The homogenized lysate was centrifuged at 10,000 × g and 4 °C for 10 min to separate nuclear fraction. The supernatant was centrifuged at 125,000 × g and 4 °C for 60 min, and the resulting supernatant was used as the cytosolic fraction. Protein levels in the cytosolic fraction were measured using the method described by Lowry et al. [89]. Liver FAS activity was measured using the method described by Kelley et al. [90].

Water-soluble metabolite analysis

For water-soluble metabolite analysis, liver samples were homogenized in a solvent mixture of methanol, water, chloroform (5: 2: 2, v/v/v). The metabolites in the liver homogenates were derivatized by N-methyl-N-trimethylsilyl-trifluoroacetamide (Sigma-Aldrich, MO, USA) and determined by GC-MS analysis (GCMS-QP2020, SHIMAZU). Metabolite data were identified using the method described by Tanaka et al. [88].

Statistical analysis

Statistical analyses were performed using Excel 2011 (Microsoft, USA). Data are presented as the mean and standard error of the mean (SEM). Comparisons between two groups in the animal experiment were analyzed using the Student's *t*-test. Differences were considered statistically significant at $p < 0.05$.

Results

Growth parameters and organ weights show differences in starch and sucrose fed rats

As shown in **Table 4**, food intake and final body weight were not significantly different between starch- and sucrose-fed rats. Food efficiency was significantly increased in the sucrose group. The weights of the liver, abdominal (sum of perirenal, peritoneal, mesenteric, and epididymal) adipose tissue, subcutaneous adipose tissue, and brown adipose tissue were significantly higher in the sucrose group than those in the starch group. The weight of the femoral muscle did not differ significantly between the starch and sucrose groups.

Serum biochemical parameters are different in starch and sucrose fed rats

Compared with the starch diet, the sucrose diet significantly increased the serum levels of ALT, FFA, TAG, PL, glucose, insulin, and HOMA-IR values (**Table 4**). Serum levels of phytosterols (campesterol and β-sitosterol) were significantly lower in the sucrose group than those in the starch group. No significant differences in the serum levels of cholesterol, HDL-c, or non-HDL-c were observed between the two groups.

Table 4. Growth parameters, organ weights, and serum biochemical parameters

	Groups		
	Starch	Sucrose	p-value
Growth parameters			
Food intake (g/day)	23.5 ± 0.2	24.2 ± 0.2	N.S.
Initial body weight (g)	137.2 ± 2.5	136.5 ± 2.6	N.S.
Final body weight (g)	355.9 ± 8.3	369.0 ± 6.6	N.S.
Food efficiency (mg body weight gain/g total food intake)	332.3 ± 4.3	345.4 ± 4.5	*<0.05*
Organ weights (g/100g body weight)			
Liver	3.96 ± 0.14	4.78 ± 0.20	*<0.05*
White adipose tissue			
Abdominal	3.33 ± 0.36	4.43 ± 0.17	*<0.05*
Perirenal	0.17 ± 0.02	0.23 ± 0.02	*<0.05*
Peritoneal	1.05 ± 0.12	1.36 ± 0.06	*<0.05*
Mesenteric	1.06 ± 0.18	1.52 ± 0.10	*<0.05*
Epididymal	1.05 ± 0.09	1.32 ± 0.09	*<0.05*
Femoral muscle	1.24 ± 0.02	1.13 ± 0.06	N.S.
Serum			
ALT (IU/L)	9.1 ± 0.6	11.2 ± 0.8	*<0.05*
FFA (mEq/L)	0.84 ± 0.05	1.05 ± 0.09	*<0.05*
Triacylglycerol (mg/dL)	132.2 ± 23.4	210.6 ± 28.9	*<0.05*
Phospholipid (mg/dL)	165.5 ± 9.6	190.3 ± 13.1	*<0.01*
Glucose (mg/dL)	135.7 ± 5.1	174.0 ± 13.2	*<0.05*
Insulin (μIU/mL)	2.06 ± 0.64	14.8 ± 3.46	*<0.01*
HOMA-IR	0.72 ± 0.24	5.39 ± 1.22	*<0.01*
Cholesterol (mg/dL)	110.3 ± 6.7	114.1 ± 5.7	N.S.
HDL-c (mg/dL)	54.3 ± 2.9	57.6 ± 3.3	N.S.
non-HDL-c (mg/dL)	56.0 ± 5.1	56.6 ± 5.3	N.S.
Campesterol (mg/dL)	0.32 ± 0.01	0.20 ± 0.02	*<0.01*
β-Sitosterol (mg/dL)	0.46 ± 0.04	0.30 ± 0.02	*<0.01*

Values represent the mean ± standard error of the mean (SEM) (n = 6/each group). Significant differences between mean values were evaluated using the Student's *t*-test. Differences were considered significant if the P-values were <0.05. N.S., not significant; ALT, alanine aminotransferase; FFA, free fatty acid; HDL-c, high-density lipoprotein cholesterol

Liver biochemical parameters are distinctive in starch and sucrose fed rats

Biochemical parameters of the liver are presented in **Table 5**. The liver contents of total, free, and esterified cholesterol were significantly decreased in sucrose diet-fed rats. Rats fed with the sucrose diet showed an increasing trend the levels of liver TAG and glycogen (p = 0.07 and 0.09, respectively). The liver phospholipid content tended to be reduced in sucrose-diet-fed rats (p = 0.09).

Liver FA composition of TAG and PL fractions from starch- and sucrose-fed rats exhibit unique profile

Tables 6 and 7 list the fatty acid composition of the TAG and PL fractions, respectively. In the TAG fraction, sucrose diet-fed rats showed significantly higher levels of monounsaturated fatty acids (MUFAs) and significantly lower levels of polyunsaturated fatty acids (PUFAs) than those in the starch diet-fed rats. Saturated fatty acids (SFAs) levels tended to be rising in the liver of sucrose-fed rats (p = 0.07). Palmitic acid (C16:0), methyl myristoleate (C14:1, n-5), palmitoleic acid (C16:1, n-7), oleic acid (C18:1, n-9), and C16:1(n-7)/C16:0 ratios in the hepatic TAG fraction were significantly increased in the sucrose group (**Table 6**). The sucrose diet led to a significant reduction in the levels of lauric acid (C12:0), behenic acid (C22:0), pentadecylic acid (C15:0), vaccenic acid (C18:1, n-7), gondoic acid (C20:1, n-9), erucic acid (C22:1, n-9), linolelaidic acid (C18:2, n-6), γ-linolenic acid (C18:3, n-6), dihomo-γ-linolenic acid (C20:3, n-6), arachidonic acid (C20:4, n-6), docosatetraenoic acid (C22:4, n-6), docosapentaenoic acid (C22:5, n-6), eicosapentaenoic acid (C22:5, n-3), and docosahexaenoic acid (C22:6, n-3) (**Table 6**). In the PL fraction, behenic

acid (C22:0), C16:1(n-7)/C16:0, and C18:3 (n-6)/C18:2 (n-6) were significantly higher in the sucrose group (**Table 7**). C20:4 (n-6)/C20:3 (n-6) in the PL fraction of sucrose-diet-fed rats also showed an upward tendency (p = 0.08).

Liver mRNA levels, enzyme activity, cholesterol contents, and fecal sterol contents are distinct in starch- and sucrose-fed rats

Compared to the starch group, the mRNA levels of *Scd-1*, *Srebf-1c*, and phosphoenolpyruvate carboxykinase-1 (*Pck-1*) were significantly higher in the livers of the sucrose group than those in the livers of the starch group (**Fig. 3A**). Similarly, an increasing tendency in the *Fasn* mRNA levels (p = 0.06) was observed in the liver of the sucrose group compared to those in the starch group (**Fig. 3A**). The mRNA levels of *Cd36*, diacylglycerol O-acyltransferase 1 (*Dgat1*), *Mttp*, *SERBf-2*, and glucose-6-phosphatase (*G6p*) were not altered by the starch or sucrose diets (**Fig. 3A**). Hepatic FAS activity increased 3.4-fold with the sucrose diet (**Fig. 3B**).

The levels of phytosterols, campesterol, and β-sitostanol were decreased in the livers of sucrose diet-fed rats (**Fig. 3C**). There was no significant difference in liver cholesterol precursors and oxidized cholesterol levels between the starch and sucrose groups (**Fig. 3D and E**).

The fecal sterol results are shown in Fig 2. Fecal total neutral steroids, coprostanol (**Fig. 4A**), total phytosterols, lathosterol, campesterol, and β-sitosterol content (**Fig. 4B**) were significantly higher in the sucrose group than those in the starch group. The conversion rate of cholesterol into coprostanol in feces also tended to be increasing in the sucrose group (p = 0.06) (**Fig. 4C**).

Fecal cholesterol levels, however, did not differ between the starch and sucrose groups (**Fig. 4A**).

Table 5. Liver biochemical parameters

	Groups		
	Starch	Sucrose	p-value
	(mg/g liver)		
Triacylglycerol	67.8 ± 8.49	93.5 ± 13.7	0.07
Phospholipid	34.6 ± 0.74	32.6 ± 1.09	0.09
Cholesterol			
Total	17.8 ± 1.24	13.6 ± 1.20	*<0.05*
Free	2.42 ± 0.05	2.08 ± 0.10	*<0.05*
Esterified	15.4 ± 1.21	11.5 ± 1.16	*<0.05*
Glycogen	11.3 ± 3.63	20.7 ± 5.69	0.09

Values represent the mean ± standard error of the mean (SEM) (n = 6/each group). Significant differences between mean values were evaluated using the Student's *t*-test. Differences were considered significant if the P-values were < 0.05.

Table 6. Fatty acid compositions in liver triacylglycerol fraction

		Groups		
		Starch	Sucrose	p-value
		(mmol/Total mol)		
Saturated fatty acids		31.2 ± 5.55	40.4 ± 1.16	*0.07*
Even numbered fatty acids		30.7 ± 5.51	40.1 ± 1.19	*0.06*
	C12:0	1.93 ± 0.44	0.85 ± 0.24	*p<0.05*
	C14:0	2.27 ± 0.25	1.79 ± 0.40	N.S.
	C16:0	28.8 ± 0.58	35.3 ± 1.04	*p<0.05*
	C18:0	2.36 ± 0.21	2.09 ± 0.47	N.S.
	C20:0	0.06 ± 0.01	0.04 ± 0.02	N.S.
	C22:0	0.06 ± 0.01	0.02 ± 0.00	*p<0.01*
Odd numbered fatty acids		0.52 ± 0.05	0.27 ± 0.04	*p<0.01*
	C15:0	0.35 ± 0.05	0.14 ± 0.04	*p<0.01*
	C17:0	0.17 ± 0.01	0.13 ± 0.02	*0.05*
Mono saturated fatty acids		36.0 ± 4.77	50.9 ± 1.55	*p<0.01*
	C14:1(n-5)	0.06 ± 0.01	0.13 ± 0.02	*p<0.05*
	C16:1(n-9)	0.57 ± 0.04	0.61 ± 0.13	N.S.
	C16:1(n-7)	5.25 ± 0.40	8.82 ± 0.31	*p<0.01*
	C18:1(n-9)t	0.45 ± 0.09	0.52 ± 0.10	N.S.
	C18:1(n-9)	29.0 ± 0.94	38.3 ± 1.67	*p<0.01*
	C18:1(n-7)	5.11 ± 0.63	3.81 ± 0.33	*p<0.05*
	C20:1(n-9)	0.28 ± 0.03	0.09 ± 0.04	*p<0.01*
	C22:1(n-9)	0.09 ± 0.02	0.06 ± 0.02	*p<0.05*
Polyunsaturated fatty acids		21.8 ± 3.43	7.31 ± 1.42	*p<0.01*
n-6 Polyunsaturated fatty acids		18.0 ± 3.19	5.66 ± 1.25	*p<0.01*
	C18:2(n-6)	15.8 ± 3.21	4.77 ± 1.14	*p<0.01*
	C18:3(n-6)	0.28 ± 0.03	0.10 ± 0.03	*p<0.01*
	C20:2(n-6)	0.15 ± 0.04	0.14 ± 0.03	N.S.
	C20:3(n-6)	0.12 ± 0.02	0.04 ± 0.00	*p<0.01*
	C20:4(n-6)	0.76 ± 0.06	0.24 ± 0.04	*p<0.01*
	C22:4(n-6)	0.83 ± 0.20	0.35 ± 0.10	*p<0.01*
	C22:5(n-6)	0.11 ± 0.02	0.02 ± 0.00	*p<0.01*
n-3 Polyunsaturated fatty acids		3.78 ± 0.76	1.65 ± 0.29	*p<0.05*
	C18:3(n-3)	0.25 ± 0.07	0.16 ± 0.05	N.S.
	C20:3(n-3)	0.19 ± 0.02	0.21 ± 0.05	N.S.
	C20:4(n-3)	0.09 ± 0.02	0.12 ± 0.03	N.S.
	C22:5(n-3)	0.15 ± 0.04	0.05 ± 0.02	*p<0.05*
	C22:6(n-3)	3.11 ± 0.73	1.12 ± 0.25	*p<0.05*
Branched chain fatty acids		0.28 ± 0.02	0.28 ± 0.02	N.S.
	i-C17:0	0.05 ± 0.01	0.06 ± 0.00	N.S.
	i-C18:0	0.23 ± 0.02	0.22 ± 0.02	N.S.

Values represent the mean ± standard error of the mean (SEM) (n = 6/each group). Significant differences between mean values were evaluated using the Student's *t*-test. Differences were considered significant if the P-values were < 0.05. N.S., not significant.

Table 7. Fatty acid compositions in liver phospholipid fraction

		Groups		
		Starch	Sucrose	p-value
		(mmol/Total mol)		
Saturated fatty acids		50.5 ± 2.32	51.0 ± 0.72	N.S.
Even numbered fatty acids		49.6 ± 2.21	50.1 ± 0.65	N.S.
	C10:0	0.74 ± 0.19	0.60 ± 0.08	N.S.
	C12:0	1.34 ± 0.37	1.18 ± 0.15	N.S.
	C14:0	0.33 ± 0.13	0.53 ± 0.03	N.S.
	C16:0	27.6 ± 1.84	26.2 ± 1.03	N.S.
	C18:0	18.4 ± 1.16	20.5 ± 0.45	N.S.
	C20:0	0.18 ± 0.03	0.15 ± 0.01	N.S.
	C22:0	0.43 ± 0.03	0.73 ± 0.05	*p<0.05*
	C24:0	0.32 ± 0.02	0.28 ± 0.01	N.S.
Odd numbered fatty acids		0.90 ± 0.15	0.78 ± 0.05	N.S.
	C15:0	0.40 ± 0.13	0.35 ± 0.03	N.S.
	C17:0	0.50 ± 0.06	0.42 ± 0.04	N.S.
Mono unsaturated fatty acids		18.2 ± 1.90	17.5 ± 1.03	N.S.
	C16:1(n-9)	0.27 ± 0.07	0.29 ± 0.05	N.S.
	C16:1(n-7)	1.34 ± 0.16	1.61 ± 0.08	N.S.
	C18:1(n-9)t	0.88 ± 0.14	0.89 ± 0.13	N.S.
	C18:1(n-9)	12.4 ± 1.89	11.6 ± 1.15	N.S.
	C18:1(n-7)	3.05 ± 0.30	2.89 ± 0.21	N.S.
	C20:1(n-9)	0.29 ± 0.02	0.23 ± 0.02	N.S.
Polyunsaturated fatty acids		32.5 ± 3.47	32.8 ± 2.00	N.S.
n-6 Polyunsaturated fatty acids		29.1 ± 3.18	28.8 ± 1.72	N.S.
	C18:2(n-6)	9.92 ± 1.65	6.91 ± 0.26	*0.06*
	C18:3(n-6)	0.27 ± 0.02	0.51 ± 0.07	N.S.
	C20:2(n-6)	0.11 ± 0.05	0.07 ± 0.00	N.S.
	C20:3(n-6)	0.75 ± 0.11	0.67 ± 0.07	N.S.
	C20:4(n-6)	17.0 ± 1.93	19.4 ± 1.36	N.S.
	C22:4(n-6)	0.33 ± 0.03	0.34 ± 0.02	N.S.
	C22:5(n-6)	0.64 ± 0.14	0.91 ± 0.08	N.S.
n-3 Polyunsaturated fatty acids		3.46 ± 0.36	3.96 ± 0.30	N.S.
	C18:3(n-3)	0.11 ± 0.03	0.14 ± 0.01	N.S.
	C18:4(n-3)	0.42 ± 0.04	0.49 ± 0.06	N.S.
	C20:4(n-3)	0.25 ± 0.08	0.33 ± 0.04	N.S.
	C20:5(n-3)	0.15 ± 0.01	0.15 ± 0.01	N.S.
	C22:5(n-3)	0.27 ± 0.02	0.23 ± 0.01	N.S.
	C22:6(n-3)	2.26 ± 0.30	2.83 ± 0.20	N.S.
Branched chain fatty acids		0.60 ± 0.08	0.79 ± 0.07	N.S.
	a-C17:0	0.23 ± 0.03	0.23 ± 0.03	N.S.
	i-C18:0	0.37 ± 0.06	0.56 ± 0.06	N.S.
Plasmalogen		0.46 ± 0.17	0.46 ± 0.04	N.S.
	Dma-C16:0	0.28 ± 0.17	0.30 ± 0.03	N.S.
	Dma-C18:0	0.07 ± 0.02	0.06 ± 0.00	N.S.
	Dma-C20:0	0.11 ± 0.03	0.12 ± 0.01	N.S.
	C16:1 (n-7)/C16:0	0.05± 0.00	0.06 ± 0.00	*p<0.01*
	C18:1 (n-9)/C18:0	0.72 ± 0.06	0.61 ± 0.08	N.S.
	C20:4 (n-6)/C20:3 (n-6)	24.6 ± 1.32	35.7 ± 2.64	*0.08*
	C18:3 (n-6)/C18:2 (n-6)	0.03 ± 0.00	0.07 ± 0.01	*p<0.05*

Values represent the mean ± standard error of the mean (SEM). n = 6/each group. Significant differences between mean values were evaluated using the Student's *t*-test. Differences were considered significant if the P-values were < 0.05. N.S., not significant.

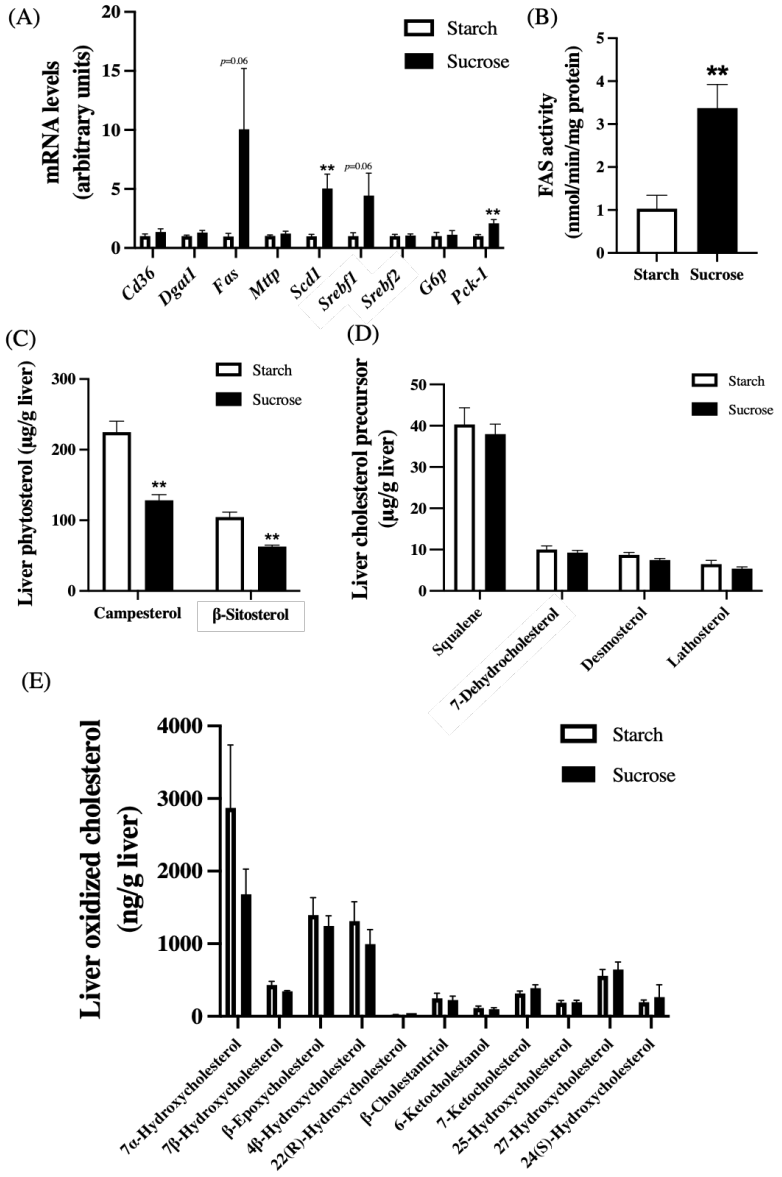

Figure 3. Liver biochemical parameters in sucrose or starch diet-fed rats

Hepatic levels of (A) mRNA expression, (B) FAS activity, (C) cholesterol precursor, (D) phytosterol, and (E) oxidized cholesterol. Values represent the mean ± standard error of the mean (SEM)(n = 6/each group). Significant differences between mean values were evaluated using Student's *t*-test (**; $p < 0.01$). Abbreviations: *Cd36*, cluster of differentiation 36; *Dgat1*, diacylglycerol O-acyltransferase 1; FAS, fatty acid synthase; *Mttp*, microsomal triglyceride transfer protein; *Scd-1*, stearoyl-CoA desaturase 1; *Srebf-1c*, sterol regulatory element-binding transcription factor 1; *Srebf-2*, sterol regulatory element-binding transcription factor 2; *G6p*, Glucose-6-phosphatase; *Pck-1*, phosphoenolpyruvate carboxykinase-1.

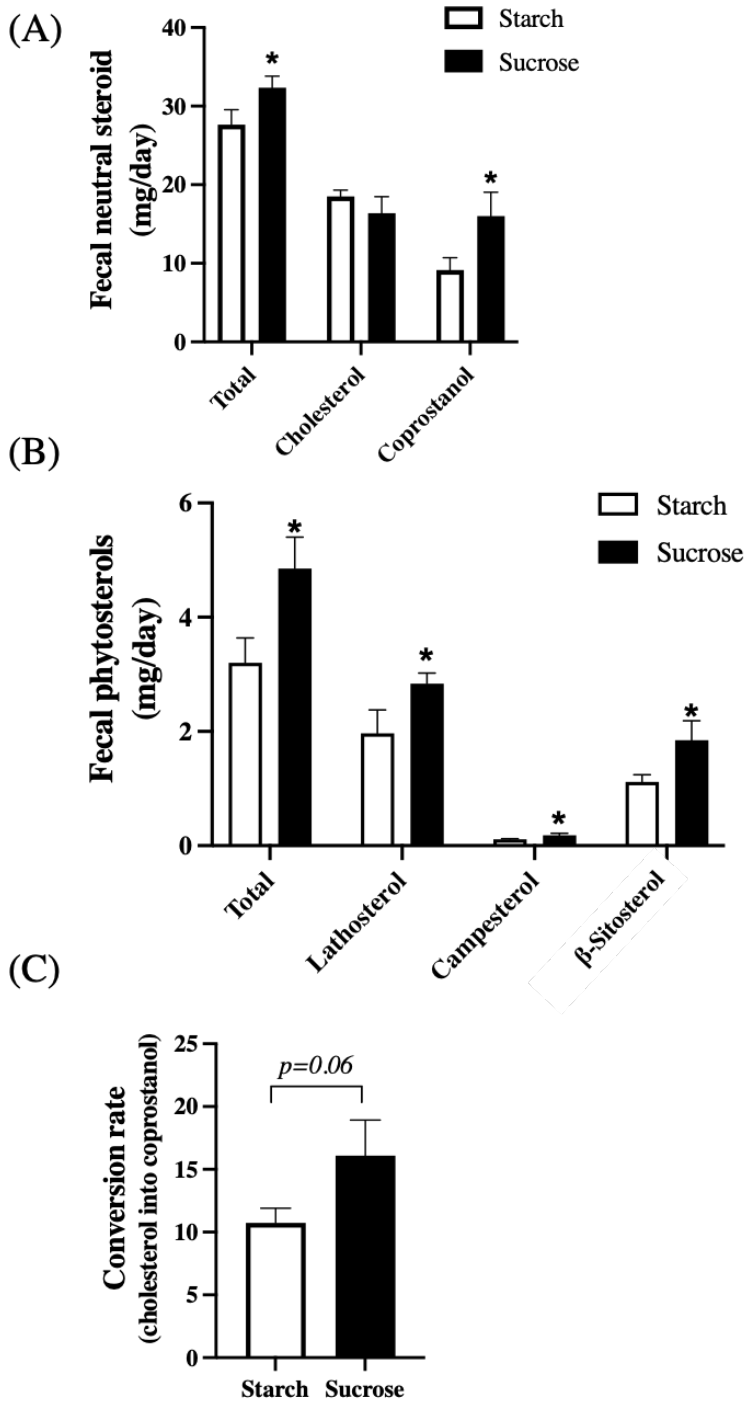

Figure 4. Fecal biochemical parameters in sucrose or starch diet-fed rats

Changes in the levels of fecal (A) neutral steroids, (B) phytosterols in starch and sucrose fed rats, (C) Cholesterol to coprostanol conversion rate in starch and sucrose fed rats. Values are means ± standard error of the mean (SEM) (n = 6/each group). Significant differences between mean values were evaluated by Student's *t*-test (*; $p < 0.05$).

Water-soluble metabolites from the livers of starch and sucrose fed rats show distinctive metabolite signatures

Seventy-four water-soluble metabolites in the rat liver were detected using GC-MS. Of these, 29 compounds, carbohydrate metabolites, and amino acids are listed in **Table 8**. In the TCA cycle, the levels of malate, fumarate, and succinate significantly decreased in the liver after the sucrose diet. Compared with the starch diet, the sucrose diet significantly increased the levels of alanine and glycine in the rat liver. Levels of phenylalanine ($p = 0.09$), serine ($p = 0.06$), and valine ($p = 0.08$) also showed an increasing tendency in the sucrose group. In the sucrose group, glucuronic acid and glycerol levels were significantly decreased. The metabolites in the glucuronic acid pathway (xylitol), urea cycle (urea and ornithine), glycolysis (glucose and lactate), pentose phosphate pathway (PPP) (ribose, ribulose 5-phosphate, xylulose 5-phosphate, and ribulose 5-phosphate), and amino acids (aspartic acid, cysteine, glutamic acid, isoleucine, leucine, methionine, proline, threonine, tryptophan, and tyrosine) were similar in the livers of starch- and sucrose-fed rats. These results suggest that water-soluble metabolites from the livers of starch- and sucrose-fed rats show a distinct abundance profile.

Table 8. Water-soluble metabolite analysis in rat liver

	Groups		
	Starch	Sucrose	p-value
	(arbitrary unit)		
Glycolysis			
Glucose	5429 ± 830	4918± 735	N.S.
Lactate	2659 ± 612	3362 ± 298	N.S.
TCA cycle			
Oxaloacetic acid & Pyruvic acid	23 ± 4	27 ± 2	N.S.
Isocitric acid & Citric acid	14 ± 2	11 ± 2	N.S.
Succinic acid	767 ± 98	556 ± 64	*<0.05*
Fumaric acid	40 ± 5	16 ± 3	*<0.01*
Malic acid	219 ± 25	83 ±16	*<0.01*
Amino acids			
Glucogenic			
Aspartic acid	149 ± 43	165 ± 41	N.S.
Alanine	1096 ± 283	1811 ± 145	*<0.05*
Cysteine	13 ± 5	21 ± 4	N.S.
Glutamic acid	543 ± 78	452 ± 45	N.S.
Glycine	1003 ± 85	1213 ± 79	*<0.05*
Proline	55 ± 17	78 ± 18	N.S.
Serine	172 ± 17	226 ± 27	*0.06*
Methionine	29 ± 5	35 ± 7	N.S.
Valine	190 ± 31	257 ± 31	*0.08*
Glucogenic & Ketogenic			
Tyrosine	110 ± 25	67 ± 22	N.S.
Isoleucine	202 ± 20	228 ± 18	N.S.
Phenylalanine	44 ± 7	57 ± 6	*0.09*
Tryptophan	33 ± 3	34 ± 3	N.S.
Threonine	110 ± 10	115 ± 13	N.S.
Ketogenic			
Leucine	211 ± 38	203 ± 37	N.S.
Pentose phosphate pathway			
Ribulose 5-phosphate	6 ± 1	5 ± 2	N.S.
Ribulose 5-phosphate & Xylulose 5-phosphate	25 ± 6	26 ± 8	N.S.
Ribose	119 ± 25	154 ± 19	N.S.
Urea cycle			
Urea	26 ± 3	19 ± 2	N.S.
Ornithine	81 ± 9	75 ± 12	N.S.
Glucuronic acid pathway			
Glucuronic acid	18 ± 2	12 ± 1	*<0.05*
Xylitol	26 ± 5	30 ± 4	N.S.
Other			
Glycerol	2989± 123	2350 ± 187	*<0.01*

Values represent the mean ± standard error of the mean (SEM) (n = 6/each group). Significant differences between mean values were evaluated using the Student's *t*-test. Differences were considered significant if the P-values were < 0.05. N.S., not significant.

Discussion

An earlier study showed that rat liver cholesterol levels did not differ between the consumption of a chow diet with or without 20% sucrose drinks [91]. The 1% cholesterol diet promoted the deposition of cholesterol compared to the no cholesterol-containing diet in rat liver [89]. Based on these previous results [91-92], we hypothesized that a cholesterol-containing sucrose diet would have an effect on the liver cholesterol levels. We observed that in the presence of 0.2% dietary cholesterol, sucrose intake decreased liver cholesterol content in rats compared with that observed upon iso-caloric starch intake (**Table 5**). The liver cholesterol pool is affected by the balance between cholesterol absorption, *de novo* cholesterol synthesis, secretion into very-low-density lipoprotein (VLDL), and conversion into bile acids. A decrease in cholesterol synthesis lowers liver cholesterol content. In addition, an increase in cholesterol conversion to oxysterols by cytochrome P450 enzymes and subsequent degradation of bile acids decreases liver cholesterol content. In this study, the reduction in liver cholesterol content by sucrose was not caused by decreasing cholesterol synthesis or increasing cholesterol excretion (**Fig 3**). Serum cholesterol concentrations did not differ between sucrose and starch diets (**Table 4**), suggesting that liver cholesterol secretion did not increase. Therefore, lowering intestinal cholesterol absorption or promoting the conversion of cholesterol to coprostanol in the intestine are possible reasons for reduced liver cholesterol levels. Ravid et al. reported that a high-glucose environment increases cholesterol uptake in Caco-2 cells [93]. In our experiments on rats, it seems that the effects of the two sugars on small intestinal epithelial cells were not different. However, based on our data, such

as the decreased cholesterol content in the livers of rats fed with the sucrose diet, dietary cholesterol was less absorbed. According to several reports, the gut microbiota converts cholesterol into non-absorbable coprostanol to remove cholesterol [94-95]. Diet composition has been shown to alter the composition and abundance of intestinal bacterial species [96]. For example, the abundance of intestinal *Lactobacillus* was higher in mice fed with a fructose diet than that in those fed with a glucose diet [97]. Lye et al. reported that lactobacilli promote the conversion of cholesterol into coprostanol [98]. In this study, dietary sucrose increased fecal neutral steroid levels by 1.2-fold and coprostanol levels by 1.8-fold (**Fig. 4A**). In addition, phytosterol content, an indicator of intestinal cholesterol absorption, was increased by 53% in the feces by the sucrose diet and decreased by 43% in the liver (**Fig. 3D**) and by 38% in the serum (**Table 4**). Taken together, our results indicate that due to the difference in dietary carbohydrates, the cholesterol-containing sucrose diet increases the bioformation of coprostanol by increasing the amount of gut microbiota, resulting in a decrease in the intestinal absorption of dietary cholesterol compared to that by the cholesterol-containing starch diet.

Liver TAG levels are affected by dietary components. In our previous studies, we reported that a high-cholesterol high-sucrose diet (1% cholesterol and 44% sucrose) promoted liver TAG deposition (2-fold) in rats [86]. In rats, liver TAG content increased 2-fold after feeding a high-sucrose diet (42% in the diet) [99]. Dietary cholesterol less than 0.5% did not change TAG content in the rat liver [100]. Therefore, dietary sucrose (65% in the diet) was regarded as the major reason for elevated liver TAG content. It is already known that the consumption of sucrose results in fatty liver via the activation of *de novo* lipogenesis in the

liver. FAS is a key enzyme in the synthesis of palmitic acid (C16:0) and stearic acid (C18:0) in *de novo* lipogenesis. When liver FAS activity is inhibited, a high-sucrose diet fails to induce liver TAG accumulation [86]. In addition, excessive C16:0 is present in the liver, leading to liver inflammation and increased serum ALT levels [101]. However, the liver FAS activity in rats did not differ between the 1% cholesterol-44% sucrose and -44% starch diets for 2 weeks in our previous study, although a 1% cholesterol-44% sucrose diet induced liver TAG deposition [86]. A high-cholesterol diet may eclipse the promotive effect of FAS activity in high-sucrose diets. A high-cholesterol diet has been reported to lead to cholesterol accumulation in rat liver [100]. When cholesterol accumulates in the rat liver, cholesterol downregulates SREBP-1 protein levels in the nucleus and decreases the transcription of target genes, especially *Fasn* [102]. Therefore, an increase in liver FAS activity (**Fig. 3B**) was caused by higher dietary sucrose (65% in diet) under conditions of low cholesterol accumulation. In addition to FAS, SCD-1 also plays a vital role in *de novo* lipogenesis in the liver. SCD-1 desaturates palmitic acid and stearic acid to palmitoleic acid (C16:1 n-7) and oleic acid (C18:1 n-9), respectively, for the biosynthesis of TAG and PL. A disruption in the *Scd-1* gene in mice decreased the liver contents of oleic acid and TAG and mRNA levels of *Fasn* and acetyl-CoA carboxylase [103]. The sucrose diet increased the contents of palmitic acid, palmitoleic acid, and oleic acid (by 1.2-, 1.9-, 1.3-folds, respectively) in FA compositions in TAG fraction (**Table 6**) and mRNA levels of *Scd-1* (**Fig. 3A**). These data suggest that dietary 0.2% cholesterol is more effective than dietary 1% cholesterol in liver *de novo* lipogenesis. Therefore, 0.2% cholesterol exacerbated the increasing

effect of dietary sucrose on *de novo* lipogenesis, causing TAG accumulation in the liver.

Increasing the enzyme activity of FAS and mRNA level of *Scd-1* means that the requirements of nicotinamide adenine dinucleotide phosphate (NADPH) and acetyl-CoA are increased in sucrose-fed rats. To provide acetyl-CoA for *de novo* lipogenesis, citrate is exported from the mitochondria to the cytosol and is converted to acetyl-CoA and oxaloacetate. Malate, which is provided by oxaloacetate, is converted to pyruvate by the cytosolic malic enzyme (ME1) and produces NADPH in the cytosol. *Fasn* mRNA expression and lipid droplet content are decreased in mice with ME1 deficiency [104]. In HCT116 human colon cancer cells, ME1 knockdown increased the accumulation of malate and fumarate and suppressed the flux of malate-pyruvate-acetyl-CoA [105]. In addition to ME1, NADPH is also produced by two enzymes in the PPP, glucose-6-phosphate dehydrogenase (G6PD), and 6-phosphogluconate dehydrogenase. The enzyme activity of G6PD was higher in the livers of rats that were fed a fructose diet than that in rats fed a glucose diet [106]. Although the gene expression of *Me1*, *G6pd*, and 6-phosphogluconate dehydrogenase was upregulated by SREBP-1 [107], in our study, the contents of PPP products in rat liver, ribulose 5-phosphate, and xylulose 5-phosphate did not change between the two diets. Dietary sucrose increased the gene expression of *Srebf-1c*, *Fasn*, and *Scd-1* and decreased the content of malate (the substrate of ME1), suggesting that a cholesterol-containing sucrose diet increases the production of liver NADPH, a substrate required for *de novo* lipogenesis in the liver.

The cholesterol-containing sucrose diet increased the liver glycogen content by approximately 80% (p = 0.09) (**Table 7**). The reason for liver glycogen accumulation may be the higher phosphorylation rate of fructose compared to that of glucose. Glucose phosphorylation is a rate-limiting step in glycolysis. In contrast, fructose can directly enter glycolysis because its phosphorylation by fructokinase bypasses the rate-limiting step [108]. The increase in liver glycogen can be interpreted as the increased conversion of glucose to glycogen storage due to the active participation of fructose in glycolysis.

In the fasting state, an increase in serum TAG levels is due to an increase in VLDL secretion from the liver. In this study, a cholesterol-containing sucrose diet significantly increased the serum levels of TAG by 1.6-fold and those of PL by 1.2-fold. The majority of serum PL is as a component of HDL and VLDL [109]. Serum HDL-c and non-HDL-c levels did not differ between the two diets. These results suggest that the increase in serum PL levels is due to increased VLDL secretion from the liver. The amount of PUFAs in liver PL increases VLDL secretion [110]. Hashidate-Yoshida et al. reported that lysophosphatidylcholine acyltransferase 3 promotes the enrichment of arachidonate-containing phospholipids in the membrane, generating an ER membrane area rich in PUFAs [111]. PUFA-rich ER membranes are more easily deformed than are MUFA-rich membranes. The more flexible PUFA-rich membrane clusters more TAG for efficient transport by *Mttp*. Δ5-desaturase (FADS1) and Δ6-desaturase (FADS2) are rate-limiting enzymes in PUFA synthesis that catalyze the formation of γ-linolenic acid, stearidonic acid, arachidonic acid (AA), and eicosapentaenoic acid. In FADS2-deficient mice, the liver was filled with tiny lipid droplets, and lipid deposition was eliminated by AA diets [111]. Intake of

sucrose diet increased the ratio of C18:3 (n-6) to C18:2 (n-6), and C20:4 (n-6) to C20:3 (n-6) in the PL fraction, which are indices of Δ5- and Δ6-desaturase activities, respectively. Moreover, hepatic Δ5- and Δ6-desaturase activities increased along with a reduction in liver microsomes cholesterol content [113], which was consistent with our observation in the sucrose group. Based on the above evidence, a cholesterol-containing sucrose diet may increase serum TAG levels due to increased PUFA content in the hepatic PL fraction.

Consistent with our results, previous studies in rats that were fed a high-sucrose diet have indicated that sucrose diets induce hyperinsulinemia [114-115]. Rats fed a high-sucrose diet (40% or 65%) for 4–5 weeks had serum insulin levels increased by 1.5-folds [114-115]. Interestingly, sucrose diets did not change serum glucose levels in previous animal studies [114-115]. In our study, cholesterol-containing sucrose diets elevated serum glucose, FFA, and hepatic glycogen levels by 1.3-, 1.25-, and 1.8-folds, respectively. Muscle glucose uptake and liver glucose production mainly regulate the serum glucose levels. In the fasting state, hepatic glycogenolysis is the main source of blood glucose. As described above, the cholesterol-containing high-sucrose diet simultaneously increased serum glucose levels and hepatic glycogen content, and hepatic glucose metabolism was considered similar between diets. A rat study indicated that dietary sucrose induces muscle insulin resistance to decrease muscle glycogen synthesis and increase blood glucose levels (45%) [114]. Additionally, high levels of circulating FFAs in rats inhibit muscle glycolysis, leading to decreased insulin-stimulated glucose uptake (37%) [116]. Taken together, the impaired glucose uptake in the muscle was a possible

cause of the increase in blood glucose after the cholesterol-containing sucrose diet.

Summary

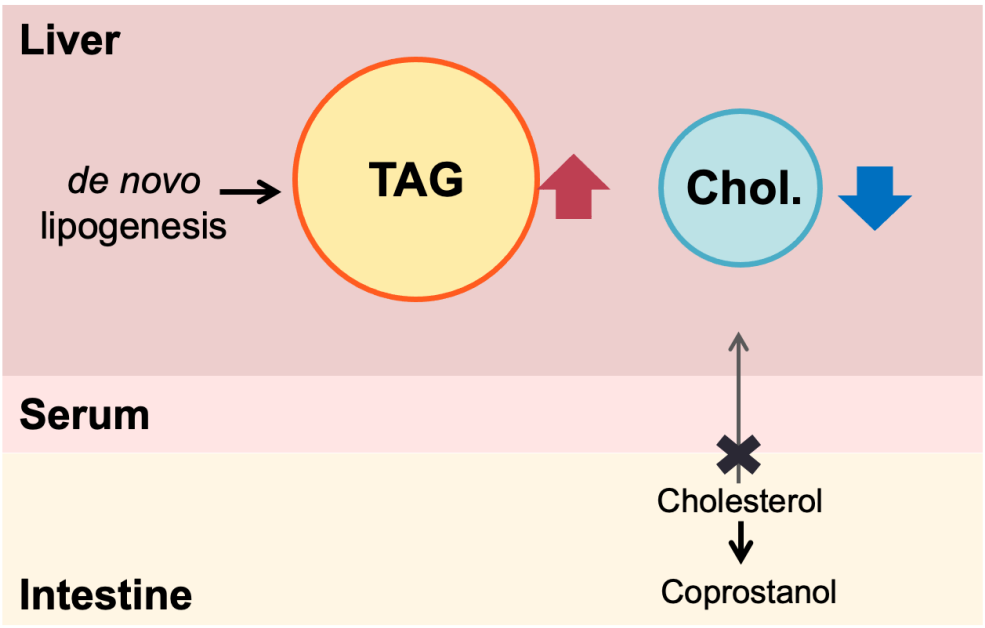

Figure 5. The effect of sucrose on lipid metabolism in animal models of NAFLD.

Although high sucrose or fructose diets are proved to promote NAFLD and liver cholesterol accumulation, limited evidence of molecular working cholesterol mechanisms of those diets is available. In most of these diets of previous studies, dietary cholesterol, which is one of the nutrients, is not to be added. Herein, we used cholesterol-containing high carbohydrate diets to clarify their effect on cholesterol metabolism in rats.

Under sucrose diet feeding, hepatic contents of cholesterol, and serum and hepatic levels of phytosterols, which is the cholesterol-absorbed marker, were decreased. The fecal contents of total neutral steroids, coprostanol, and phytosterols by sucrose diet feeding. Also, the fecal conversion rate of cholesterol into coprostanol showed an increasing trend in the sucrose group. According to these results, high sucrose consumption reduced intestinal cholesterol absorption in rats compared to high starch consumption, probably

because fructose in sucrose promotes the growth of coprostanol-forming-related bacteria, but dietary glucose does not or does so weakly.

Additionally, in TAG metabolism, hepatic TAG levels had an increasing tendency by dietary sucrose, due to fructose catabolism being faster than that of glucose to upregulate de novo lipogenesis. Intake of sucrose diet increased the activity of enzymes in PUFA synthesis in hepatic PL fraction to promote VLDL assembly and excretion, resulting in higher levels of serum PL and lower levels of hepatic PL.

Therefore, high sucrose diet prevents abnormal hepatic cholesterol metabolism in the course of NAFLD (**Fig. 5**).

CHAPTER II Effect of diet induced NAFLD in animal models

PART2

Soyasaponin ameliorates fatty liver and increases hepatic cholesterol accumulation in high-fat diet-fed male C57BL/6J mice

Introduction

Soybean is a raw material for soy foods such as tofu, natto, and soy sauce that are consumed in Asia, especially Japan. In recent years, soyasaponins in soy foods have received increasing attention from researchers [117]. Soyasaponins are oleanane triterpenoid glycosides with polar sugar chains conjugated to a nonpolar pentacyclic ring, found in soybean. Soyasaponins are classified into four groups, A, B, E, and DDMP (2,3-dihydro-2,5-dihydroxy-6-methyl-4H-pyran-4-one) based on the type of aglycones (i. e., soyasapogenol) and binding position of sugar chains. In the soyasaponin aglycone, there are two major types of soyasapogenols, soyasapogenol A and B **(Fig. 6)**. Soyasapogenols as aglycones do not exist in natural raw soybeans. After undergoing acid or alkaline hydrolysis, the saponins are deglycosylated, leaving the intact aglycone. Thus, soyasapogenols are found only in processed soy foods [118]. It has been reported that Japanese people consume 50.3 μmol of soyasaponins and 0.59 μmol of soyasapogenols daily, and that group B soyasaponin is the major source of soyasaponins in Japanese soy food products [119]. Moreover, the absorption rate of soyasapogenols is better than that of soyasaponins, and the bioavailability of group B soyasaponins is better than that of group A soyasaponins [120].

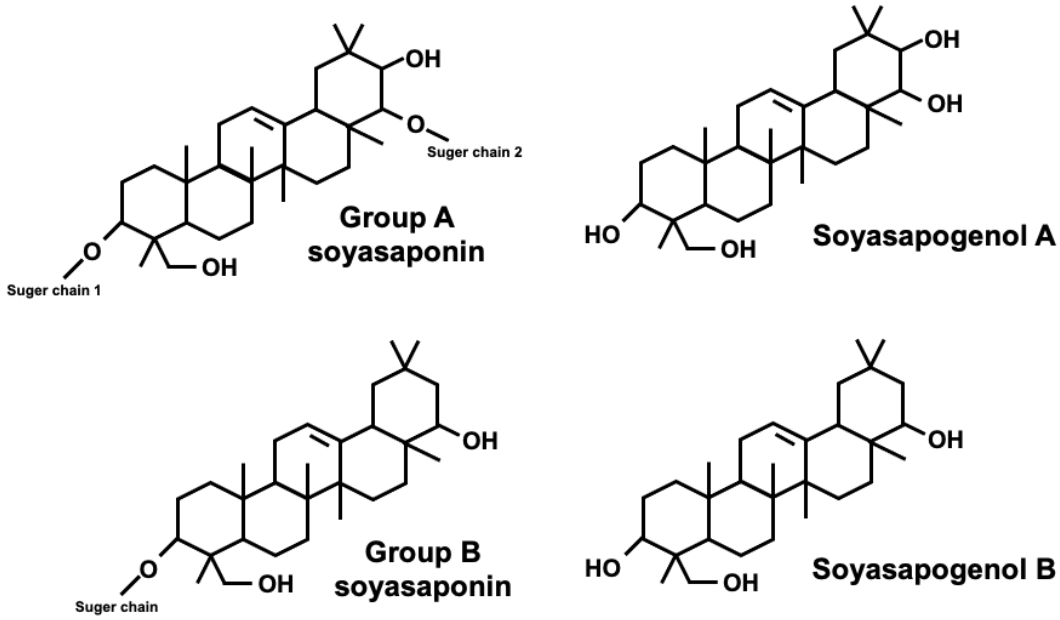

Figure 6. Structures of group A and B soyasaponin and its soyasapogenols

Several reports have shown the beneficial effects of soyasaponins on lipid metabolism in animals and cell models **(Table 9)** [121-123]. Dietary intakes of group B soyasaponins aglycone, soyasapogenol B, reportedly suppress the increasing body and white adipose tissues (WATs) weights, serum and liver TAG levels in HFD-fed C57BL6 mice [121]. Soyasaponin A_2 reduces the serum triacylglycerol level and adipocyte size, and increases fecal triacylglycerol excretion, but does not decrease the body weight in HFD-fed C57BL6/J mice [123]. Group A soyasaponins (soyasaponin Aa and Ab) inhibit lipid accumulation in 3T3-L1 adipocytes by suppressing adipocyte differentiation [124]. Soyasaponins (soyasaponin A_1, A_2, and Bb) ameliorate liver steatosis in obese mice [123]. Additionally, soyasaponins are also known to improve the cholesterol status [121-123]. In HFD-fed hamsters, group B soyasaponins

(soyasaponin I and II mixture) increase the excretion of fecal bile acids (BAs) and fecal neutral sterols, lowering the plasma cholesterol and non-high-density lipoprotein cholesterol (non-HDL-C) levels [121].

These prior studies show that soyasaponins have an effect on reducing body weight or preventing TAG accumulation in the liver [121 &123]. However, the mechanism of soyasaponins on anti-obesity and anti-fatty liver has not yet been fully understood. In order to investigate the mechanism that the soyasaponin sample (SAP) improves TAG accumulation, we administrated the SAP orally to HFD-fed mice. We used X-ray CT scanning to observe the change of adipose tissue weights in mice at the early feeding stage. Several saponins reportedly inhibit pancreatic lipase (PL) activity to prevent obesity [125-126]. For the inhibition of lipid intestinal absorption, we assayed the activity of SAP on PL *in vitro*. For assessment of the effect on adipocyte differentiation, 3T3-L1 adipocytes were treated with soyasapogenols.

Table 9. Characteristics of the previous reports on soyasaponins and soyasapogenol in HFD-fed animals

Cites	Animal	Diets	Soyasaponin		Compare to HFD group											
					Body weight	Feces				Liver		Serum				
			Types	Dose		TAG	TC	BA	Neutral sterols	TAG	TC	TAG	FFA	TC	HDL-C	Glucose
121	C57BL6 mice	High fat diet for 5 weeks (39% kcal from fat)	Group B soyasaponin aglycone (soyasapogenol A and B mixture)	0.26% in diet	↓ *	n.d.	n.d.	n.d.	n.d.	↓ *	n.r.	↓ *	n.d.	n.r.	n.r.	n.r.
122	Syrian hamster	High fat diet for 4 weeks (37% kcal from fat, 0.1% cholesterol)	Group B soyasaponin (soyasaponin I and II mixture)	128 mg/kg body weight/ daily in diet	n.d.	n.d.	n.d.	↑ *	↑ *	n.d.	n.d.	↓ *	n.d.	↓ *	n.r.	n.d.
123	C57BL/6J mice	High fat diet for 8 weeks (45% kcal from fat)	Soyasaponin A_1	20 mg/kg body weight in diet	n.r.	↑ *	↑ *	↑ *	n.d.	↓ *	↓ *	↓ *	n.r.	↓ *	↑ *	n.r.
			Soyasaponin A_2		n.r.	↑ *	↑ *	↑ *	n.d.	↓ *	↓ *	↓ *	↓ *	↓ *	↑ *	↓ *
			Soyasaponin I		n.r.	↑ *	↑ *	↑ *	n.d.	↓ *	↓ *	↓ *	n.r.	n.r.	↑ *	n.r.

*= $p<0.05$; n.d.= not determined; n.r.= not represented

Materials and methods

Reagents

1,4-Dioxane for high-performance liquid chromatography (HPLC), sodium hydrogen carbonate, sucrose, Tris (hydroxymethyl) aminomethane, hydrochloric acid, sodium chloride, proteinase K, hydroquinone, phenol, n-butanol, ammonium acetate, ascorbic acid, dexamethasone, and 3-isobutyl-1-methylxanthine were purchased from Nacalai Tesque (Kyoto, Japan). SAP (product code; 191-18652), ethylenediaminetetraacetic acid (EDTA) disodium dihydrate, insulin, α-tocopherol, 2,2,5,7,8-penta-methyl 6-hydroxycromane (PMC), and acetonitrile for HPLC were purchased from Wako Pure Chemical Industries (Osaka, Japan). Hexane and 2-propanol, both for HPLC, were purchased from Kanto Chemical Co. (Tokyo, Japan). Crystalline penicillin G potassium and streptomycin sulfate were obtained from Meiji Seika Kaisha (Tokyo, Japan). Phosphate buffer saline (-) was purchased from Nissui Pharmaceutical Co. (Tokyo, Japan). Soyasapogenol A and soyasapogenol B were purchased from Tokiwa Phytochemical Co. (Chiba, Japan). Dulbecco's modified Eagle medium (DMEM) was purchased from Gibco BRL (NY, USA). Fetal bovine serum (FBS) was obtained from Thermo Fisher Scientific (MA, USA).

Determination of ingredients in the soyasaponin (SAP) sample

The soyasapogenol A and B contents in the SAP were determined by HPLC [127]. Briefly, 10 mg of the SAP was dissolved in 1 mL of ethanol: deionized water:acetic acid (70:29.9:0.1, v/v/v), and then 100 μL of the dissolved solution was added to 1.9 mL of ethanol: deionized water:acetic acid (70:29.9:0.1, v/v/v)

and 200 μL of HCl. The solution was heated for 6 h at 80°C. After cooling, the solution was filtered through a 0.2 μm filter. In the filtered sample, soyasapogenol A and B contents were determined by HPLC (Waters 600 Controller, Nihon Waters K.K.), using an ultraviolet/visible detector (Waters 486 Tunable Absorbance Detector) at a wavelength of 210 nm. Chromatographic separation was performed using a column (Waters Puresil C18, μm, 4.6 × 150 mm). The mobile phase was 60% acetonitrile and 40% water, at a flow rate of 1.0 mL/min. The column temperature was set to 40°C. Soyasapogenols contents of the SAP was quantified using the calibration curves of external standards, soyasapogenol A and B.

The total sugar content in the SAP was determined by the phenol-sulfuric acid method [128], with glucose as the standard. The reducing sugar content in the SAP was determined by the 3,5-dinitrosalicylic acid method [129] using glucose as the standard. To determine the lipid concentration, the SAP was extracted with a solution of chloroform/methanol and the TAG concentration was determined using the Triglyceride E-Test Wako kit (Wako Pure Chemicals), with absorbance measured at 600 nm.

Measurement of PL activity *in vitro*

The PL activity was measured as described previously [130].

Animal study

Four-week-old male C57BL/6J mice were obtained from Charles River Laboratories Japan (Kanagawa, Japan). The mice were individually housed in plastic cages containing paper chips (ALPHA-dri from Shepherd Specialty

Papers, Inc., Kalamazoo, MI, USA), and were maintained in a temperature-controlled room (21–24°C) with a 12-h light-dark cycle (0800-2000), and free access to commercial chow and deionized water. After a 1-week adaptation period, mice were randomly divided into the control and SAP groups (n = 10/group). All mice were fed the HFD **(Table 10)** for 9 weeks. The SAP group food intake was pair-feeding to match the food intake of the control group. In the control group, mice were orally administered 1 % carboxymethylcellulose (CMC). In the SAP group, mice were orally administered 2 g/kg body weight of the SAP suspended in 1 % CMC, daily for 9 weeks. Body weight and food intake were recorded weekly. After a 9-week treatment, the mice were fasted for 4 h and then sacrificed, with blood collected from the heart under pentobarbital anesthesia (0.08 mg/100 g body weight). The liver, epididymal adipose tissue, femoral muscle, and small intestine mucosa from each mouse were excised, weighed, and stored at −80°C.

For all experimental animals, the handling and euthanasia were performed in accordance with nationally prescribed guidelines, and ethical approval for the experiments was granted by the Animal Care and Use Committee of Kyushu University. The authorization number was A22-159-0.

Table 10. Compositions of the experimental diets

Ingredients (g/kg diet)	Diet
Cornstarch [1]	125
Sucrose [2]	375
Casein[3]	200
Lard[4]	200
Cellulose[5]	50
Vitamin mix (AIN-76)[6]	10
Mineral mix (AIN-76)[6]	35
DL-Methionine[7]	3
Choline bitartrate[7]	2

[1] NZMP Acid Casein (Fonterra Co-operative Group Limited, Auckland, New Zealand)

[2] TK-16 (Matsutani Chemical Industry Co., Ltd., Hyogo, Japan)

[3] Nippon Beet Sugar Manufacturing Co., Ltd., Tokyo, Japan

[4] Oil Mills, Inc., Tokyo, Japan

[5] Crystalline cellulose (Ceolus PH-102, Asahi Kasei Corporation, Tokyo, Japan)

[6] Mineral mix and vitamin mix for AIN-76 (Oriental Yeast Co., Ltd., Tokyo, Japan)

[7] CLEA Japan, Inc., Tokyo, Japan

Measurement of adipose tissue weight using an X-ray CT system

At weeks 3, 5, 7, and 9 of treatment, mice were anesthetized using intraperitoneal pentobarbital, and the amount of WAT in visceral and subcutaneous fat was measured by X-ray CT (Latheta LCT-100, Hitachi Aloka Medical, Ltd., Tokyo, Japan) at a scan pitch of 2 mm (18 s/1 per slice) for mouse body parts between the diaphragm and the base of the tail.

Analysis of mRNA levels in adipose tissue and liver

Total RNA was isolated from the adipose tissue and liver using the phenol/chloroform method as described previously [91]. Complementary DNA (cDNA) was synthesized from 1 μg total RNA using the Transcriptor First Strand cDNA Synthesis Kit (Roche, Switzerland). Expression levels of genes were analyzed using quantitative real-time reverse transcription-polymerase chain reaction (qRT-PCR) with an Mx3000P Real-Time PCR System (Stratagene, CA) and SYBR Premix Ex Taq:Perfect Real-time kit (Takara Bio., Shiga, Japan). The mRNA levels were normalized using glyceraldehyde-3-phosphate-dehydrogenase (*Gapdh*) for adipose tissue and beta-actin (*Actb*) for the liver. Primer sequences used for the analysis are shown in **Table 11.**

Table 11. Mouse primers designs for qRT-PCR.

Gene	Forward primer	Reverse primer
Pparg	GCCCTTTGGTGACTTTATGG	CAGCAGGTTGTCTTGGATGT
Cebpa	CAAGAACAGCAACGAGTACCG	GTCACTGGTCAACTCCAGCAC
Fabp4	AAGACAGCTCCTCCTCGAAGGTT	TGACCAAATCCCCATTTACGC
Srebf-1	GGAGCCATGGATTGCACATT	GCTTCCAGAGAGGAGGCCAG
Fasn	TTGCTGGCACTACAGAATGC	AACAGCCTCAGAGCGACAAT
Abca1	GGTTTGGAGATGGTTATACAATAGTTGT	TTCCCGGAAACGCAAGTC
Cyp7a1	AACGGGTTGATTCCATACCTGG	GTGGACATATTTCCCCATCAGTT
Ppara	GGGCAAGAGAATCCACGAAG	GTTGTTGCTGGTCTTTCCCG
Gapdh	GAAGGTCGGTGTGAACGGATT	GAAGACACCAGTAGACTCCACGACATA
Actb	AGCCATGTACGTAGCCATCC	TCCCTCTCAGCTGTGGTGGTGAA

Cell culture and treatment

3T3-L1 preadipocytes were obtained from the JCRB cell bank (Osaka, Japan). Briefly, $2x10^3$ 3T3-L1 preadipocytes per well in 96 well were incubated in the maintenance medium (DMEM supplemented with 10% FBS, 200 μM ascorbic acid, 1.0 × 10^5 IU/L penicillin, and 100 mg/L streptomycin) at 37°C in 5% CO_2 until they reached confluence. On reaching 100% confluence (about 2 days), the cells were incubated for an additional 2 days. To initiate differentiation, on day 0, 3T3-L1 preadipocytes were incubated in the differentiation medium (maintenance medium supplemented with 0.25 μM dexamethasone, 0.5 mM 3-isobutyl-1-methylxanthine, 10 μg/mL insulin, and 0, 5, 15, 30, or 40 μM soyasapogenol A or B) for 2 days. On day 2, the medium was replaced with the maturation medium (the maintenance medium supplemented with 10 μg/mL insulin), with fresh medium added every 2 days until day 14. On day 14, the area and lipid droplets in differentiated 3T3-L1 cells were measured using IN Cell Analyzer 1000 (GE Healthcare, Little Chalfont Buckinghamshire, UK), according to a previous study [131].

Analysis of metabolic variables in serum

Serum samples were obtained from blood collected by cardiac puncture and stored at −80°C until analysis. For TAG, FFA, glucose, and ALT, serum levels were measured using commercial enzyme assay kits (Triglyceride E-Test, NEFA C-Test, Glucose C II-test, Transaminase C II-test, respectively; Wako Pure Chemicals). Serum adiponectin levels were measured using a commercial ELISA kit (Mouse/rat adiponectin ELISA kit from Otsuka Pharmaceutical, Tokyo, Japan). Serum TC was measured using a commercial enzyme assay kit (T-CHO Kainos kit from Kainos Laboratories Inc., Tokyo, Japan). For measuring serum HDL-C levels, the serum HDL-C fraction was collected as previously described [129] and HDL-C levels were measured using the enzyme assay kit (T-CHO Kainos kit).

Measurement of lipid content in tissues

Liver, muscle, and small intestine lipids were extracted using chloroform/methanol according to the method described by Folch, Lees, & Sloane Stanley (1957) [80]. In the liver, muscle, and small intestine, the TAG content was measured using a commercial enzyme assay kit (Triglyceride E-Test). The phospholipid content in the liver was measured using the method described by Rouser, Siakotos, & Fleischer (1966) [133]. Furthermore, TC and FC contents in the liver were measured using the method described by Sperry, & Webb (1950) [134]. EC in the liver was calculated as the difference between TC and free cholesterol contents.

Measurements of hepatic carnitine palmitoyltransferase II (CPT-II) and acyl-CoA oxidase (ACO) activities

Briefly, a piece of liver was homogenized in 6 volumes of a 0.25 M sucrose solution, containing 1 mM EDTA in 10 mM Tris-HCl buffer (pH 7.4). The homogenate was centrifuged at 500 × *g* for 10 min at 4°C to obtain the supernatant without the nuclei fraction. The protein concentration in the supernatant was determined using a commercial kit (BioRad, Hercules, CA) with bovine serum albumin (BSA) as the standard. The enzyme activities of CPTII and ACO in the supernatant were determined as described previously [135-136].

Measurement of hepatic α-tocopherol (α-Toc) content

The α-Toc content in hepatic total lipids was determined by HPLC as previously described [130]. The hepatic α-Toc content was quantified using linear regression from the calibration curve of an external standard, PMC.

Measurement of fecal lipid content

Briefly, feces were collected for 7 days at the end of the experiment, lyophilized, weighed, and stored at −20°C until analysis. Fecal cholesterol and coprostanol were derivatized into trimethylsilyl ethers and quantified by gas-liquid chromatography as previously described. Fecal fatty acids (FAs) were determined by the titration method as previously described [130].

Statistical analysis

Data are presented as mean ± standard error of the mean (SEM). Comparisons between 2 groups in the animal experiment were analyzed using Student's *t*-test. Comparisons among 5 groups in the cell experiment were analyzed using one-way ANOVA, followed by Dunnett's multiple comparison post-hoc test. Differences were considered statistically significant at $p < 0.05$. Statistical analysis was performed using Excel 2011.

Results and Discussion

Determination of the SAP composition

Zhang et al. have reported that crude or total soyasaponin extracts are typically mixtures of group A and B soyasaponins with small amounts of soyasapogenols [137]. Following the deglycosylation of soyasaponins by acid or base hydrolysis to produce soyasapogenols, the concentration of soyasapogenols can be used to determine the soyasaponin composition [138-139]. As shown in **Table 12**, the SAP contained 36.3 mg/g of soyasapogenol A, and 78.1 mg/g of soyasapogenol B, 258.8 mg/g of total sugars, including 56.9 mg/g of reducing sugars, and 2.29 mg/g of TAG.

In Japanese soy food products, the content of group B soyasaponins is higher than that of group A soyasaponins [119]. Soyasapogenol B was the most abundant soyasaponin aglycone and was higher than soyasapogenol A in our SAP after acid hydrolysis **(Table 12)**. As mentioned in prior studies, soyasaponin A1 and I are the major components of group A and group B soyasaponins, respectively [140]. Soyasapogenol is the plasma major metabolite after consumption of soybean diet [141]. Reportedly, soyasaponin is converted to soyasapogenol by the human gut microbiota [141], which represents that the sugar chains of soyasaponin were removed in the intestine, and then absorbed in the form of soyasapogenol. Additionally, in Caco-2, a colon cell model, the absorption of soyasapogenol B is favored over that of soyasapogenol A [142]. Based on these findings, we speculate that soyasaponin I was the major soyasaponin in our SAP, and the primary form absorbed was soyasapogenol B.

Table 12. Composition of SAP

Ingredients (mg/g powder)	SAP
Soyasapogenol A	36.3
Soyasapogenol B	78.1
Total sugars	258.8
Triacylglycerol	2.29

The SAP significantly reduced the body weight gain in C57BL/6J mice fed an HFD for 9 weeks

It has been reported that mice fed an HFD can induce obesity [143]. To determine whether the anti-obesity effect of the SAP, male C57BL/6J mice were fed an HFD and orally administered the SAP for 9 weeks, starting at 5 weeks of age. Simultaneously, mice in the control group were fed an HFD. Wu et al. (2017) showed that HFD increased 4g of body weight in mice after 9 weeks [144]. At the end of the feeding, the control group gained 5.1g of body weight **(Table 13)**, which demonstrated that our HFD could induce obesity. As shown in **Table 13**, although food intake did not differ between the 2 groups, the SAP significantly reduced the final body weight and food efficiency by 7 % and 29 %, respectively. Furthermore, no significant difference was observed in the body weights between the 2 groups until week 4 of treatment; however, after week 5 of the SAP treatment, the body weight was significantly reduced by 5 % **(Fig. 7)**.

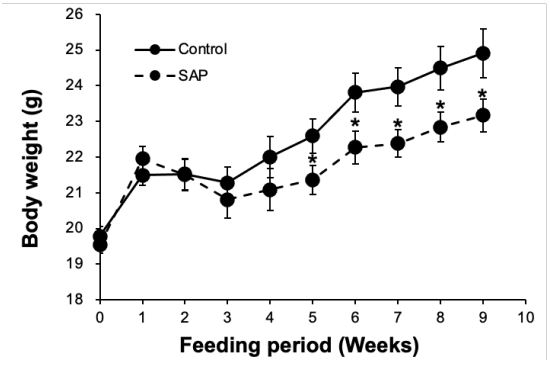

Figure 7. Changes in body weight of male C57BL/6J mice fed HFD with or without SAP for 9 weeks

Values are means ± standard error of the mean (SEM) (n = 9 or 10/group). Significant differences between mean values were evaluated by Student's *t*-test (*$p < 0.05$).

Table 13. Growth and serum parameters of C57BL/6J mice fed HFD with or without SAP for 9 weeks

	Control	SAP
Growth parameters		
Food intake (g/day)	2.12 ± 0.04	2.13 ± 0.05
Initial body weight (g)	19.8 ± 0.3	19.5 ± 0.2
Final body weight (g)	24.9 ± 0.7	23.2 ± 0.5 *
Food efficiency	37.8 ± 3.8	26.9 ± 1.9 *
(mg body weight gain/g total food intake)		
Serum		
Triacylglycerol (mg/dL)	59.2 ± 6.0	52.5 ± 4.1
Free fatty acids (mg/dL)	20.0 ± 2.5	14.7 ± 1.2 (p = 0.0760)
Total cholesterol (mg/dL)	124.1 ± 5.5	126.1± 7.8
HDL-cholesterol (mg/dL)	89.8 ± 2.7	80.6 ± 5.4
Glucose (mg/dL)	230.6 ± 8.7	238.0 ± 12.1
Alanine aminotransferase (IU/L)	6.7 ± 0.9	11.5 ± 1.16 **
Adiponectin (μg/mL)	17.44 ± 0.65	16.26 ± 1.00
β-Hydroxybutyrate (mmol/L)	0.47 ± 0.08	0.59 ± 0.07

Values are means ± standard error of the mean (SEM) (n = 9 or 10/group). Significant differences between mean values were evaluated using Student's *t*-test (*$p < 0.05$, **$p < 0.01$). If P-values are < 0.05, the difference is considered significant. N.S., not significant; SAP, Soyasaponin sample; HDL, high-density cholesterol.

Table 14. Metabolic parameters in the liver, small intestinal mucosa, muscle, and feces of C57BL/6J mice fed HFD with or without SAP for 9 weeks.

	Control	SAP
Liver		
Weight (g)	0.9 ± 0.04	1.09 ± 0.06 *
Relative weight (g/100 g B.W.)	3.61 ± 0.11	4.72 ± 0.22 **
Triacylglycerol (mg/g liver)	20.2 ± 2.8	12.7 ± 1.0 *
Phospholipids (mg/g liver)	30.4 ± 0.7	30.1 ± 0.7
Cholesterol (mg/g liver)		
Total	3.09 ± 0.14	4.27 ± 0.21 **
Free	1.90 ± 0.08	2.24 ± 0.08 **
Esterified	1.19 ± 0.11	2.03 ± 0.23 **
ACO (nmol/min/mg protein)	4.49 ± 0.31	2.76 ± 0.12 **
CPT-II (nmol/min/mg protein)	6.16 ± 0.38	4.79 ± 0.18 **
α-Tocopherol (μg/g liver)	9.27 ± 1.44	1.17 ± 0.48 **
Small intestinal mucosa		
Relative weight (g/100 g B.W)	3.00 ± 0.09	3.45 ± 0.06 **
Triacylglycerol (mg/g tissue)	22.8 ± 1.6	18.5 ± 1.7 (p = 0.0752)
Muscle		
Relative weight (g/100g B.W.)	1.49 ± 0.04	1.57 ± 0.05
Triacylglycerol (mg/g tissue)	15.7 ± 1.8	16.0 ± 1.6
Feces		
Feces dry weight (mg/day)	170.0 ± 8.4	195.0 ± 8.7 (p = 0.0534)
Fatty acids (mg/day)	17.7 ± 1.2	14.6 ± 1.2 (p = 0.0727)
Fatty acids excretion rate (%day)	4.17 ± 0.21	3.45 ± 0.24 *
Cholesterol (mg/day)	0.58 ± 0.04	0.34 ± 0.02 **
Coprostanol (mg/day)	0.01 ± 0.01	0.003 ± 0.000

Values are means ± standard error of the mean (SEM) (n = 9 or 10/group). Significant differences between mean values were evaluated using Student's *t*-test (*$p < 0.05$, **$p < 0.01$). N.S., not significant; SAP, Soyasaponin sample; ACO, Acyl-CoA oxidase; CPT-II, Carnitine palmitoyltransferase II.

The SAP significantly inhibited adipose tissue weight gain in C57BL/6J mice fed an HFD for 9 weeks

The body weight gain caused by a high-fat diet is mainly due to the increase in adipose tissue weight. To determine whether the inhibitory effect of the SAP on body weight in HFD-fed mice similarly inhibits the adipose tissue weight gain at the early feeding stage. We assessed the effect of the SAP on the body fat mass by tomographic analysis using an experimental X-ray CT system. Compared with the control group, at weeks 3, 5, 7, and 9, the SAP significantly reduced visceral (by 28 %, 37 %, 37 % and 44 %, respectively) and subcutaneous adipose tissue weights (by 26 %, 35 %, 39 % and 47 %, respectively) **(Fig. 8B & C)**. From week 3 until week 9, the weight of visceral and subcutaneous fats did not significantly change in the SAP group **(Fig. 8B & C)**. As shown in **Fig. 8D**, after the 9-week treatment period, the SAP significantly reduced the relative adipose tissue weights of the total, visceral, and subcutaneous tissues by 35 %, 37 % and 32 %, respectively. These results suggested that the SAP suppressed the adipose tissue weight gain from the early feeding stage, which led to the final suppression of the body weight gain. Similar to our results, group B soyasaponin aglycone (soyasapogenol B) has revealed an early inhibitory effect on body weight gain (by 8 % at 3 weeks of feeding) through the early suppression of adipose tissue weight in HFD-fed mice [121].

We assessed inhibitory activity of the SAP on PL in vitro. Inhibition of PL activity has been known to result in anti-obesity effects by reducing lipid absorption via the intestine, and several saponins reportedly inhibit PL activity [125-126]. In contrast to these findings, the SAP increased the PL activity at

concentrations of 0.5-10 mg/mL **(Fig. 9)**. Meanwhile, fecal fatty acid excretion rate was significantly decreased by 17 % as well as fecal FA levels tended to be lower by 18 % (p = 0.0727) in the SAP-treated mice **(Table 14)**. These data suggested that the SAP increased lipid absorption via the intestine.

Bidesmoside triterpenoid saponins from Platycodi radix, which is composed of an aglycone moiety with sugar moieties at C-3 and C-28, exhibits inhibitory effects on PL [125]. Among them, low molecular weight saponins such as platycodin A, C, D, and deapioplatycodin D are known to possess higher inhibitory activity than high-molecular-weight saponins with more than one or two more glucose moieties in the structure [125]. Saponins isolated from Kochia scoparia are known to demonstrate an inhibitory effect on PL activity, which requires a structure with a free carboxylic acid group at position C-28 in the triterpene skeletons and a free carboxylic acid in the β-D-glucopyranosiduronic acid sugar moiety [126]. In addition to the combined properties of the aglycone and the sugar moieties mentioned in the above studies, there exists another possible explanation for the increased PL activity demonstrated by the SAP. Soyasaponins possess surfactant characteristics, with the coexistence of a water-soluble sugar part and water-insoluble triterpene part in the molecule. Therefore, soyasaponins may increase lipase activity by utilizing conformational changes or increasing substrate access to the specific area of the enzyme, similar to other surfactants [145].

These results suggested that the SAP prevented obesity by suppressing lipid accumulation in adipose tissue but not inhibiting intestinal lipid absorption.

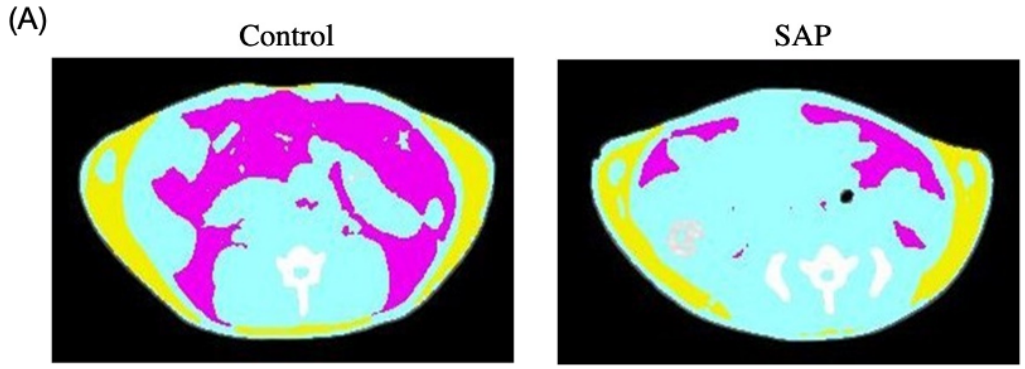
(A)
Control
SAP

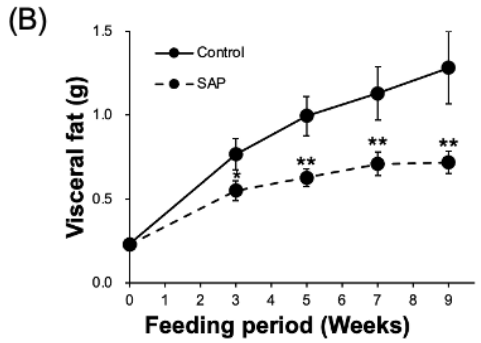
(B)
Visceral fat (g)
Control
SAP
Feeding period (Weeks)

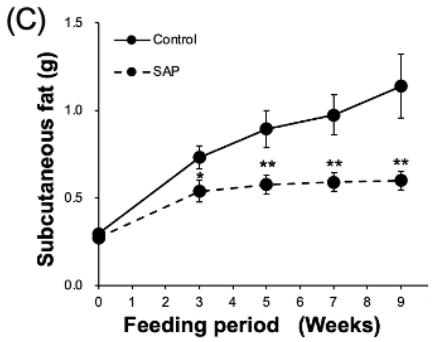
(C)
Subcutaneous fat (g)
Control
SAP
Feeding period (Weeks)

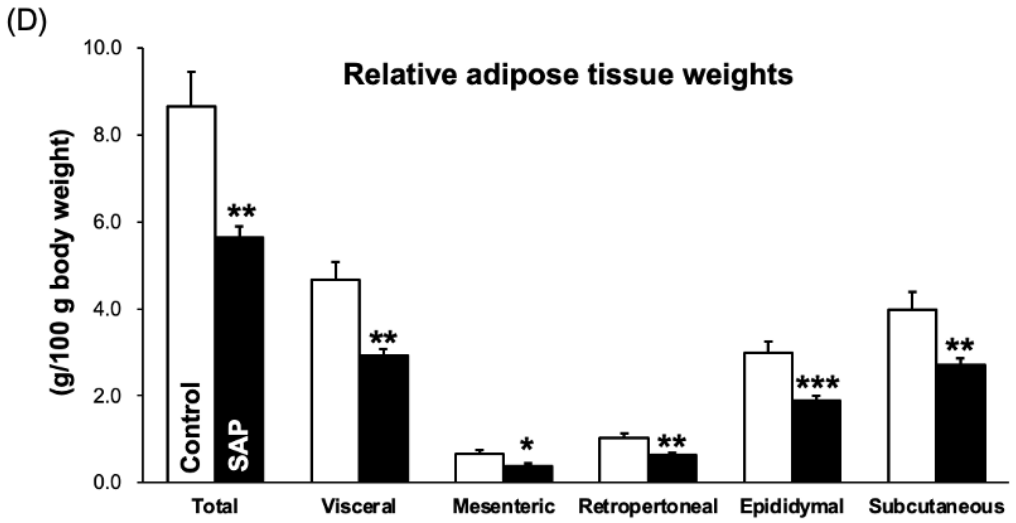
(D)
Relative adipose tissue weights
(g/100 g body weight)
Control
SAP
Total
Visceral
Mesenteric
Retropertoneal
Epididymal
Subcutaneous

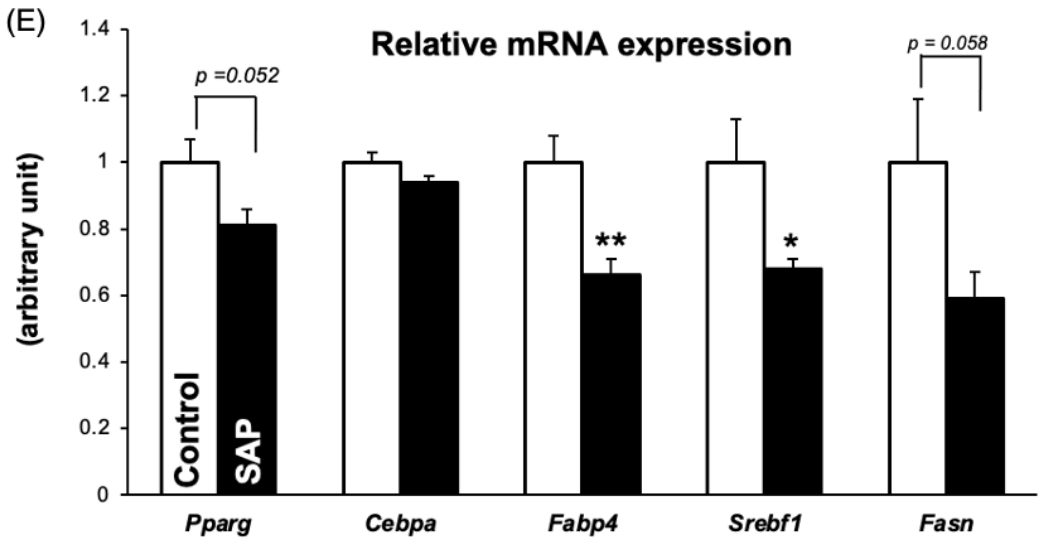
(E)
Relative mRNA expression
p =0.052
p = 0.058
(arbitrary unit)
Control
SAP
Pparg
Cebpa
Fabp4
Srebf1
Fasn

Figure 8. White adipose tissue weights of C57BL/6J mice fed HFD with or without SAP for 9 weeks.

(A) A photographic representation of the changes in the visceral and subcutaneous fat areas of mice treated with the SAP (purple, visceral fat; yellow, subcutaneous fat). Temporal weight changes in visceral fat (B) and subcutaneous fat (C) were calculated by tomographic analysis. Relative adipose tissue weight (D) of mice fed a high-fat diet and treated with the SAP for 9 weeks was calculated by body weight and each part of the adipose weight. (E) The lipogenic-related gene expression levels in white adipose tissue (epididymitis) were analyzed by qRT-PCR. Values are presented as means ± standard error of the mean (SEM) (n = 9 or 10/group). Significant differences between mean values were evaluated by Student's t-test (*$p < 0.05$, **$p < 0.01$, ***$p < 0.001$). Fabp4, fatty acid binding protein 4; Cebpa, CCAAT/enhancer binding protein (C/EBP) alpha; Fasn, Fatty acid synthase; Pparg, Peroxisome proliferator-activated receptor-gamma; SAP, Soyasaponin sample; Srebf1, Sterol regulatory element binding transcription factor 1.

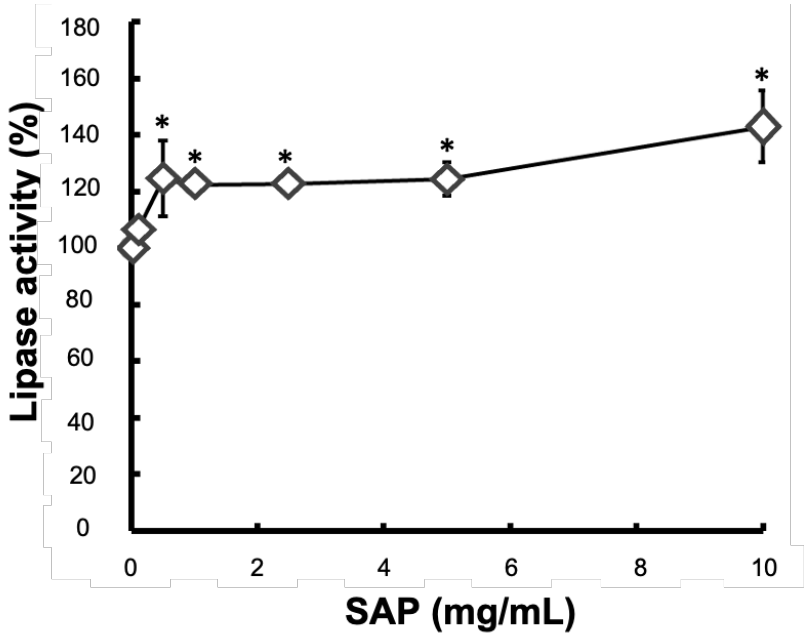

Figure 9. Effect of the SAP on the activity of pancreatic lipase *in vitro*

The enzyme activity at 0 mg/mL was considered 100%. Values are means of triplicate determinations ± standard error of the mean (SEM). Significant differences from the 0 mg/mL SAP group were evaluated by Student's *t*-test (*$p < 0.05$).

The SAP and soyasapogenol B respectively inhibited lipogenesis in HFD-fed C57BL/6J mice and 3T3-L1 cells.

In obesity, adipose tissue weight gain results from an imbalance between lipogenesis and lipolysis. The rate of lipogenesis is associated with the adipocyte differentiation rate under the HFD feeding [146]. Notably, adipocyte differentiation is controlled by two key transcriptional regulators, Peroxisome proliferator-activated receptor-γ (*Pparg*) and CCAAT/enhancer-binding protein α (*Cebpa*), which differentiate preadipocytes into adipocytes [147]. When preadipocytes are differentiating, it activates the lipogenic genes, including *Srebf1*, *Fasn*, and fatty acid binding protein 4 (*Fabp4*), to convert into lipid-filled mature adipocytes. To further examine the effects of the SAP on WATs, mRNA levels related to lipogenesis were analyzed in epididymal WAT. As observed in **Fig 8E**, mRNA levels of *Srebf1* and *Fabp4* were significantly lower by 32 % and 34 %, respectively, in the SAP group. Moreover, the *Pparg* and *Fasn* mRNA levels tended to be lower by 19 % ($p = 0.052$) and 41 % ($p = 0.058$), respectively, in the SAP group.

Soyasapogenol A and B are aglycones that release from the SAP following acid hydrolysis. To further confirm the effects of the SAP on adipogenesis during adipocyte differentiation of 3T3-L1 preadipocytes, 3T3-L1 preadipocytes were incubated in the differentiation medium with 0, 5, 15, 30, and 40 μM soyasapogenol A or B for 2 days (days 0-2). On day 14, the lipid count and lipid area in 3T3-L1 adipocytes were measured. Soyasapogenol B significantly decreased lipid counts (lipid droplets) in 3T3-L1 adipocytes in a dose-dependent manner, with no significant change observed with soyasapogenol A **(Fig. 10A)**. Additionally, the lipid area was significantly reduced following

treatment with 30 and 40 μM soyasapogenol B **(Fig. 10B**). No significant difference was observed in the lipid area of 3T3-L1 cells treated with soyasapogenol A **(Fig. 10B)**. Therefore, soyasapogenol B, the lack of hydroxyl group on the C-23 position compared to soyasapogenol A, had a better inhibitory effect on lipid accumulation.

At the early stages of adipocyte differentiation, PPARγ and C/EBPa as major transcriptional regulators cross-regulate to promote the expression of lipogenic genes [148]. Deleting PPARγ blocks adipocyte differentiation and prevents HFD-induced obesity in mice [149]. In the present study, the SAP inhibited the increasing body and WAT weight in mice at the early HFD feeding period **(Fig 7 & 8A-C)**. In the WAT, the SAP suppressed the expression of PPAR-γ and inhibited the expression of SREBP-1c, aP2, and FAS **(Fig. 8E)**. In 3T3-L1 cells, soyasapogenol B demonstrated a better inhibitory effect on lipogenesis than soyasapogenol A **(Fig. 10)**. Taken together, we speculate that soyasapogenol B, the major form of the absorbed SAP, inhibits adipocyte differentiation via the PPAR-γ pathway and results in a decrease in early WAT and body weight gain. A similar mechanism is observed in Platycodin D, which suppresses PPAR-γ and C/EBPα protein levels through 5'AMP-activated protein kinase (AMPK) activation to decrease epididymal fat (by 39 %) and early body weight gain (by 18 % at 2 weeks of feeding) in HFD-fed mice [150]. Therefore, platycodin D, with four sugar units at C-28 compared to soyasaponins, has a strong anti-obesity effect.

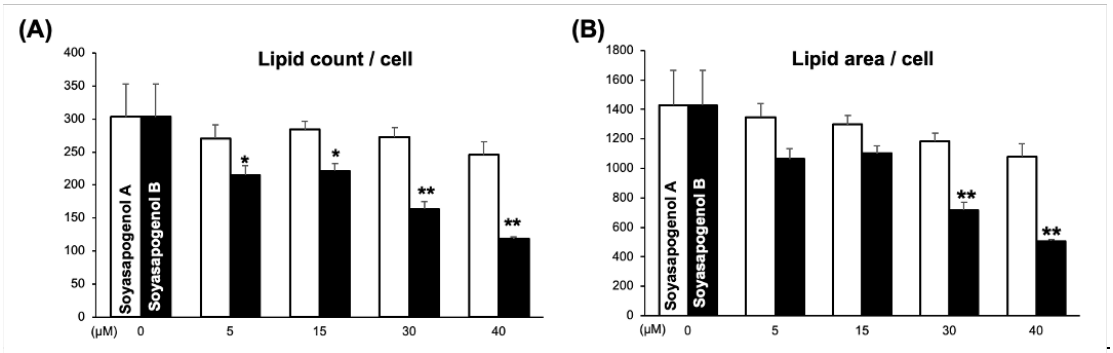

Figure 10. The effect of soyasapogenol A or B on the differentiated 3T3-L1 adipocytes.

After reaching 100% confluency, 3T3-L1 preadipocytes were incubated in a differentiation medium containing soyasapogenol A and B (0, 5,15, 30, and 40 μM) for 14 days. Lipid droplets in adipocytes were stained with BODIPY 493/503. The lipid count (A) and lipid area (B) of 3T3-L1 adipocytes were measured using IN Cell Analyzer 1000 (GE Healthcare). Values are presented as means ± standard error of the mean (SEM) (n = 6/group). Significant differences between mean values were evaluated by Dunnett's test (*$p < 0.05$, **$p < 0.01$).

The SAP inhibited hepatic lipogenesis in HFD-fed C57BL/6J mice

In obesity, a high level of circulating FFA promotes the uptake of FFA by extra-adipose tissues, resulting in ectopic fat deposition and, insulin resistance, and hyperglycemia [151-152]. Serum FFA levels tended to be lower ($p = 0.076$) in the SAP-treated mice **(Table 13)**. As shown in **Table 14**, hepatic TAG and α-Toc levels were significantly reduced by 37 % and 89 %, respectively, in the SAP-treated mice. Between the 2 groups, no significant difference was observed in the relative weights of the femoral muscle, TAG contents of the small intestine mucosa and femoral muscle, serum levels of TAG, glucose, β-hydroxybutyrate and adiponectin, and hepatic phospholipids levels **(Tables 13 and 14)**.

The reason for hepatic TAG accumulation is the input rate of FFA (uptake, *de novo* lipogenesis, and esterification into TAG) is greater than the output rate of FFA (β-oxidation and export within VLDL). In the previous reports in HFD-fed mice, soyasaponins lowered TAG accumulation in the liver [121-122]. However, the mechanism through which soyasaponin improves fatty liver remains unclear. Typically, the inhibition of fatty acid synthesis or activation of fatty acid oxidation plays an important role in the improvement of fatty liver. To elucidate the effects of the SAP on hepatic TAG metabolism, we analyzed mRNA levels of lipogenesis-related genes in the liver. The qRT-PCR result analysis showed a significant decrease in *Srebp1, Fasn*, and peroxisome proliferator-activated receptor-α (*Ppara*) mRNA levels by 52 %, 61 % and 31 %, respectively, in the SAP group when compared with the control group **(Fig 11A)**. Next, we analyzed fatty acid oxidation related enzyme activities in the liver. As shown in **Table 14**, the SAP decreased the activities of CPT-II by 22 % and ACO by 39 %, enzymes involved in fatty acid β-oxidation regulated by PPAR-α.

In the present study, the SAP suppressed the expression of SREBP-1c and FAS **(Fig. 11A)**. Several studies have demonstrated the improvement of fatty liver by regulating the lipogenic protein, SREBP-1c [153]. Crude triterpenoid saponins extracted from Ilex latifolia ameliorate hepatic lipid accumulation in HFD-fed mice by decreasing the mRNA levels of lipogenic genes such as *Srebf1*, acetyl-CoA carboxylase (*Acc*), *Fasn*, and *Scd1* [154]. 20(S)-Protopanaxatriol, an aglycone steroid saponin categorized as a ginsenoside, demonstrates inhibitory activity against LXRα-mediated lipogenic genes such as *Srebf1*, decreasing TAG accumulation in hepatocytes [155]. Enhancement

of β-oxidation is also one of the pathways to ameliorate fatty liver [156]. In β-oxidation related gene and enzymes, the SAP inhibited the activities of CPT-II and ACO and mRNA level of *Ppara* **(Table 14 & Fig 11A)**. Our results indicated that the SAP had a decreasing hepatic TAG accumulation effect by reducing lipogenic gene levels of *Srebf1* and *Fasn* but not through the β-oxidation mechanism. The most likely explanation for the suppression of β-oxidation by the SAP is that the SAP decreases the flux of fatty acids by reducing lipogenesis in the liver, thereby lowering the rate of β-oxidation.

The SAP increased hepatic cholesterol contents in HFD-fed C57BL/6J mice

In investigations assessing the relationship between saponins and cholesterol, most have focused on the inhibition of intestinal cholesterol absorption and the promotion of fecal cholesterol excretion by saponins [122 & 142]. For example, group B soyasaponins decrease cholesterol micelle formation and interfere with intestinal cholesterol absorption [142]. Group B soyasaponins play a role in lowering plasma cholesterol (by 19 %) by reducing the intestinal absorption of cholesterol and increasing the excretion of neutral sterols by 1.9-fold and BAs by 2.1-fold in hamster feces [122]. Contrary to previous studies, no significant difference was observed in the level of serum cholesterol and HDL-c between the 2 groups **(Fig 11B)**. The fecal cholesterol content was significantly decreased by 41 % in the SAP-treated mice **(Fig 11C)**, indicating that the SAP may increase cholesterol absorption in the intestine or reduce the excretion of cholesterol from the liver.

The cholesterol content in the liver is determined by a balance between absorption from the intestines (from the diet), *de novo* cholesterol synthesis, consumption by conversion to BAs, and secretion into blood. As shown in Fig 6D, the SAP significantly increased hepatic levels of TC by 1.2-fold, FC by 1.2-fold, and EC by 1.7-fold. EC is the form that hepatic uptake of dietary cholesterol [157], indicating that the SAP elevated intestinal cholesterol absorption. To investigate the effects of the SAP on hepatic cholesterol metabolism, we analyzed related mRNA levels. *Hmgcr* is a critical enzyme in *de novo* cholesterol synthesis and be activated in obesity followed by elevating hepatic cholesterol levels [158]. However, the SAP significantly lowered the mRNA level of *Hmgcr* by 70 % **(Fig 11A)**, suggesting that the SAP caused liver cholesterol accumulation was not through cholesterol biosynthesis. ABCA1 is a membrane transporter protein that effluxes hepatic cholesterol into the bloodstream to nascent HDL particles. Inhibition of ABCA1 expression reduces cholesterol efflux to HDL in the liver [159]. The SAP significantly decreased the expression of hepatic *Abca1* by 41 % **(Fig 11A)**. The repression of ABCA1 expression may underlie the increase in hepatic cholesterol content induced by the SAP. CYP7A1 is a rate-limiting enzyme in the BA biosynthetic pathway, which excrete cholesterol into feces. Suppression of CYP7A1 expression or activity leads to enhanced serum and liver cholesterol levels [160]. *Cyp7a1* mRNA levels tended to be lower by 32 % (p = 0.06) in the SAP group **(Fig 11A)**. Results indicated that the accumulation of hepatic cholesterol by the SAP may be a complex consequence of increased intestinal cholesterol absorption, inhibited liver cholesterol excretion into feces, and suppressed efflux into HDL **(Fig 11E)**.

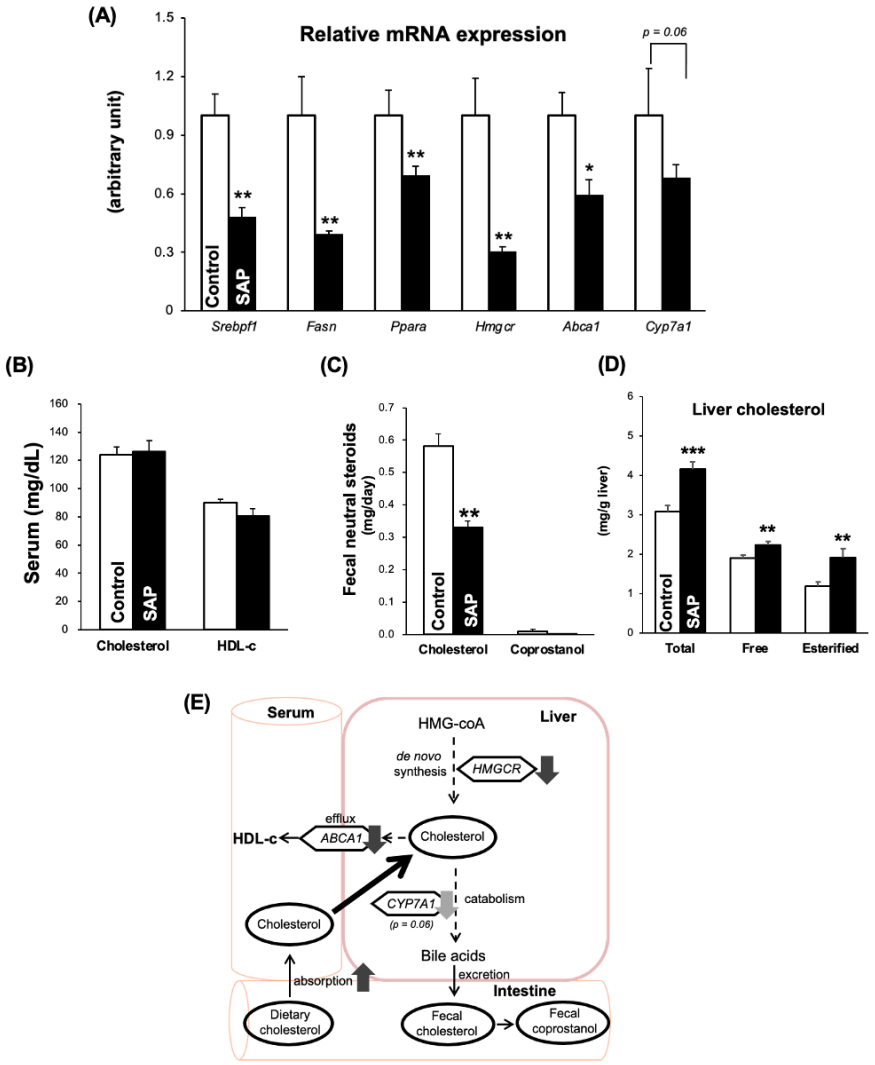

Figure 11. Liver metabolic parameters of C57BL/6J mice fed HFD with or without SAP for 9 weeks.

(A) The lipogenic-related or cholesterol-related gene expression levels in the liver were analyzed by qRT-PCR. The level of cholesterol and HDL in serum (B), and neutral steroids in feces (C), and the content of total, free, esterified cholesterol in the liver (D) of C57BL/6J mice fed HFD for 9 weeks. (E) The mechanism of the SAP on cholesterol accumulation in the liver. Values are presented as means ± standard error of the mean (SEM) (n = 9 or 10/group). Significant differences between mean values were evaluated by Student's t-test (*$p < 0.05$, **$p < 0.01$, ***$p < 0.001$). Abca1, ATP-binding cassette transporter 1; Cyp7a1, Cytochrome P450 family 7 subfamily A member 1; Fasn, Fatty acid synthase; HDL, high-density lipoprotein; Hmgcr, HMG-CoA reductase; Ppara, Peroxisome proliferator-activated receptor-alpha; SAP, Soyasaponin sample; Srebf1, Sterol regulatory element binding transcription factor 1.

Effect of the SAP on metabolism parameters

In the SAP group, the relative weight of the small intestine mucosa and liver as well as serum ALT were significantly increased by 1.2-fold, 1.1-fold, and 1.7-fold, respectively **(Tables 13 and 14)**. Reportedly, atrophy of the small intestine and intestinal hyperpermeability is induced by HFD [161]. The possible reason that the SAP increased the weight of mucosa was that oligosaccharides released from the SAP may prevent damage to the intestinal mucosa by HFD [162].

Blood ALT concentration is positively correlated with liver weight [163]. The SAP elevated the weight of liver in mice, explaining why serum ALT levels were increased by the SAP. The reason resulted in the SAP increased mice liver weight may be the total intake of the SAP (126 g) is higher than the total soy saponin intake (84 g) in previous study [154]. For example, dietary sesamin has been reported to have a hepatic protective effect with an increase in liver weight [165-166].

Summary

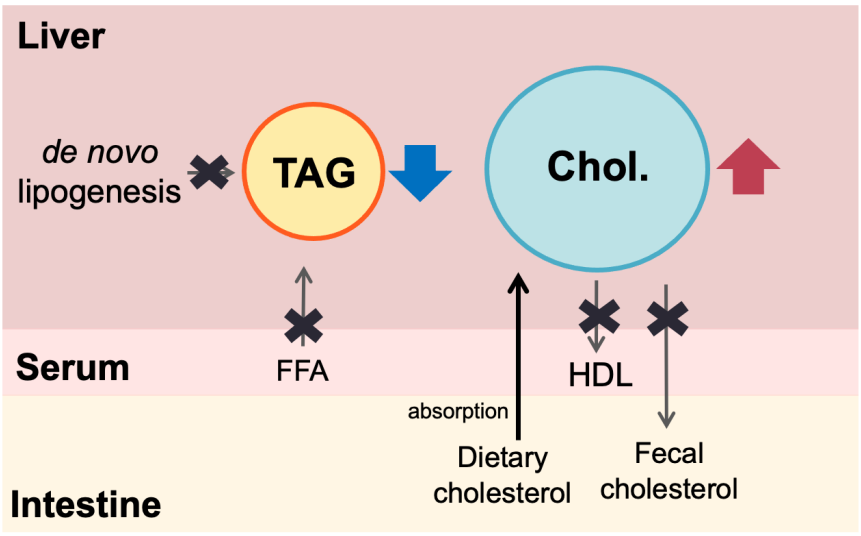

Figure 12. The effect of SAP on lipid metabolism in animal models of NAFLD.

It has been described that the relationship between SAP and intestinal cholesterol absorption; however, the working mechanisms of liver cholesterol metabolism by SAP are not well understood. In this study, we focused on the effect of SAP on the liver cholesterol metabolism of HFD-induced NAFLD in C57BL/6J mice.

Contrary to previous studies' results, SAP promoted cholesterol absorption in the intestine. SAP increased the accumulation of hepatic cholesterol via increasing intestinal cholesterol absorption, inhibiting liver cholesterol excretion into feces, and suppressing efflux into HDL. These evidence indicated that SAP is an inducer of abnormal hepatic cholesterol metabolism.

Moreover, this animal study showed that the SAP can potently reduce body weight and WAT weight and that the early phase of adipogenesis is the key stage for this effect. This report revealed that our SAP effectively suppressed TAG formation and accumulation by inhibiting the mRNA levels of aP2 and

SREBP-1c in the adipose tissue, without inhibiting the intestinal absorption of lipids. In mouse adipocytes, soyasapogenol B, one of the main absorption forms of soyasaponin in vivo, inhibited 3T3-L1 differentiation to reduce TAG accumulation. The SAP significantly lowered lipogenesis-related gene expression in mice livers, including SREBP-1c and FAS, to prevent excessive TAG accumulation. Although the dosage and structure of soyasaponins differ, the inhibitory effect of soyasaponins on hepatic TAG accumulation has been presented in the present study, as well as in previous reports.

In conclusion, the SAP, a mixture of soyasaponin A and B, has a double-sided effect on liver lipid metabolisms that can prevent hepatic TAG accumulation but accelerates hepatic cholesterol accumulation in HFD-fed induced NAFLD (**Fig. 12**).

CHAPTER III Effect of free fatty acid induced NAFLD in cell model

D-Psicose improves palmitic acid induced cholesterol accumulation and cellular senescence in HepG2 cells

Introduction

Liver content of lipids (particularly TAG) higher than 5 % (i.e., steatosis) is regarded as the beginning of NAFLD, followed by a series of liver diseases, including NASH and liver fibrosis. Recently, many studies revealed that the dysregulation of cholesterol metabolism has occurred in NAFLD, especially the accumulation of FC in the liver [8]. In patients with NASH, it has been observed that the liver content of FC is higher roughly 1.7-fold than in healthy subjects [43]. Clinical studies have shown a positive correlation between liver FC accumulation and histological severity of NAFLD [44]. A reduction in liver FC overload by using cholesterol-lowering drugs, such as statins, improves the liver disease severity in NASH [9-10]. Thus, the prevention of dysregulated cholesterol metabolism may effectively prevent the development of NASH.

Cellular senescence has been proposed as a risk factor in the development of NAFLD. Cellular senescence is a process that features irreversible cell cycle arrest, which is triggered by deleterious stress and leads to an increase in the secretion of senescence-associated secretory phenotype (e.g., pro-inflammatory factors) and activation of the cyclin-dependent kinase inhibitors (e.g., cyclin dependent kinase inhibitor 1A (p21) or cyclin-dependent kinase inhibitor 2A (p16), etc.) to cause cellular dysfunction [167]. The activity of

senescence-associated β-galactosidase (SA-β-gal), one of the lysosomal enzymes, is a widely accepted biomarker to detect senescence, due to the increased lysosomal biogenesis in senescent cells [168]. Lower nuclear area, telomere shortening, and p21 expression are recognized to be indicators of NAFLD progression [169-170]. Moreover, in senescence models of mice, hepatocyte senescence drives steatosis and cholesterol accumulation [171], while eliminated hepatocyte senescence has a lipid-lowering effect in the liver [171]. There may be a close association between senescence and cholesterol metabolism in NAFLD.

D-Psicose is well known as a low-calorie sweetener, it only provides approximately 0.4 calories per gram [172]. Pharmacokinetic studies both in humans and rats have demonstrated that D-allulose is readily absorbed into the circulation and rapidly excreted into the urine (roughly 6 h in humans and 1 h in rats) [172-174]. Although it is the C3 epimer of D-fructose, D-psicose has different biological functions in comparison with fructose, such as anti-hyperglycemic [174], and anti-obese [175-176]. D-Psicose is reported to inhibit postprandial blood glucose elevation by suppressing the activities of intestinal α-glucosidases in Wistar rats [177]. D-Psicose has been shown to increase the hepatic utilization of blood glucose via promoting activities of glucokinase and inhibiting activities of glucose-6-phosphatase in rat models [178-179]. However, there are still few studies about the effect of D-psicose on hepatic lipid metabolism **(Table 15)**. Chen et al. demonstrated that 5% of dietary D-psicose decreases lipogenesis gene expression (SREBP-1c, FAS, and ACCα) and upregulates fatty acid oxidation gene expression (AMP-activated protein kinase 2α (AMPK2α), HSL and PPARα) to prevent lipid accumulation in the liver of

AIN76-diet-fed Wistar rats [176]. Matsuo T et al. revealed that rats fed d-psicose had lowered activity of lipogenic enzymes including, FAS and glucose-6 phosphate dehydrogenase (G6PDH), in the liver in comparison with that fed glucose or fructose [180]. In diabetic mice, D-Psicose showed a lowering effect on TAG and total cholesterol in the liver [181]. Our previous study on hamsters has revealed that D-psicose suppresses serum PCSK9, which is a degrader of hepatic LDL receptors, resulting in decreasing the serum ratio of LDL/HDL [66]. 3% dietary D-psicose increased liver TAG contents when rats were fed the normal diet, while it did not affect liver TAG levels when rats were fed HFD [66]. In a rat hepatocytes study, uptake of HDL-c is promoted by D-psicose, resulting from upregulating the protein expression of SR-B1 [182]. Similarly, in a double-blinded placebo-controlled trial, the daily consumption of D-psicose (5g or 15g) for 48 weeks has lowered serum HDL-c levels in subjects with high LDL-c levels [183]. Moreover, dietary D-psicose (3%) has been shown to downregulate gene expression of hepatic cholesterol synthesis (SREBP-2 and HMGCR) in AIN-93G diet-fed rats, despite increasing liver cholesterol content [184]. Elevating liver levels of cholesterol, cholesterol precourse (desmosterol), plant sterols (campesterol, β-sitosterol, and stigmasterol), and bile acids (cholic acid and taurocholic acid) by dietary D-psicose (3%) have also been reported in another study of rats [185]. According to these previous studies, the regulation of cholesterol metabolism by D-psicose under non-disease conditions has been assessed [66.182-185]. However, the effect of D-psicose on cholesterol metabolism in the progression of NAFLD was not yet clarified.

In this study, a NAFLD cell model was induced by palmitic acid, which is lipotoxic lipid and widely used to promote hepatocyte lipid accumulation, to

examine the effect of D-psicose on cholesterol metabolism. Moreover, the working mechanisms underlying D-psicose protection against hepatocyte senescence was investigated.

Table15. Characteristics of the previous reports on d-psicose in lipid metabolism.

Models	Diets	D-Psicose dose	lipid metabolism	Cites
Wistar rats	AIN-76A diets	5%	Serum TAG level ↓ Serum FFA level ↓ Serum LDL-c level ↓ Liver Weight ↓ Liver Catalase level ↑ Liver Succinate dehydrogenase level ↑ Liver *Srebpf1* mRNA level ↓ Liver *Fans* mRNA level ↓ Liver *Acc* mRNA level ↓ Liver *Prkaa2* (AMPKα2) mRNA level ↑ Liver *Ppara* mRNA level ↑	176
Wistar rats	Normal diets CE-2	5%	Liver activities of FAS ↓ Liver activities of G6PDH ↓	180
C57BL/6J db/db mice	High-fat diet (60% energy of fat) for 4 weeks	%	(Compare to diabetic control) Liver triglyceride ↓ Liver cholesterol ↓	181
Golden Syrian hamsters	Normal diets 20% protein, 6% fat, and 74% carbohydrate, 0.1% cholesterol for 8 weeks HFD 20% protein, 15% fat, and 65% carbohydrate, 0.1% cholesterol for 4 weeks	3%	<u>Normal diets</u> Liver TAG ↑ Liver cholesterol - Liver phospholipid ↑ Serum PCSK9 ↓ <u>HFD</u> Liver TAG - Liver cholesterol - Liver phospholipid – Serum PCSK9 ↓	66
Rats	AIN-93G-based diets for 2 weeks	3%	<u>Rats</u> Serum total cholesterol ↑ Serum LDL ↓ Serum HDL ↓ <u>Primary rats hepatocytes</u>	182

			HDL uptake ↑ SR-B1 protein ↑	
Adult men and women	D-psicose beverage for 8 or 48 weeks	High-dose 15 g Low-dose 5 g	<u>High-dose</u> Serum HDL ↓ VLDL-TG/VLDL-c ↓ <u>Low-dose</u> VLDL-TG/VLDL-c ↓	183
Rats	A modified AIN-93G diet for 4 weeks	3%	Liver TAG - Liver Activities of FAS ↓ Liver Total cholesterol ↑ Liver *Hmgcr* mRNA level ↑ Liver *Srebpf2* mRNA level ↑	184
Wistar rats	AIN-93G diet for 4 weeks	3%	Serum total cholesterol - Serum free fatty acid – Liver cholesterol level ↑ Liver campesterol level ↑ Liver sitosterol level ↑ Liver stigmasterol level ↑ Liver desmosterol level ↑ Liver cholic acid level ↑ Liver taurocholic acid level ↑	185

Materials and Methods

Chemicals

Palmitic acid (PA), fatty acid-free bovine serum albumin (BSA), ethanol, D-psicose, ascorbic acid, chloroform, methanol, 5α-cholestane, KOH, hexane were purchased from Nacalai Tesque (Kyoto, Japan). Crystalline penicillin G potassium and streptomycin sulfate were obtained from Meiji Seika Kaisha (Tokyo, Japan). Phosphate buffer saline (-) was purchased from Nissui Pharmaceutical Co. (Tokyo, Japan). Fetal bovine serum (FBS) was obtained from Capricorn Scientific (Ebsdorfergrund, Germany).

Preparation of fatty acid and d-psicose

PA- BSA stock was made as follows: For the preparation of 100 mM PA stock, palmitate powder was melted in 99% ethanol solution at 55°C. For the preparation of 10% fatty acid (FA)-free BSA solution, FA-free BSA powder was dissolved in double-distilled water (ddH_2O) at 37°C. Subsequently, 100 mM PA stock was mixed with 10% FA-free BSA solution at 55°C with a volume ratio of 1:19 (the molar ratio was 3.5:1). The vehicle control was composed of 99% ethanol solution with 10% FA-free BSA solution. PA-BSA stock and vehicle were stored at −20 °C after filtering through a filter (Thermo Fisher Scientific, MA, USA).

D-Psicose powder was dissolved in DMEM and subsequently filtered by a filter. D-Psicose stock was stored at −20 °C for further treatment.

Cell culture

HepG2 cells were obtained from JCRB Cell Bank (Osaka, Japan) and cultured in DMEM (Nissui Pharmaceutical CO., Tokyo, Japan) supplemented with 10% FBS, 200 μM ascorbic acid, 1.0 × 10^5 IU/L penicillin, and 100 mg/L streptomycin in a humidified incubator maintained at 37 °C with 5% CO_2. The cells were seeded in 96-well plates, 30 mm dishes, and 60 mm dishes at a density of 1 × 10^4 cells/well, 0.5 × 10^6 cells/dish, and 1× 10^6 cells/dish, respectively. After reaching confluence, cells were treated with vehicle control, 100 μM PA-BSA, and 25 mM D-psicose for 24 h and then harvested for future experiments.

Cell viability assay

Cell viability was assessed by cell counting kit-8 (CCK-8) (Dojindo Laboratories Co., Kumamoto, Japan). HepG2 cells were seeded in 96-well plate by 1 x 10^4 cells per well. After treatment was complete, 10 μL of CCK-8 solution was added to each well of supernatant. The 96-well plate was incubated for 1 h in humidified incubator at 37 °C with 5% CO_2. When the incubation finished, the formazan dye was quantified by measuring the absorbance at 450 nm using a microplate reader (Multiskan GO, Thermo Scientific).

Analysis of the content of cholesterol and its precursors in HepG2 cells

For analysis of the content of cellular cholesterol and its precursors, HepG2 cells were seeded by 1 x 10^6 cells in 60 mm dishes. After treatment was complete, cells were harvested with 2 mL of cold-PBS. 0.2 mL of cell

suspensions were used for protein assay, and 1.8 mL of cell suspensions were used for cholesterol precursors analysis. Cell lipids of 1.8 mL of cell suspensions were extracted using chloroform/methanol according to the description by Folch's method [83]. Cell lipid extractions were added 10 μg of 5α-cholestane, as an internal standard, and saponified in 2 mL of 0.71 M ethanolic KOH at 65 °C for 1 h. After saponification, 2 mL of n-hexane were added, after homogeneous mixing, the mixtures were centrifuged at 18°C and 1,500×g for 10 min by repeating 3 times. 6 mL of supernatants (hexane layer) were collected and dried under nitrogen gas. Once dry had finished, 200 μL of *N*, *N*, *O*-bis (trimethylsilyl)trifluoroacetamide with 1% trimethylchlorosilane (99:1 mixture of BSTFA+TMCS) (TCI Chemicals, Kyoto, Japan) were added and heated at 70 °C for 1 h to derivatization of trimethylsilyl esters.

Cellular cholesterol precursors contents were detected by GC-FID (GC-2014) (Shimadzu Co.) equipped with an SPB-1 capillary column (60 m x 0.25 mm x 0.25 μm) (Sigma-Aldrich, MO, USA). The temperature of the injection port and detection was set to 300 °C. The column temperature was 275 °C. The flow rate of helium as the carrier gas was 32.5 cm/s.

Immunofluorescence of LDLR

Preparation of solutions

1X PBS

9.6 g PBS powder was dissolved in 1000 mL ddH_2O.

Fixation solution

10% formalin neutral buffer solution (containing 4% formaldehyde) (Nacalai Tesque, Kyoto, Japan).

Blocking solution

3% BSA solution was made by 0.3 g BSA powder dissolving in 1 mL PBS.

LDLR staining solution

LDLR staining solution was prepared with 1 µL of LDL antibody (sc-18823, Santa Cruz Biotechnology, TX, USA) in 200 µL of PBS.

Fluorochrome-conjugated secondary antibody solution

Fluorochrome-conjugated secondary antibody solution was prepared with 1 µL of secondary antibody (Anti-mouse IgG (H+L), F(ab')2 Fragment (Alexa Fluor® 488 Conjugate); Cell Signaling, Danvers, USA) in 1000 µL of PBS.

Hoechst staining solution

Hoechst solution was prepared by 1 µL of 1 mg/1 mL Hoechst 33342 solution (Dojindo Laboratories, Kumamoto, Japan) in 1 mL of PBS.

Cell staining protocol

HepG2 cells were seeded 1 x 10^4 cells per well in µclear fluorescence black 96-well plate (Greiner Bio-One, Tokyo, Japan). After treatment was complete, cells were washed twice with 100 µL of PBS. 100 µL of fixation solution were added into each well for 10 min at room temperature. Aspirated fixation solution, cells washed twice in PBS following by incubating in 100 µL blocking solution for 30 min at room temperature. Cells were stained with 50 µL of LDLR staining solution overnight at 4°C after aspirated blocking solution. After washing three times with 100 µL of PBS, cells were incubated with 100 µL of fluorochrome-conjugated secondary antibody solution for 1 hr at room temperature in the dark. During the last 15 min of secondary antibody incubation, 30 µL of hoechst

staining solution were added into each well. Aspirated all solution, cells were rinsed three times in 100 μL of PBS and stored in 100 μL of PBS for imaging.

Quantification of images

Fluorescence images were obtained using IN Cell Analyzer 1000 (GE Healthcare, Amersham Place, UK), analyzed using IN Cell Developer Toolbox 1.9 (GE Healthcare), and visualized by Spotfire DecisionSite Client 8.2 software (PerkinElmer, Waltham, MA, USA).

Fluorescence SA-β-gal assay

Preparation of solutions

PBS (pH 6.0)

Mix solution containing 40 mM disodium hydrogen phosphate (Na_2HPO_4) and 150 mM sodium chloride (NaCl) with solution containing 40 mM monosodium phosphate (NaH_2PO_4) and 150 mM NaCl to final pH 6.0.

Fixation solution

5.4 mL of 37% formaldehyde and 1 mL of 20% glutaraldehyde were mixed in ddH_2O until the final volume was 50 mL.

SA-β-gal solution

ImaGene Green C_{12}FDG (Thermo Fisher Scientific, MA, USA), a fluorescein-based β-galactosidase substrate, was dissolved in DMSO to the concentration was 20 mM. The SA-β-gal solution, containing 33 μM C_{12}FDG, was prepared with 1 μL of 20 mM C_{12}FDG stock in 605 μL of PBS (pH 6.0).

Hoechst solution

Hoechst solution was prepared by 1 µL of 1 mg/1 mL Hoechst 33342 solution in 1 mL of PBS (PH 6.0).

Cell staining protocol

HepG2 cells were seeded 1 x 10^4 cells per well in µclear fluorescence black 96-well plate (Greiner Bio-One, Tokyo, Japan). After treatment was complete, the supernatant was removed. Cells were fixed in 100 µL of fixation solution for 10 min at room temperature, then cells were washed twice with PBS (pH 6.0). Cells were incubated with 50 µL of SA-β-gal solution for 10 min at room temperature and followed by washed twice with PBS (pH 6.0). After that, cells were stained with 50 µL of Hoechst solution for 30 min. When incubation finished, the solution was removed and added 100 µL of PBS (pH 6.0) to each well.

Quantification of images

The image of C12FDG and Hoechst 33342 from each well was obtained by an IN Cell Analyzer 1000 (GE Healthcare, Amersham Place, UK) using 360-nm and 480-nm excitation filters, separately, with a 20 × objective. The images of Hoechst 33342 and fluorescent SA-β-Gal staining were quantified using Spotfire DecisionSite Client 8.2 software. The quantified image results were revealed as SA-β-Gal intensity (mean fluorescence intensity per cells) and the number of SA-β-Gal positive/negative cells. The setting of the threshold of SA-β-Gal intensity was 75% of all control cells as negative.

RNA isolation and quantitative real time polymerase chain reaction (qPCR)

HepG2 cells were seeded by 0.5 × 10^6 cells in 30 mm dishes. After treatment was complete, cells were washed with 1 mL of cold-PBS and were scraped with 0.5 mL of solution D reagent (4 M guanidinium thiocyanate, 25 mM sodium citrate, 0.5% (wt/vol) *N*-laurosylsarcosine, and 0.1 M 2-mercaptoethanol). Cell samples were mixed with solutions sequentially, including 50 μL of 2 M sodium acetate, 500 μL of water-saturated phenol, and 100 μL of chloroform: isoamyl alcohol (49:1, vol/vol), and were allowed to react on ice for 15 min, then centrifuged at 15,000 rpm for 15 min. Five hundred μL of the supernatant was collected and was mixed with 500 μL of isopropanol, following by reacting on -20 °C for 1h. After centrifugation at 15,000 rpm for 20 min, the supernatant was discarded, and the RNA pellet was stored in 75% ethanol or dissolved in DEPC water for quantification. Complementary DNA (cDNA) was synthesized from 1 μg total RNA using the Transcriptor First Strand cDNA Synthesis Kit (Roche, Switzerland). Expression levels of genes were analyzed using qRT-PCR with an Mx3000P Real-Time PCR System (CA, USA) and SYBR Premix Ex Taq:Perfect Real-time kit (Takara Bio., Shiga, Japan). The mRNA levels were normalized using ACTB (β-actin). Primer sequences used for the analysis are shown in **Table 16.**

Table 16. Human primers for qRT-PCR.

Gene name	Forward primer	Reverse primer
PCSK9	ATCCACGTTCCTGCTGC	CACGGTCACCTGCTCCTG
LDLR	AGGSGSCGTGCTTGTCTGTC	CTGAGCCGTTGTCGCAGT
SR-B1	TCCTCACTTCCTCAACGCTG	TCCCAGTTTGTCCAATGCC
HMGCR	CAGGACCCTTTGCTTAGATG	ACCTCCACCAAGACCTATTGCTC
SREBP-2	TGTGTATGTCCTGTGCCTTTTC	TGGGACACAGTGACTGATTGAT
ACAT1	CCACTGGTCCAGATGAGTTTAG	GGGAACATGCAGAGTACCTT

ACAT2	ACGTTGCCAGGCATCTTCAT	AGTCATGGACCACCACGTTC
ABCA1	CGAACAGTACACATTTGTCAGC	GTGTCTGGGATTGGGTTTCCTTC
apo-A1	GCCGTGCTCTTCCTGACGG	TGGGACACATAGTCTCTGCCGC
CHOP	AAGGCACTGAGCGTATCATGT	TGAAGATACACTTCCTTCTTGAACA
XBP1	CCTGGTTGCTGAAGAGGAGG	CCATGGGGAGATGTTCTGGAG
p16	GGCACCAGAGGCAGTAACCA	GGACCTTCGGTGACTGATGATCTAA
p21	TCAAATCGTCCAGCGACCTTC	GTCCATAGCCTCTACTGCCACCA
ACTB	GAGCTACGAGCTGCCTGACG	GTAGTTTCGTGGATGCCACAG

Western blot analysis

HepG2 cells were seeded by 0.5 × 10^6 cells in 30 mm dishes. After treatment was complete, cells were washed with 1 mL of cold-PBS and were scraped with 100 μL of RIPA buffer (50 mM Tris-HCl, pH 7.4, 150 mM NaCl, 1% Trition X-100, 1 mM EDTA, 0.5% sodium deoxycholate, 0.1% SDS, 1% protease inhibitor and 1x phosphatase inhibitor). Cell homogenates were centrifuged at 15,000 rpm for 15 min at 4 °C. The supernatant was collected for protein quantification. The total protein was determined by use of the Bio-Rad DC protein assay dye reagent concentrate (Bio-Rad). Protein samples for electrophoresis were diluted to 1 μg/mL by 4x sample buffer (0.5 M Tris-HCl, pH 6.8, 20% SDS, 100% glycerol, bromophenol blue, and 2-mercaptoethanol) and RIPA buffer and heated at 95 °C for 5 min. Diluted protein samples (10 μg protein for each lane) were electrophoresed in 12% SDS-polyacrylamide gels for 2h at 100 V and transferred onto a polyvinylidene fluoride (PVDF) membrane (Hybond-P, GE Healthigh-carbohydrateare) for 1 h at 39 mA. After then, PVDF membranes were blocked with 5 % nonfat dry milk in phosphate buffered saline containing Tween® 20 (PBST) buffer at room temperature for 2 h, and then washed with PBST twice for three times (5 min/each time). Membranes were probed with primary antibodies with anti-PCSK9 (1:1000, #sc-515082, Santa Cruz

Biotechnology, TX, USA), anti-α-Tubulin (1:6000), anti-p-p38 MAPK (1:1000, #sc-166182, Santa Cruz Biotechnology, TX, USA), and p-21 Waf1/Cip1 (1:1000, #sc-6246, Santa Cruz Biotechnology, TX, USA) at 4°C for overnight, and then incubated in secondary antibody with anti-mouse-IgG (1:1000) or anti-rabbit-IgG (1:1000) for 1 h at room temperature. The bands were visualized by using an ECL prime detection reagents (GE Healthigh-carbohydrateare, IL, US) and were scanned by a Image Quant LAS 4000 (GE Healthigh-carbohydrateare IL, US). The bands were quantitated with **ImageJ software (2020 ver.)**.

Statistical analysis

Data were analyzed by using analysis of SPSS version 20 (IBM Japan, Ltd., Tokyo, Japan). The significance of the difference between mean values was determined by one-way analysis of variance followed by Tukey's test; p values <0.05 were taken to be statistically significant.

Results

Effect of D-psicose on the cell viability of HepG2 in the presence of PA

The CCK-8 assay was used to test whether the concentrations of D-psicose used in the presence of PA caused cell damage. As shown in **Fig. 13**, HepG2 cells in the presence of D-psicose (25 mM) and PA (100 μM) did not exhibit adverse cell viability after 24 h incubation.

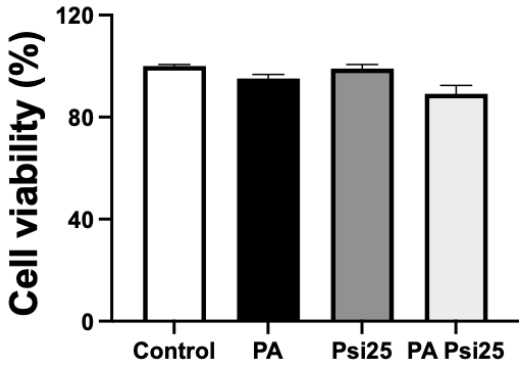

Figure 13. Effect of d-psicose on the cell viability of HepG2 in the presence of PA.

Cells were treated with 100 μM PA and 25 mM d-psicose for 24 h. Cell viability was determined by using the CCK-8 assay. Values are presented as means ± standard error of the mean (SEM) (n = 3/group). PA, Palmitic acid; Psi25, D-psicose 25 mM; PA Psi25, Palmitic acid with D-psicose 25 mM.

D-psicose inhibits PA-induced cholesterol accumulation

To examine the role of D-psicose in PA-induced cholesterol accumulation, cells were treated with 25 mM D-psicose and PA for 24h. The content of cholesterol and lathosterol were significantly increased by PA, and this observation was reversed by D-psicose **(Fig 14)**.

Subsequently, we examined the related mechanism about cholesterol metabolism. The mRNA expression of main transcription factor and rate-limiting enzyme about cholesterol synthesis, SREBP-2 and HMGCR, were enhanced by PA, and the increase was attenuated by D-psicose **(Table 17)**. In cholesterol esterification, the mRNA level of ACAT2 was higher in D-psicose with PA group than control group **(Table 17)**. Both mRNA expression of LDLR and PCSK9 were induced by PA, and this induction of PCSK9 was inhibited by D-psicose, however, D-psicose elevated LDLR about this induction **(Table 17)**. Regarding

protein expression of PCSK9, the same result was observed as at the mRNA level, which was increased by PA, and this induction was suppressed by D-psicose **(Fig. 15)**. The content of LDLR areas was inhibited in the presence of PA, but D-psicose abolished this decrease **(Fig. 15)**. In addition, mRNA level of ABCA1 was significantly elevated in D-psicose with PA group, and mRNA level of apo-A1 was significantly increased in both of PA group and D-psicose with PA group **(Table 17)**.

D-psicose reverses PA-induced ER stress

The main transcription factor of cholesterol metabolism SREBP-2 is storage in ER by non-active form under the case of cellular sufficient sterols. When cellular sterols are insufficient or ER stress occurs, SREBP-2 translocate to Golgi and is activated, then enters the nucleus to upregulate target genes expression [14]. ER stress instigates by unfolded protein response (UPR). There are three key UPR signaling pathways, including inositol requiring enzyme 1α/β (IRE1)-X-box-binding protein 1 (XBP1) pathway, PKR-like ER kinase (PERK)-activation transcription factor 4 (ATF4) pathway, and activation transcription factor 6 (ATF6) pathway [184]. Activation of those three UPR pathways leads to the upregulation of C/EBP-homologous protein (CHOP), which is a transcription factor to mediate apoptosis. PA is proved to inspire ER stress in hepatocytes. In the present study, we focused on ER stress downstream transcription factors in attenuation of PA-induced activation by D-psicose. As shown in **Table 17**, the presence of PA-induced the gene expression of CHOP and XBP-1, and the induction was attenuated by D-

psicose. These data suggested that D-psicose improved ER stress which resulted from PA.

D-psicose ameliorates PA-induced cellular senescence

Reportedly, cellular senescence was observed in hepatocytes under the condition of PA-induced lipid accumulation. Zhang et al. study showed that liver cholesterol content was elevated in the senescence mice model [172]. Thus, we speculated that there had a relationship between cellular senescence and dysregulated cholesterol metabolism. As shown in **Fig. 16A**, D-psicose reduced the activity of SA-β-galactosidase which was elevated by PA. Thereafter, we determined the role of D-psicose in the mechanism of PA-induced cell senescence. As shown in **Fig. 16B**, PA significantly increased p38 phosphorylation and p21 protein level, and D-psicose inhibited those enhancements. As for the gene expression, both mRNA levels of p16 and p21 were elevated by PA, but only the increase of p21 was abolished by D-psicose.

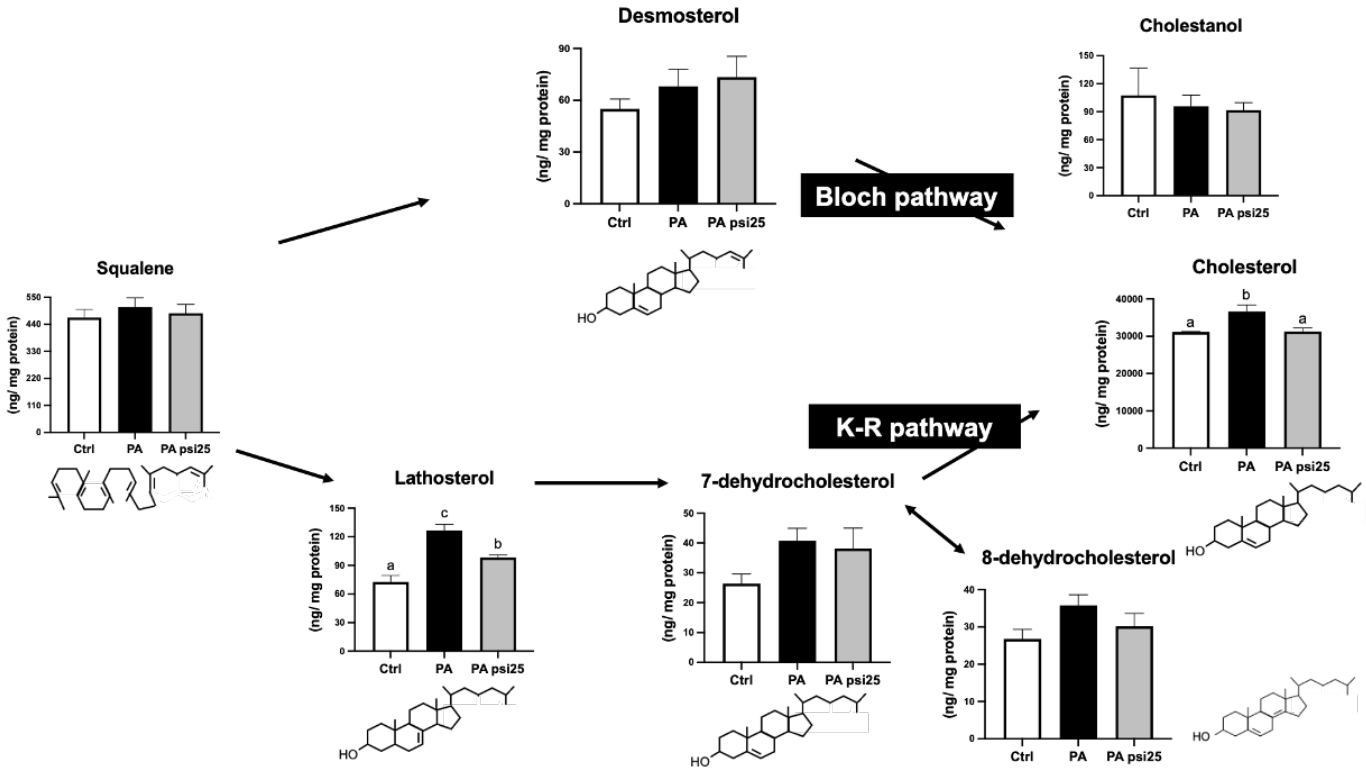

Figure 14. Effect of d-psicose on the hepatic cholesterol precursors of HepG2 in the presence of palmitic acid (PA).

Cells were treated with 100 μM PA and 25 mM D-psicose for 24 h. Cholesterol and its precursors was measured by GC-FID. Values are presented as means ± standard error of the mean (SEM) (n = 5/group). Values not sharing the same letter are significantly different ($p<0.05$). Ctrl, control; PA, Palmitic acid; PA Psi25, Palmitic acid with D-psicose.

Table 17. Effects of D-psicose on PA-induce cholesterol metabolism, ER stress, and cell senescence related gene expression levels in HepG2 cells

	Control	Palmitic acid 100 μM	Palmitic acid 100 μM + D-Psicose 25 mM
	(Fold of control)		
Cholesterol uptake			
PCSK9	1.0 ± 0.00 a	1.5 ± 0.06 b	0.9 ± 0.17 a
LDLR	1.0 ± 0.00 a	1.4 ± 0.09 b	2.1 ± 0.09 c
SR-B1	1.0 ± 0.00 a	1.6 ± 0.10 c	1.3 ± 0.06 b
Cholesterol synthesis			
HMGCR	1.0 ± 0.00 a	1.5 ± 0.07 b	1.1 ± 0.07 a
SREBP-2	1.0 ± 0.00 a	1.3 ± 0.04 b	0.8 ± 0.09 a
Cholesterol esterification			
ACAT1	1.0 ± 0.00	1.2 ± 0.10	1.3 ± 0.14
ACAT2	1.0 ± 0.00 a	1.3 ± 0.05 ab	1.5 ± 0.13 b
Cholesterol excretion			
ABCA1	1.0 ± 0.00 a	1.0 ± 0.09 a	1.7 ± 0.11 b
apo-A1	1.0 ± 0.00 a	1.9 ± 0.16 b	1.6 ± 0.13 b
ER stress			
CHOP	1.0 ± 0.00 b	1.2 ± 0.03 c	0.7 ± 0.05 a
XBP1	1.0 ± 0.00 a	1.3 ± 0.02 b	1.1 ± 0.05 a
Cell senescence			
p16	1.0 ± 0.00 a	1.5 ± 0.07 b	1.3 ± 0.15 ab
p21	1.0 ± 0.00 a	1.4 ± 0.03 c	1.2 ± 0.02 b

Values are means ± standard error of the mean (SEM). Significant differences between mean values were evaluated using Tukey test. Values not sharing the same letter are significantly different ($p<0.05$). PCSK9, Proprotein convertase subtilisin/kexin type 9; LDLR, Low-density lipoprotein receptor; SR-B1, Scavenger receptor class B type 1; HMGCR, 3-hydroxy-3-methylglutaryl-coenzyme A reductase; SREBP-2, Sterol regulatory element-binding protein 2; ACAT-1, Acetyl-coenzyme A acetyltransferase 1; ACAT-2, Acetyl-coenzyme A acetyltransferase 2; ABCA1, ATP binding cassette subfamily A member 1; apo-A1, Apolipoprotein A1; CHOP, CCAAT-enhancer-binding protein homologous protein; XBP1, X-box binding protein 1; p16, cyclin-dependent kinase inhibitor 2A; p21, cyclin-dependent kinase inhibitor 1A.

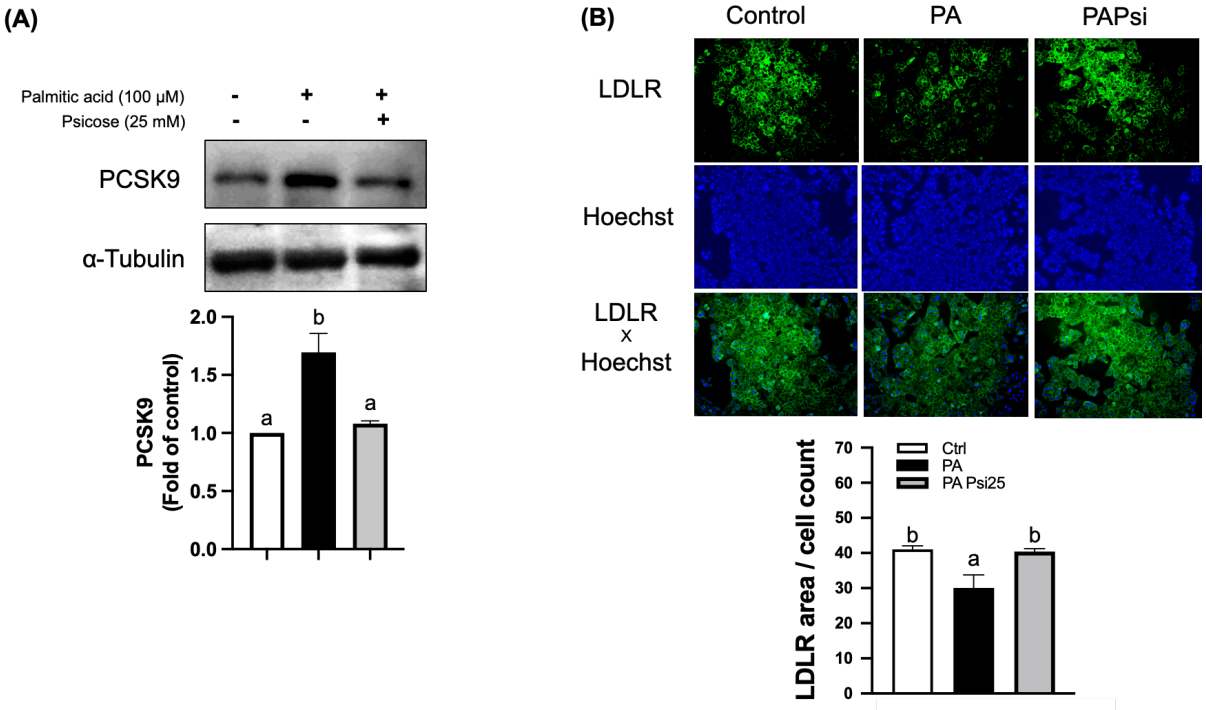

Figure 15. D-psicose reverses PA-induced increasing expression of PCSK9 and suppressing expression of LDLR.

Cells were treated with 100 μM PA and 25 mM D-psicose for 24 h. (A) PCSK9 protein expression was determined by Western blot analysis. (B) LDLR area was determined by Immunofluorescence staining. Values are presented as means ± standard error of the mean (SEM) (n = 3/group). Values not sharing the same letter are significantly different ($p<0.05$). PCSK9, Proprotein convertase subtilisin/kexin type 9; LDLR, Low-density lipoprotein receptor.

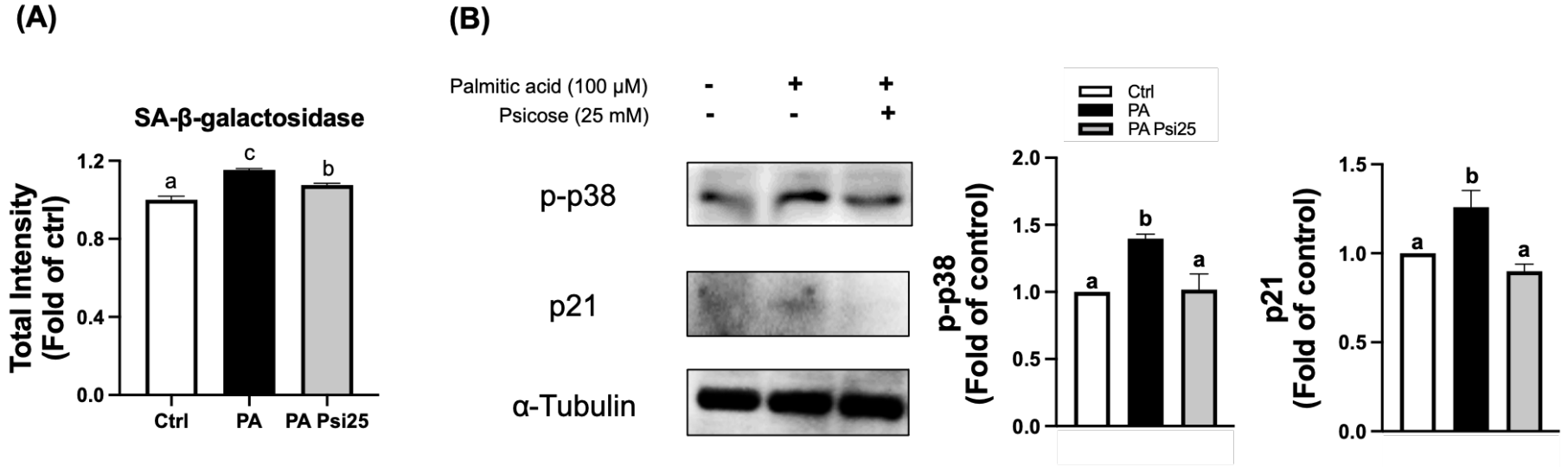

Figure 16. D-psicose attenuate PA-activation p-p38 and p-21 expression.

Cells were treated with 100 μM PA and 25 mM D-psicose for 24 h. (A) Activity of SA-β-Gal was measured by Immunofluorescence staining. (B) p-p38 and p-21 protein expression was determined by Western blot analysis. Values are presented as means ± standard error of the mean (SEM) (n = 3/group). Values not sharing the same letter are significantly different ($p<0.05$). p-p38, Phospho-p38 mitogen-activated protein kinase; p21, cyclin-dependent kinase inhibitor 1A.

Discussion

The abnormalities in cholesterol homeostasis are correlated with the severity of NAFLD [44]. Inhibition of cholesterol accumulation in the liver is contributing to decelerating the development of NAFLD. In this study, we found in the cell model of NAFLD that D-psicose ameliorates PA-induced hepatic cholesterol accumulation via decreasing cholesterol synthesis and promoting cholesterol excretion. Moreover, this is the first study showing the improvement effect on PA-induced hepatocyte senescence by D-psicose which inhibits the activation of p38-p21 pathway.

D-psicose has been proved to regulate the serum level of lipoprotein cholesterol in studies of humans and animals [66.182-183]. Our previous study on hamsters showed that D-psicose significantly suppressed serum PCSK9 levels and led to reducing serum LDL levels. As a negative regulator of hepatic LDLR, hepatic synthetic and secreted PCSK9 mediates the degradation of LDLR through binding to LDLR and then directing it to lysosomes [187]. Thus, effective suppression of synthetic and secreted PCSK9 in the liver is contributed to the elimination of circulating LDL-c. It is known that the expression of both the PCSK9 and LDLR genes is transcriptionally regulated by SREBP-2. SREBP-2 upregulates PCSK9 gene expression by binding to SRE in the PCSK9 promoter [188]. Lebeau et al reported that caffeine reduced mRNA and protein expression of PCSK9 in hepatocytes by blocking transcriptional activation of SREBP-2 [189]. Similar to this observation, our results suggested that the inhibition effect of D-psicose on PCSK9 expression occurred at the transcriptional level. Although *LDLR* mRNA expression is transcriptional regulated by SREBP-2, but LDLR protein level on the cell

surface is post-translational regulated by PCSK9. Our finding indicated that D-psicose against the PA-induced reduction of LDLR protein, thereby increasing the LDL uptake.

ER stress has been reported to be responsible for the activation of the SREBP2-induced hepatic PCSK9 expression [190]. Hepatic lipid accumulation has been implicated in ER stress, and palmitic acid and high-fat diet promote steatosis in the liver [61]. In the case of ER stress, ER stress marker expression (GRP78, XBP1, CHOP, e.t.) is upregulated, and SREBP is activated [191]. The possible mechanisms of SREBP activation by ER stress have been proposed including decreasing expression of Insig-1 (a negative regulator of the SREBPs) [192], activating S1P (production of mature forms of SREBP) [193], or promoting dissociation of GRP78 from the SCAP-SREBP complex (liberation of SREBP from ER) [194]. Some phytochemicals such as caffeine are recently reported to against ER stress and suppress the activation of SREBP [189]. To date, whether D-psicose protects against PA-induced ER stress plays remains unclear. In this study, our data showed that D-psicose inhibited PA-induced expression of ER stress (XBP1and CHOP), suggesting that D-psicose suppressed the activation of the SREBP-2-PCSK9 pathway through alleviating ER stress.

In addition to upregulating PCSK9 transcription, SREBP-2 mediates the expression of *de novo* cholesterol-related genes, such as *HMGCR*. Analysis of *HMGCR* mRNA level and cholesterol precursors revealed that D-psicose suppressed PA-enhanced *de novo* cholesterol synthesis **(Fig. 14)**. The cholesterol synthesis pathway begins with the formation of lanosterol from acetate via a series of multistep enzymatic processes. Lanosterol can follow

either the Bloch or the Kandutsch-Russell (K-R) pathway to ultimately the conversion into cholesterol. Some human studies have reported that an increase in K-R pathway intermediate lathosterol is positive correlate with liver lipid content [195-196]. In this study, D-psicose decreased hepatic lathosterol levels, indicating that D-psicose blocked PA-induced *de novo* cholesterol synthesis through the K-R pathway.

SR-B1 is another lipoprotein receptor that mediates HDL selective uptake by the liver. Studies have demonstrated that hepatic SR-B1 expression affects atherosclerosis: liver-specific lack of SR-B1 induces atherosclerosis [197], while overexpression of hepatic SR-B1 shows the preventive effect of atherosclerosis [198]. In addition, SR-B1 is regarded as the anti-NAFLD receptor [199-200]. The enhancement of liver SR-B1 expression has been shown to attenuate the development of NAFLD in rats and mice [199-200]. D-psicose increases HDL-C uptake by elevating protein expression of SR-B1 had been previously reported in rat's primary hepatocyte [182]. But in this study, we found that D-psicose suppressed the increase in SR-B1 gene levels induced by PA **(Table 18)**. In HepG2 cells of saturated fatty acid-induced lipid accumulation models, PA elevates the gene and protein expression of PPAR-γ [201], which upregulates SR-B1 [202]. Reportedly, The suppression of HFD-induced hepatic SR-B1 expression in mice by KMUP-1 (7-[2-[4-(2-chlorophenyl) piperazinyl]ethyl]1,3-dimethylxanthine) was attributed to its down-regulation of PPAR-γ [203]. In this study, the PA-induced increase in SR-B1 expression was attenuated by D-psicose, it is likely that mediated by PPAR-γ.

The efflux of cholesterol from the liver to the circulation is mediated by ABCA1 to prevent hepatic excess cholesterol accumulation. ABCA1 regulates

the transport of cholesterol and phospholipid on the cell membrane to apo-A1 for the formation of HDL particles [204]. In this study, we detected a significant increase in hepatic ABCA1 and apo-A1 mRNA levels in presence of D-psicose, which suggested that D-psicose promotes hepatic cholesterol efflux.

Several clinical studies have indicated that hepatocyte senescence is associated with the progression of NAFLD [205-206]. Decreased ability to metabolize lipids by hepatocyte senescence that drives lipid accumulation has been reported in high-fat diet-fed or old age mice [205-206]. The expression of cell cycle suppressors (p16 and p21) and SA-β-gal are an indicator of cellular senescence [205]. p16 and p21 prevent cell cycle progression through combing to CDK to inhibit the phosphorylation of Rb [208]. Cell studies have shown that mitogen-activated protein kinases (MAPK), especially p38, play crucial roles in the activation of those cell cycle arrest pathways [206. 209-210]. In addition, an increase in the activity of SA-β-gal is accompanied by increases in lysosomal content and size in senescent cells [211]. An expansion in lysosomal volume has also been observed in the process of autophagy [212]. Senescence and autophagy may induce simultaneously by oxidative stress, this process is mediated by p38α activation [213-214]. In this study, D-psicose diminished PA-induced SA-β-gal activity and p-p38 and P21 protein expression, which suggests that D-psicose improves PA-induced hepatocyte senescence via inhibiting MAPK p-38-p21 pathway. Regulation mechanisms of D-psicose on autophagy need to be clarified in future studies.

Summary

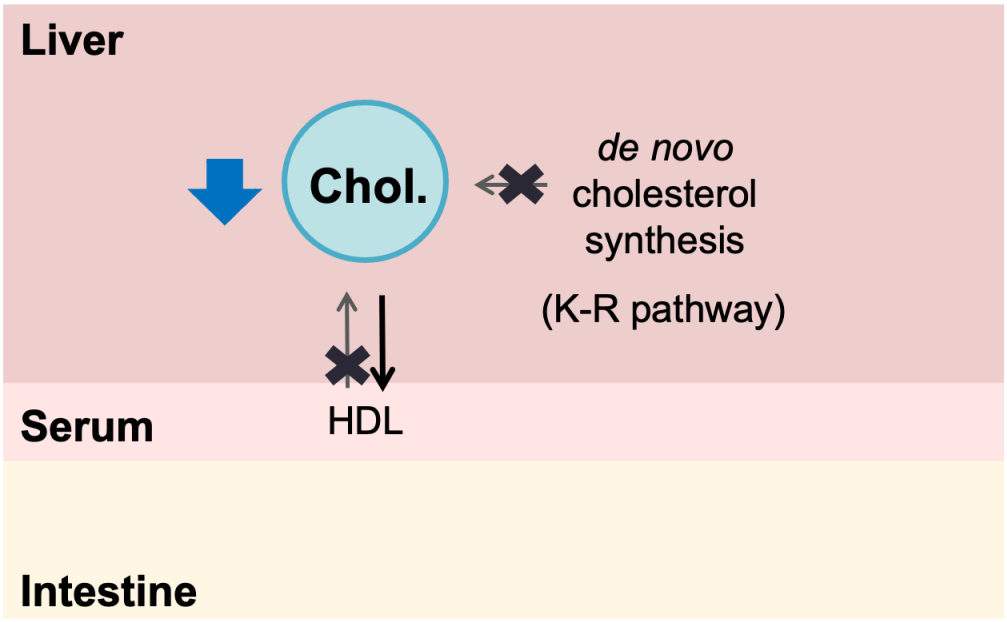

Figure 17. The effect of D-psicose on cholesterol metabolism in PA-induce NAFLD.

D-psicose had been proved to prevent hepatic fat accumulation by suppressing lipogenesis and elevating fatty acid oxidation. However, studies on the effect of D-psicose on cholesterol metabolism are still few. Our previous hamster study shows that D-psicose significantly reduces serum PCSk9 levels. Herein, we investigated the effect of D-psicose on PA-induced dysregulated cholesterol metabolism in HepG2 cells.

D-psicose abolished PA-inhibited protein expression of LDLR resulting from significantly decreasing PCSK9 protein expression. D-psicose suppressed the mRNA level of SREBP-2, thus downregulating PCSK9 expression at the transcriptional level. A decreasing activation of SREBP-2 to reduce SREBP-2 gene expression is attributed to D-psicose ameliorating PA-induced ER stress. Moreover, D-psicose reversed PA-induced cholesterol synthesis by inhibiting the flux of the K-R pathway. D-psicose greatly increased

mRNA expression of ABCA1 and apo-A1 to promote cholesterol efflux from hepatocytes. Based on our findings, D-psicose improved PA-induced hepatic cholesterol accumulation by decreasing cholesterol synthesis and increasing cholesterol efflux.

We also found that D-psicose significantly decreased PA-enhanced senescence marker protein expression of p21 and activity of SA-β-gal. Additionally, D-psicose diminished the phosphorylation of p38, which is the activator of cell cycle arrest. These data showed that D-psicose ameliorates PA-induced hepatocyte senescence through preventing cell cycle arrest of the p-p38-p21 pathway.

According to these findings, D-psicose exhibits an improved effect on cholesterol accumulation in the NAFLD progression (**Fig. 17**).

Summary and Conclusions

Table 18. The effect of food ingredients on lipid metabolism with cell or animal models in NAFLD.

	Study I	Study II	Study III
Food ingredients	Sucrose	Soyasaponins	D-psicose
Liver TAG	↑	↓	↓
Liver cholesterol	↓	↑	↓
Steatosis (Fatty liver)	High	Low	Low
Steatohepatitis	Low	High	Low

In this paper, we examined the effect of food ingredients on cholesterol metabolism in NAFLD cell or animal models and further described its working mechanism.

In CHAPTER II PART 1, we studied the effect of dietary ingredients on cholesterol metabolism. It has been known that excessive consumption of carbohydrates increased the risk of suffering from NAFLD. In this study, rats were fed equivalent carbohydrate diets (sucrose or starch, 67% of total calories) containing 0.2% cholesterol. From the results, high sucrose diet had lower hepatic cholesterol accumulation than high starch diet, resulting from high sucrose diet promoting the bioformation of coprostanol from cholesterol. in addition, high sucrose diet has an increased tendency in hepatic TAG content. The above results indicated that dietary sucrose has a prevention effect on overaccumulation of hepatic cholesterol (**Table 18)**.

In CHAPTER II PART 2, the effects of SAP on cholesterol metabolism were investigated. Herein, we fed mice HFD (39 % energy from fats) to induce NAFLD. Mice were fed for 9 weeks, and SAP markedly increased the deposition of hepatic cholesterol, because of elevating intestinal cholesterol absorption and inhibiting the excretion and utilization of cholesterol. Moreover, SAP had an improved effect on HFD-induced hepatic TAG accumulation by suppressing lipogenesis. These evidences showed that SAP exacerbated the abnormality of hepatic cholesterol metabolism (**Table 18**).

In CHAPTER III, the effect of D-psicose on cholesterol metabolism in the NAFLD cell model was investigated. In this study, we used the PA-induced NAFLD on the HepG2 cell model. D-psicose effectively disturbed *de novo* cholesterol synthesis and promoted cholesterol efflux to reverse PA-caused accumulation of hepatic cholesterol. Due to the alleviation of ER stress to block the SREBP-2 and PCSK9 pathways, D-psicose promoted an increase in hepatic LDLR levels. Furthermore, D-psicose inhibited the activation of the p38-p21 pathway for ameliorating PA-induced hepatocyte senescence. These results suggested that D-psicose can improve the disorder of cholesterol metabolism in NAFLD status (**Table 18**).

In summary, in animal models of NAFLD, sucrose increases hepatic TAG contents coincident with reducing hepatic cholesterol levels, whereas SAP improves hepatic TAG accumulation and simultaneously accelerates hepatic cholesterol deposition. In cell models of NAFLD, D-psicose prevents cholesterol accumulation in hepatocytes. These findings suggest that the regulations by each food ingredient on hepatic cholesterol metabolism in NAFLD development are in different mechanisms.

Acknowledgments

The author is especially indebted to my supervisor, Dr. Masao Sato, Professor of Laboratory of Nutrition Chemistry, for his patient guidance, enthusiastic encouragement, and useful critiques of this research. This paper and the research behind it would not have been possible without his exceptional support.

The author would also like to extend her deep thanks to Dr. Yasutake Tanaka, Assistant Professor of Laboratory of Nutrition Chemistry, for his advice, and guidance on my experiment as well as his constructive comments on my doctoral thesis.

The author is also immensely grateful to Dr. Bungo Shirouchi, Associate Professor of University of Nagasaki, for his encouragement and professional guidance in my doctoral course.

The author's grateful thanks are also extended to Dr. Yoshinori Katakura, Professor of Laboratory of Cellular Regulation Technology, for his help in doing the cell data analysis.

The author wishes to thank her family members, especially her father, Haumin Tsai, for inspiring her to study in Japan and providing their spiritual support, encouragement, and financial support throughout her doctoral life.

The author wants to acknowledge Japan-Taiwan Exchange Association for providing a scholarship that has been provided in the past a year and a half so that she could concentrate on her doctoral study without worrying about finances.

Moreover, the author also expresses appreciation to Zhe Jiang, Ai Takeyama, Xingyu Yuan, Yuki Nakamura, Saki Inoue, and all the other members of Laboratory of Nutrition Chemistry for their numerous help during the past three years.

Literature cited

Introduction

1. Soccio RE, Breslow JL. Intracellular cholesterol transport. Arterioscler Thromb Vasc Biol. 2004, 24:1150-1160.

2. Hu J, Zhang Z, Shen WJ et al. Cellular cholesterol delivery, intracellular processing and utilization for biosynthesis of steroid hormones. Nutr Metab (Lond). 2010, 7:47.

3.Luu W, Sharpe LJ, Capell-Hattam I et al. Oxysterols: old tale, new twists. Annu Rev Pharmacol Toxicol. 2016, 56: 447-467.

4. Ministry of Health, Labour and Welfare. 2020. Dietary Reference Intakes for Japanese.

5. Musso G, Gambino R, De Michieli F et al. Dietary habits and their relations to insulin resistance and postprandial lipemia in nonalcoholic steatohepatitis. 2003, 37:909-916.

6. Allard JP, Aghdassi E, Mohammed S et al. Nutritional assessment and hepatic fatty acid composition in non-alcoholic fatty liver disease (NAFLD): a cross-sectional study. J Hepatol. 2008, 48:300-307.

7. Neuschwander-Tetri BA. Hepatic lipotoxicity and the pathogenesis of nonalcoholic steatohepatitis: the central role of nontriglyceride fatty acid metabolites. Hepatology. 2010, 52: 774-788.

8. Wouters K, van Bilsen M, van Gorp PJ et al. Intrahepatic cholesterol influences progression, inhibition and reversal of non-alcoholic steatohepatitis in hyperlipidemic mice. FEBS Lett. 2010, 584:1001-1005.

9. Nascimbeni F, Aron-Wisnewsky J, Pais R et al. Statins, antidiabetic medications and liver histology in patients with diabetes with non-alcoholic fatty liver disease. BMJ Open Gastroenterol. 2016, 3: e000075.

10. Kim RG, Loomba R, Prokop LJ et al. Statin use and risk of cirrhosis and related complications in patients with chronic liver diseases: a systematic review and meta-analysis. Clin Gastroenterol Hepatol. 2017, 15: 1521-1530.

11. Dietschy JM. Central nervous system: cholesterol turnover, brain development and neurodegeneration. Biol Chem. 2009, 390: 287-293.

12. Altmann SW, Davis HR Jr, Zhu LJ et al. Niemann–Pick C1 like 1 protein is critical for intestinal cholesterol absorption. Science. 2004, 303:1201-1204.
13.Brown MS, Goldstein JL et al. The SREBP pathway: regulation of cholesterol metabolism by proteolysis of a membrane-bound transcription factor. Cell. 1997, 89: 331-340.
14. Gong X, Qian H, Shao W et al. Complex structure of the fission yeast SREBP-SCAP binding domains reveals an oligomeric organization. Cell Res. 2016, 26, 1197-1211.
15. Brown MS, Radhakrishnan A, Goldstein JL et al. Retrospective on cholesterol homeostasis: the central role of Scap. Annu Rev Biochem. 2018, 87, 783-807.
16. Wijers M, Kuivenhoven JA, van de Sluis B et al. The life cycle of the low-density lipoprotein receptor: insights from cellular and in-vivo studies. Curr Opin Lipidol. 2015, 26, 82-87.
17. Brown MS, Herz J, Goldstein JL et al. LDL-receptor structure. Calcium cages, acid baths and recycling receptors. Nature. 1997, 388, 629-630.
18. Goldstein JL, DeBose-Boyd RA, Brown MS et al. Protein Sensors for Membrane Sterols. Cell. 2006, 124, 35-46.
19. Lagace TA. PCSK9 and LDLR degradation: regulatory mechanisms in circulation and in cells. Curr Opin Lipidol. 2014, 25 :387-393.
20. Horton JD, Goldstein JL, Brown MS. SREBPs: activators of the complete program of cholesterol and fatty acid synthesis in the liver. J Clin Invest. 2002, 109: 1125-1131.
21. Papale GA, Nicholson K, Hanson PJ et al. Extracellular hydrophobic regions in scavenger receptor BI play a key role in mediating HDL-cholesterol transport. Arch Biochem Biophys. 2010 , 496: 132-139.
22. Pittman RC, Knecht TP, Rosenbaum MS et al. A nonendocytotic mechanism for the selective uptake of high density lipoprotein-associated cholesterol esters. J Biol Chem. 1987, 262: 2443-2450.
23. Dong B, Singh AB, Guo GL et al. Activation of FXR by obeticholic acid induces hepatic gene expression of SR-BI through a novel mechanism of transcriptional synergy with the nuclear receptor LXR. Int J Mol Med. 2019, 43: 1927-1938.

24. Nes WD. Biosynthesis of cholesterol and other sterols. Chem Rev. 2011, 111:6423-6451.
25. Goldstein JL, Brown MS. Regulation of the mevalonate pathway. Nature. 1990, 343: 425-430.
26. Gill S, Stevenson J, Kristiana I et al. Cholesterol-dependent degradation of squalene monooxygenase, a control point in cholesterol synthesis beyond HMG-CoA reductase. Cell Metab. 2011, 13:260-273.
27. Sun LP, Seemann J, Goldstein JL et al. Sterol-regulated transport of SREBPs from endoplasmic reticulum to Golgi: Insig renders sorting signal in Scap inaccessible to COPII proteins. Proc Natl Acad Sci U S A. 2007, 104:6519-6526.
28.Radhakrishnan A, Goldstein JL, McDonald JG et al. Switch-like control of SREBP-2 transport triggered by small changes in ER cholesterol: a delicate balance. Cell Metab. 2008, 8: 512-521.
29. Mitsche MA, McDonald JG, Hobbs HH et al. Flux analysis of cholesterol biosynthesis in vivo reveals multiple tissue and cell-type specific pathways. Elife. 2015, 4:e07999.
30. Simonen M, Männistö V, Leppänen J et al. Desmosterol in human nonalcoholic steatohepatitis. Hepatology. 2013, 58: 976-982.
31. Oelkers P, Behari A, Cromley D et al. Characterization of two human genes encoding acyl coenzyme A:cholesterol acyltransferase-related enzymes. J Biol Chem. 1998, 273: 26765-26771.
32. Langston TB, Hylemon PB, Grogan WM. Over-expression of hepatic neutral cytosolic cholesteryl ester hydrolase in mice increases free cholesterol and reduces expression of HMG-CoAR, CYP27, and CYP7A1. Lipids. 2005 , 40: 31-38.
33. Li H, Yu XH, Ou X et al. Hepatic cholesterol transport and its role in non-alcoholic fatty liver disease and atherosclerosis. Prog Lipid Res. 2021, 83:101109.
34. Chiang JY. Regulation of bile acid synthesis: pathways,nuclear receptors, and mechanisms. J Hepatol. 2004, 40:539-551.
35. Chiang JY. Bile acids: regulation of synthesis. J Lipid Res. 2009, 50: 1955-1966.

36. Vaz FM, Ferdinandusse S. Bile acid analysis in human disorders of bile acid biosynthesis. Mol Aspects Med. 2017, 56: 10-24.
37. Goodwin B, Jones SA, Price RR et al. A regulatory cascade of the nuclear receptors FXR, SHP-1, and LRH-1 represses bile acid biosynthesis. Mol Cell. 2000, 6:517-526.
38. Wang Y, Liu X, Pijut SS et al.The combination of ezetimibe and ursodiol promotes fecal sterol excretion and reveals a G5G8-independent pathway for cholesterol elimination. J Lipid Res. 2015, 56: 810-820.
39. Repa JJ, Berge KE, Pomajzl C et al. Regulation of ATP-binding cassette sterol transporters ABCG5 and ABCG8 by the liver X receptors alpha and beta. J Biol Chem. 2002, 277:18793-18800.
40. Sabeva NS, Liu J, Graf GA et al. The ABCG5 ABCG8 sterol transporter and phytosterols: implications for cardiometabolic disease. Curr Opin Endocrinol Diabetes Obes. 2009, 16:172-177.
41. Luo J, Yang H, Song BL et al. Mechanisms and regulation of cholesterol homeostasis. Nat Rev Mol Cell Biol. 2020, 21: 225-245.
42. Janowski BA, Willy PJ, Devi TR. An oxysterol signalling pathway mediated by the nuclear receptor LXR alpha. Nature. 1996, 383(6602): 728-731.
43. Puri P, Baillie RA, Wiest MM et al. A lipidomic analysis of nonalcoholic fatty liver disease. Hepatology. 2007, 46: 1081-1090.
44. Min HK, Kapoor A, Fuchs M et al. Increased hepatic synthesis and dysregulation of cholesterol metabolism is associated with the severity of nonalcoholic fatty liver disease. Cell Metab. 2012, 15: 665-674.
45. Lake AD, Novak P, Shipkova P et al. Decreased hepatotoxic bile acid composition and altered synthesis in progressive human nonalcoholic fatty liver disease. Toxicol Appl Pharmacol. 2013, 268:132-140.
46. Raselli T, Hearn T, Wyss A et al. Elevated oxysterol levels in human and mouse livers reflect nonalcoholic steatohepatitis. J Lipid Res. 2019, 60:1270-1283.
47. Jensen T, Abdelmalek MF, Sullivan S et al. Fructose and sugar: A major mediator of non-alcoholic fatty liver disease. J Hepatol. 2018, 68:1063-1075.

48. Chung M, Ma J, Patel K et al. Fructose, high-fructose corn syrup, sucrose, and nonalcoholic fatty liver disease or indexes of liver health: a systematic review and meta-analysis. Am J Clin Nutr. 2014, 100:833-849.
49. Geidl-Flueck B, Hochuli M, Németh Á et al. Fructose- and sucrose- but not glucose-sweetened beverages promote hepatic de novo lipogenesis: A randomized controlled trial. J Hepatol. 2021, 75:46-54.
50. Softic S, Cohen DE, Kahn CR. Role of Dietary Fructose and Hepatic De Novo Lipogenesis in Fatty Liver Disease. Dig Dis Sci. 2016, 61:1282-1293.
51. Flister KFT, Pinto BAS, França LM et al. Long-term exposure to high-sucrose diet down-regulates hepatic endoplasmic reticulum-stress adaptive pathways and potentiates de novo lipogenesis in weaned male mice. J Nutr Biochem. 2018, 62: 155-166.
52. Fernandes-Lima F, Monte TL, Nascimento FA et al. Short Exposure to a High-Sucrose Diet and the First 'Hit' of Nonalcoholic Fatty Liver Disease in Mice. Cells Tissues Organs. 2015 -2016, 201:464-472.
53. Apro J, Beckman L, Angelin B et al. Influence of dietary sugar on cholesterol and bile acid metabolism in the rat: Marked reduction of hepatic Abcg5/8 expression following sucrose ingestion. Biochem Biophys Res Commun. 2015, 461:592-597.
54. Berger JM, Moon YA. Increased Hepatic Lipogenesis Elevates Liver Cholesterol Content. Mol Cells. 2021, 44:116-125.
55. Oliveira LS, Santos DA, Barbosa-da-Silva S. The inflammatory profile and liver damage of a sucrose-rich diet in mice. J Nutr Biochem. 2014, 25:193-200.
56. Berger JM, Moon YA. Hepatic cholesterol synthesis and lipoprotein levels impaired by dietary fructose and saturated fatty acids in mice: Insight on PCSK9 and CD36. Mol Cells. 2021; 44: 116-125.
57. Ichigo Y, Takeshita A, Hibino M et al. High-Fructose Diet-Induced Hypertriglyceridemia Is Associated With Enhanced Hepatic Expression of ACAT2 in Rats. Physiol Res. 2019, 68, 1021-1026.
58. Lai YS, Lee WC, Lin YE et al. Ginger Essential Oil Ameliorates Hepatic Injury and Lipid Accumulation in High Fat Diet-Induced Nonalcoholic Fatty Liver Disease. J Agric Food Chem. 2016, 64: 2062-71.

59. Kant R, Lu CK, Nguyen HM et al. 1,2,3,4,6 penta-O-galloyl-β-D-glucose ameliorates high-fat diet-induced nonalcoholic fatty liver disease and maintains the expression of genes involved in lipid homeostasis in mice. Biomed Pharmacother. 2020, 129:110348.
60. Fan Y, Yan LT, Yao Z et al. Biochanin A Regulates Cholesterol Metabolism Further Delays the Progression of Nonalcoholic Fatty Liver Disease. Diabetes Metab Syndr Obes. 2021, 14: 3161-3172.
61. Ichimura M, Kawase M, Masuzumi M et al. High-fat and high-cholesterol diet rapidly induce non-alcoholic steatohepatitis with advanced fibrosis in Sprague-Dawley rats. Hepatol Res. 2015, 45:458-469.
62. Ioannou GN, Subramanian S, Chait A et al. Cholesterol crystallization within hepatocyte lipid droplets and its role in murine NASH. J Lipid Res. 2017, 58:1067-1079.
63. Boden G, Shulman GI. Free fatty acids in obesity and type 2 diabetes: defining their role in the development of insulin resistance and beta-cell dysfunction. Eur J Clin Invest. 2002, 32:14-23.
64. Mayer C, Côme M, Blanckaert V et al. Effect of Carotenoids from Phaeodactylum tricornutum on Palmitate-Treated HepG2 Cells. Molecules. 2020, 25:2845.
65. Wu L, Guo T, Deng R et al. Apigenin Ameliorates Insulin Resistance and Lipid Accumulation by Endoplasmic Reticulum Stress and SREBP-1c/SREBP-2 Pathway in Palmitate-Induced HepG2 Cells and High-Fat Diet-Fed Mice. J Pharmacol Exp Ther. 2021, 377:146-156.
66. Lebeau PF, Byun JH, Platko K et al. Diet-induced hepatic steatosis abrogates cell-surface LDLR by inducing de novo PCSK9 expression in mice. J Biol Chem. 2019, 294:9037-9047.

CHAPTER II PART1

67. Sievenpiper JL, de Souza RJ, Mirrahimi A et al. Effect of fructose on body weight in controlled feeding trials: a systematic review and meta-analysis. Ann Intern Med 156, 2012: 291-304.
68. Maersk M, Belza A, Stødkilde-Jørgensen H, Ringgaard S et al. Sucrose-sweetened beverages increase fat storage in the liver, muscle, and visceral fat

depot: a 6-mo randomized intervention study. Am J Clin Nutr. 2012, 95: 283-289.
69. Basu S, Yoffe P, Hills N et al. The relationship of sugar to population-level diabetes prevalence: an econometric analysis of repeated cross-sectional data. PLoS One. 2013, 8:e57873.
70. Prinz P. The role of dietary sugars in health: molecular composition or just calories? Eur J Clin Nutr.2019, 73:1216-1223.
71. Bouwman LMS, Nieuwenhuizen AG, Swarts HJM et al. Metabolic effects of the dietary monosaccharides fructose, fructose–glucose, or glucose in mice fed a starch-containing moderate high–fat diet. Physiol Rep 2020, 8:e14350.
72. Softic S, Gupta MK, Wang GX et al. Divergent effects of glucose and fructose on hepatic lipogenesis and insulin signaling. J Clin Invest. 2017, 127:4059-4074.
73. Mastrocola R, Collino M, Rogazzo M et al. Advanced glycation end products promote hepatosteatosis by interfering with SCAP-SREBP pathway in fructose-drinking mice. Am J Physiol Gastrointest Liver Physiol. 2013, 305:G398-407.
74. Rajasekar P, Anuradha CV. Fructose-induced hepatic gluconeogenesis: Effect of l-carnitine. Life Sci. 2007, 80:1176-1183.
75. Arguello G, Balboa E, Arrese M et al. Recent insights on the role of cholesterol in non-alcoholic fatty liver disease. Biochim Biophys Acta. 2015, 1852:1765-1778.
76. Musso G, Gambino R, De Michieli F et al. Dietary habits and their relations to insulin resistance and postprandial lipemia in nonalcoholic steatohepatitis. Hepatology. 2003, 37:909-916.
77. Ichimura M, Kawase M, Masuzumi M et al. High-fat and high-cholesterol diet rapidly induces non-alcoholic steatohepatitis with advanced fibrosis in Sprague-Dawley rats. Hepatol Res. 2015, 45:458-469.
78. Fujiwara A, Murakami K, Asakura K et al. Estimation of Starch and Sugar Intake in a Japanese Population Based on a Newly Developed Food Composition Database. Nutrients. 2018, 10:1474.
79. Kimberly MM, Leary ET, Cole TG et al. Selection, Validation, Standardization, and Performance of a Designated Comparison Method for

HDL-Cholesterol for Use in the Cholesterol Reference Method Laboratory Network. Clin Chem. 1999, 45:1803-1812.
80. Folch J, Lees M, Sloane Stanley GH. A simple method for the isolation and purification of total lipides from animal tissues. J Biol Chem. 1957,226:497-509.
81. Tsai WT, Nakamura Y, Akasaka T et al. Soyasaponin ameliorates obesity and reduces hepatic triacylglycerol accumulation by suppressing lipogenesis in high-fat diet-fed mice. J Food Sci. 2021, 86:2103-2117.
82. Rouser G, Fkeischer S, Yamamoto A. Two dimensional then layer chromatographic separation of polar lipids and determination of phospholipids by phosphorus analysis of spots. Lipids. 1970, 5:494-496.
83. Lo S, Russell JC, Taylor AW. Determination of glycogen in small tissue samples. J Appl Physiol. 1970, 28:234-236.
84. Jiang Z, Kimura Y, Shirouchi B et al. Dietary Egg White Protein Hydrolysate Improves Orotic Acid-Induced Fatty Liver in Rats by Promoting Hepatic Phospholipid Synthesis and Microsomal Triglyceride Transfer Protein Expression. J Nutr Biochem. 2021, 98:108820.
85. Kanasaki A, Jiang Z, Mizokami T et al. Dietary d-allulose alters cholesterol metabolism in Golden Syrian hamsters partly by reducing serum PCSK9 levels. J Funct Foods, 2019, 60:103429.
86. Shirouchi B, Kashima K, Horiuchi Y et al. 27-Hydroxycholesterol suppresses lipid accumulation by down-regulating lipogenic and adipogenic gene expression in 3T3-L1 cells. Cytotechnology. 2017, 69:485-492.
87. Chirgwin JM, Przybyla AE, MacDonald RJ et al. Isolation of biologically active ribonucleic acid from sources enriched in ribonuclease. Biochemistry. 1979, 18:5294-5299.
88. Tanaka Y, Ono M, Miyago M et al. Low utilization of glucose in the liver causes diet-induced hypercholesterolemia in exogenously hypercholesterolemic rats. PLoS One. 2020, 15:e0229669.
89. Lowry OH, Rosebrough NJ, Farr AL et al. Protein measurement with the Folin phenol reagent. J Biol Chem. 1951, 193:265-275.
90. Kelley DS, Nelson GJ, Hunt JE. Effect of prior nutritional status on the activity of lipogenic enzymes in primary monolayer cultures of rat hepatocytes. Biochem J. 1986, 235:87-90.

91. Torres-Villalobos G, Hamdan-Pérez N, Tovar AR et al. Combined high-fat diet and sustained high sucrose consumption promotes NAFLD in a murine model. Ann Hepatol. 2015, 14: 540-546.
92. Liu CH, Huang MT, Huang PC. Sources of triacylglycerol accumulation in livers of rats fed a cholesterol-supplemented diet. Lipids. 1995, 30:527-531.
93. Ravid Z, Bendayan M, Delvin E et al. Modulation of intestinal cholesterol absorption by high glucose levels: impact on cholesterol transporters, regulatory enzymes, and transcription factors. Am J Physiol Gastrointest Liver Physiol. 2008, 295:G873-885.
94. Sadzikowski MR, Sperry JF, Wilkins TD. Cholesterol-reducing bacterium from human feces. Appl Environ Microbiol. 1977, 34:355-362.
95. Snog-Kjaer A, Prange I, Dam H. Conversion of cholesterol into coprosterol by bacteria in vitro. J Gen Microbiol. 1956, 14:256-260.
96. Singh RK, Chang HW, Yan D et al. Influence of diet on the gut microbiome and implications for human health. J Transl Med. 2017,15:73.
97. Silva JCP, Mota M, Martins FO et al. Intestinal Microbial and Metabolic Profiling of Mice Fed with High-Glucose and High-Fructose Diets. J Proteome Res. 2018, 17: 2880-2891.
98. Lye HS, Rusul G, Liong MT. Removal of cholesterol by lactobacilli via incorporation and conversion to coprostanol. J Dairy Sci. 2010, 93:1383-1392.
99. Cahova M, Dankova H, Palenickova E et al. The opposite effects of high-sucrose and high-fat diet on Fatty Acid oxidation and very low density lipoprotein secretion in rat model of metabolic syndrome. J Nutr Metab.2012, 2012:757205.
100. Lee JH, Ikeda I, Sugano M. Dietary cholesterol influences on various lipid indices and eicosanoid production in rats fed dietary fat desirable for the protection of ischemic heart disease. J Nutr Sci Vitaminol (Tokyo). 1991, 37:389-399.
101. Ogawa Y, Imajo K, Honda Y et al. Palmitate-induced lipotoxicity is crucial for the pathogenesis of nonalcoholic fatty liver disease in cooperation with gut-derived endotoxin. Sci Rep. 2018, 8:11365.

102. Korn BS, Shimomura I, Bashmakov Y et al. Blunted feedback suppression of SREBP processing by dietary cholesterol in transgenic mice expressing sterol-resistant SCAP(D443N). J Clin Invest. 1998, 102:2050-2060.
103. Miyazaki M, Dobrzyn A, Man WC et al. Stearoyl-CoA desaturase 1 gene expression is necessary for fructose-mediated induction of lipogenic gene expression by sterol regulatory element-binding protein-1c-dependent and -independent mechanisms. J Biol Chem. 2004, 279:25164-25171.
104. Al-Dwairi A, Pabona JM, Simmen RC et al. Cytosolic malic enzyme 1 (ME1) mediates high fat diet-induced adiposity, endocrine profile, and gastrointestinal tract proliferation-associated biomarkers in male mice. PLoS One. 2012, 7: e46716.
105. Murai S, Ando A, Ebara S et al. Inhibition of malic enzyme 1 disrupts cellular metabolism and leads to vulnerability in cancer cells in glucose-restricted conditions. Oncogenesis 2017, 6:e329.
106. Koo HY, Wallig MA, Chung BH et al. Dietary fructose induces a wide range of genes with distinct shift in carbohydrate and lipid metabolism in fed and fasted rat liver. Biochim Biophys Acta. 2008, 1782:341-348.
107. Shimomura I, Shimano H, Korn BS et al. Nuclear sterol regulatory element-binding proteins activate genes responsible for the entire program of unsaturated fatty acid biosynthesis in transgenic mouse liver. J Biol Chem. 1998, 273:35299-35306.
108. Bizeau ME, Pagliassotti MJ. Hepatic adaptations to sucrose and fructose. Metabolism. 2005, 54:1189-1201.
109. Timmins JM, Lee JY, Boudyguina E et al. Targeted inactivation of hepatic Abca1 causes profound hypoalphalipoproteinemia and kidney hypercatabolism of apoA-I. J Clin Invest. 2015, 115:1333-1342.
110. Rong X, Wang B, Dunham MM et al. Lpcat3-dependent production of arachidonoyl phospholipids is a key determinant of triglyceride secretion. Elife. 2015, 4:e06557.
111. Hashidate-Yoshida T, Harayama T, Hishikawa D et al. Fatty acid remodeling by LPCAT3 enriches arachidonate in phospholipid membranes and regulates triglyceride transport. Elife. 2014, 4:e06328.

112. Stoffel W, Hammels I, Jenke B et al. Obesity resistance and deregulation of lipogenesis in Δ6-fatty acid desaturase (FADS2) deficiency. EMBO Rep. 2014, 15:110-120.
113. Leikin AI & Brenner RR. In vivo cholesterol removal from liver microsomes induces changes in fatty acid desaturase activities. Biochim Biophys Acta. 1988, 963:311-319.
114. Pagliassotti MJ, Prach PA, Koppenhafer TA et al. Changes in insulin action, triglycerides, and lipid composition during sucrose feeding in rats. Am J Physiol . 1996, 271:R1319-1326.
115. Castro RQ, Soto Rodriguez I, Deschamps Lago RA et al. Dietary sucrose regulates the expression of the Cd36 gene in hepatic tissue of rats with obesity and Non Alcoholic Fatty Liver Disease (NAFLD). Biomed Pap Med Fac Univ Palacky Olomouc Czech Repub 2018, 162:99-106.
116. Kim JK, Wi JK, Youn JH. Plasma free fatty acids decrease insulin-stimulated skeletal muscle glucose uptake by suppressing glycolysis in conscious rats. Diabetes. 1996, 45:446-453.

CHAPTER II PART2

117. Guang C, Chen J, Sang S et al. Biological functionality of soyasaponins and soyasapogenols. Journal of Agricultural and Food Chemistry. 2014, 62:8247−8255.
118. Kang J, Badger TM, Ronis MJ et al. Non-isoflavone phytochemicals in soy and their health effects. Journal of Agricultural and Food Chemistry. 2010, 58:8119−8133.
119. Kamo S, Suzuki S, Sato T. The content of soyasaponin and soyasapogenol in soy foods and their estimated intake in the Japanese. Food Science & Nutrition. 2014, 2:289−297.
120. Kamo S, Suzuki S, Sato T. Comparison of bioavailability (I) between soyasaponins and soyasapogenols, and (II) between group A and B soyasaponins. Nutrition. 2014, 30:596−601.
121. Kamo S, Takada Y, Yamashita T et al. Group B soyasaponin aglycone suppresses body weight gain and fat levels in high fat-fed mice. Journal of Nutritional Science and Vitaminology. 2018, 64:222−228.

122. Lee SO, Simons AL, Murphy PA et al. Soyasaponins lowered plasma cholesterol and increased fecal bile acids in female golden Syrian hamsters. Experimental Biology and Medicine, 2005, 230:472−478.
123.Xie Q, Gu X, Chen J et al. Soyasaponins reduce inflammation and improve serum lipid profiles and glucose homeostasis in high fat diet-induced obese mice. Molecular Nutrition & Food Research. 2018, 62:e1800205.
124. Yang SH, Ahn EK, Lee JA et al. Soyasaponins Aa and Ab exert an anti-obesity effect in 3T3-L1 adipocytes through downregulation of PPARγ. Phytotherapy Research. 2015, 29:281−287.
125. Xu BJ, Han LK, Zheng YN et al. In vitro inhibitory effect of triterpenoidal saponins from Platycodi Radix on pancreatic lipase. Archives of Pharmacal Research. 2005, 28:180−185.
126. Han LK, Nose R, Li W et al. Reduction of fat storage in mice fed a high-fat diet long term by treatment with saponins prepared from Kochia scoparia fruit. Phytotherapy Research. 2006, 20:877−882.
127. Saeki T, Nikaido T. Evaluations of saponin properties of HPLC analysis of Platycodon grandiflorum A.DC. Yakugaku Zasshi. 2003, 123: 431-444.
128. DuBois M, Gilles KA, Hamilton JK et al. Colorimetric method for determination of sugars and related substances. Analytical Chemistry. 1956, 28: 350−356.
129. Miller G. Use of dinitrosalicylic acid reagent for determination of reducing sugars. Analytical Chemistry. 1959, 31:426−428.
130. Sato M, Ueda T, Nagata K et al. Dietary kakrol (Momordica dioica Roxb.) flesh inhibits triacylglycerol absorption and lowers the risk for development of fatty liver in rats. Experimental Biology and Medicine. 2011, 236:1139−1146.
131. Inoue C, Kozaki T, Morita Y et al. Kibizu concentrated liquid suppresses the accumulation of lipid droplets in 3T3-L1 cells. Cytotechnology. 2015, 67:721−725.
132. Niibo M, Shirouchi B, Umegatani M et al. Probiotic Lactobacillus gasseri SBT2055 improves insulin secretion in a diabetic rat model. Journal of Dairy Science. 2019, 102:997−1006.

133. Rouser G, Siakotos AN, Fleischer S. Quantitative analysis of phospholipids by thin-layer chromatography and phosphorus analysis of spots. Lipid. 1966, 1:85−86.
134. Sperry WM, Webb M. A revision of the Schoenheimer-Sperry method for cholesterol determination. Journal of Biological Chemistry. 1950, 187: 97−106.
135. Markwell MA, McGroarty EJ, Bieber LL et al. The subcellular distribution of carnitine acyltransferases in mammalian liver and kidney. A new peroxisomal enzyme. Journal of Biological Chemistry. 1973, 248: 3426−3432.
136. Hashimoto T, Miyazawa S, Gunarso D et al. alpha-Amanitin inhibits the oxidation of long chain fatty acids in mouse liver. Journal of Biochemistry. 1981, 90:415−421.
137. Zhang W, Popovich DG. Effect of soyasapogenol A and soyasapogenol B concentrated extracts on Hep-G2 cell proliferation and apoptosis. Journal of Agricultural and Food Chemistry. 2008, 56:2603−2608.
138. Isoa K, Masayuki S, Toshio T et al. Saponin and sapogenol. XXXVIII. Structure of soyasaponin A2, a bisdesmoside of soyasapogenol A, from soybean, the seeds of Glycine max Merrill Chem. Chemical and Pharmaceutical Bulletin. 1985, 33: 598−608.
139. Yoshiki Y, Kudou S, Okubo K. Relationship between chemical structures and biological activities of triterpenoid saponins from soybean. Bioscience, Biotechnology, and Biochemistry. 1998, 62: 2291−2299.
140. Goda Y, Akiyama H, Suyama E et al. Comparison of soyasaponin and isoflavone contents between genetically modified (GM) and non-GM soybeans. Shokuhin Eiseigaku Zasshi. 2002, 43:339−347.
141. Neacsu M, Raikos V, Benavides-Paz Y et al. Sapogenol is a major microbial metabolite in human plasma associated with high protein soy-based diets: the relevance for functional food formulations. Foods. 2020, 9:422.
142. Chávez-Santoscoy RA, Gutiérrez-Uribe JA, Serna-Saldívar SO. Effect of flavonoids and saponins extracted from black bean (Phaseolus vulgaris L.) seed coats as cholesterol micelle disruptors. Plant Foods for Human Nutrition. 2013, 68:416−423.
143. Hariri N, Thibault L. High-fat diet-induced obesity in animal models. Nutrition Research Reviews. 2010, 23:270-299.

144. Wu T, Guo X, Zhang M et al. Anthocyanins in black rice, soybean and purple corn increase fecal butyric acid and prevent liver inflammation in high fat diet-induced obese mice. Food & Function. 2017, 8:3178-3186.
145. Delorme V, Dhouib R, Canaan S et al. Effects of surfactants on lipase structure, activity, and inhibition. Pharmaceutical Research. 2011, 28:1831−1842.
146. Cristancho AG, Lazar MA. Forming functional fat: a growing understanding of adipocyte differentiation. Nature Reviews Molecular Cell Biology. 2011, 12:722−734.
147. Wu Z, Rosen ED, Brun R et al. Cross-Regulation of C/EBPα and PPARγ Controls the Transcriptional Pathway of Adipogenesis and Insulin Sensitivity. Molecular Cell. 1999, 3:151-158.
148. Jones JR, Barrick C, Kim KA et al. Deletion of PPARγ in adipose tissues of mice protects against high fat diet-induced obesity and insulin resistance. Proceedings of the National Academy of Sciences of the United States of America. 2005, 102:6207-6212.
149. Lee EJ, Kang M, Kim YS. Platycodin D inhibits lipogenesis through AMPKα-PPARγ2 in 3T3-L1 cells and modulates fat accumulation in obese mice. Planta Medica. 2012, 78:1536−1542.
150. Byrne CD. Ectopic fat, insulin resistance and non-alcoholic fatty liver disease. Proceedings of the Nutrition Society. 2013, 72:412-419.
151. Kahn SE, Hull RL, Utzschneider KM. Mechanisms linking obesity to insulin resistance and type 2 diabetes, Nature. 2006, 444:840-846.
152. Li Y, Xu S, Mihaylova MM et al. AMPK phosphorylates and inhibits SREBP activity to attenuate hepatic steatosis and atherosclerosis in diet-induced insulin-resistant mice. Cell Metabolism. 2011, 13:376−388.
153. Feng RB, Fan CL, Liu Q et al. Crude triterpenoid saponins from Ilex Latifolia (Da Ye Dong Qing) ameliorate lipid accumulation by inhibiting SREBP expression via activation of AMPK in a non-alcoholic fatty liver disease model. Chinese Medicine. 2015, 10:23.
154. Oh GS, Yoon J, Lee GG, et al. 20(S)-protopanaxatriol inhibits liver X receptor α-mediated expression of lipogenic genes in hepatocytes. Journal of Pharmacological Sciences. 2015, 128: 71−77.

155. Lee HJ, Jung H, Cho H et al. Black Raspberry Seed Oil Improves Lipid Metabolism by Inhibiting Lipogenesis and Promoting Fatty-Acid Oxidation in High-Fat Diet-Induced Obese Mice and db/db Mice. Lipids. 2018, 53:491-504.
156. Wang QA, Tao C, Gupta RK et al. Tracking adipogenesis during white adipose tissue development, expansion and regeneration. Nature Medicine. 2013, 19:1338-1344.
157. Lu, K., Lee, M.H., & Patel, S.B. (2001). Dietary cholesterol absorption; more than just bile. Trends in Endocrinology & Metabolism, 12(7), 314-320.
158. Wu N, Sarna LK, Hwang SY et al. Activation of 3-hydroxy-3-methylglutaryl coenzyme A (HMG-CoA) reductase during high fat diet feeding. Biochimica et Biophysica Acta. 2013 1832:1560-1568.
159. Yang Y, Jiang Y, Wang Y et al. Suppression of ABCA1 by unsaturated fatty acids leads to lipid accumulation in HepG2 cells. Biochimie. 2010, 92:958−963.
160. Pullinger CR, Eng C, Salen G et al. Human cholesterol 7alpha-hydroxylase (CYP7A1) deficiency has a hypercholesterolemic phenotype. Journal of Clinical Investigation. 2002, 110: 109−117.
161. Tanaka S, Nemoto Y, Takei Y et al. High-fat diet-derived free fatty acids impair the intestinal immune system and increase sensitivity to intestinal epithelial damage. Biochemical and Biophysical Research Communications. 2020, 522:971-977.
162. Zheng J, Cheng G, Li Q et al. Chitin Oligosaccharide Modulates Gut Microbiota and Attenuates High-Fat-Diet-Induced Metabolic Syndrome in Mice. Marine Drugs. 2018,16:66.
163. Jiang Z, Hayashi T, Kashima K et al. Alteration of Serum Phospholipid n-6 Polyunsaturated Fatty Acid Compositions in Nonalcoholic Fatty Liver Disease in the Japanese Population: A Cross-Sectional Study. Lipids. 2020, 55:599-614.
164. MacDonald RS, Guo J, Copeland J et al. Environmental influences on isoflavones and saponins in soybeans and their role in colon cancer. Journal of Nutrition. 2005, 135:1239−1242.
165. Hirose N, Inoue T, Nishihara K et al. Inhibition of cholesterol absorption and synthesis in rats by sesamin. Journal of Lipid Research. 1991, 32:629-638.

166. Kamal-Eldin A, Frank J, Razdan A et al. Effects of dietary phenolic compounds on tocopherol, cholesterol, and fatty acids in rats. Lipids. 2002, 35:427-435.

CHAPTER III

167. Meijnikman AS, Herrema H, Scheithauer TPM et al. Evaluating causality of cellular senescence in non-alcoholic fatty liver disease. JHEP Rep. 2021, 3:100301.

168. Debacq-Chainiaux F, Erusalimsky JD, Campisi J et al. Protocols to detect senescence-associated beta-galactosidase (SA-β-gal) activity, a biomarker of senescent cells in culture and in vivo. Nat Protoc. 2009, 4:1798-1806.

169. Aravinthan A, Scarpini C, Tachtatzis P et al. Hepatocyte senescence predicts progression in non-alcohol-related fatty liver disease. J Hepatol. 2013, 58: 549-556.

170. Nakajima T, Nakashima T, Okada Y et al. Nuclear size measurement is a simple method for the assessment of hepatocellular aging in non-alcoholic fatty liver disease: Comparison with telomere-specific quantitative FISH and p21 immunohistochemistry. Pathol Int. 2010, 60:175-183.

171. Zhang J, Li Y, Wang B et al. Erratum: The p66shc-Mediated Regulation of Hepatocyte Senescence Influences Hepatic Steatosis in Nonalcoholic Fatty Liver Disease. Med Sci Monit. 2020, 26:e926160.

172. Iida T, Hayashi N, Yamada T. Failure of d-psicose absorbed in the small intestine to metabolize into energy and its low large intestinal fermentability in humans. Metabolism. 2010, 59: 206-214.

173. Tsukamoto I, Hossain A, Yamaguchi F et al. Intestinal absorption, organ distribution, and urinary excretion of the rare sugar D-psicose. Drug Des Devel Ther. 2014, 8:1955-1964.

174. Baek SH, Park SJ, Lee HG. D-psicose, a sweet monosaccharide, ameliorate hyperglycemia, and dyslipidemia in C57BL/6J db/db mice. J Food Sci. 2010, 75:H49-53.

175. Han Y, Kwon EY, Yu MK et al. A Preliminary Study for Evaluating the Dose-Dependent Effect of d-Allulose for Fat Mass Reduction in Adult Humans:

A Randomized, Double-Blind, Placebo-Controlled Trial. Nutrients. 2018; 10:160.
176. Chen J, Huang W, Zhang T et al. Anti-obesity potential of rare sugar d-psicose by regulating lipid metabolism in rats. Food Funct. 2019, 10: 2417-2425.
177. Matsuo T, Izumori K. d-Psicose Inhibits Intestinal alpha-Glucosidase and Suppresses the Glycemic Response after Ingestion of Carbohydrates in Rats. J Clin Biochem Nutr. 2009, 45: 202-206.
178. Shintani T, Yamada T, Hayashi N et al. Rare Sugar Syrup Containing d-Allulose but Not High-Fructose Corn Syrup Maintains Glucose Tolerance and Insulin Sensitivity Partly via Hepatic Glucokinase Translocation in Wistar Rats. J Agric Food Chem. 2017, 65:2888-2894.
179. Nagata Y, Kanasaki A, Tamaru S et al. D-psicose, an epimer of D-fructose, favorably alters lipid metabolism in Sprague–Dawley rats. J Agric Food Chem. 2015, 63:3168-3176.
180. Matsuo T, Baba Y, Hashiguchi M et al. Dietary D-psicose, a C-3 epimer of D-fructose, suppresses the activity of hepatic lipogenic enzymes in rats. Asia Pac J Clin Nutr. 2001,10:233-237.
181. Baek SH, Park SJ, Lee HG. D-psicose, a sweet monosaccharide, ameliorate hyperglycemia, and dyslipidemia in C57BL/6J db/db mice. J Food Sci. 2010,75: H49-53.
182. Kanasaki A, Iida T, Murao K et al. D-Allulose enhances uptake of HDL-cholesterol into rat's primary hepatocyte via SR-B1. Cytotechnology. 2020, 72: 295-301.
183. Tanaka M, Kanasaki A, Hayashi N et al. Safety and efficacy of a 48-week long-term ingestion of D-allulose in subjects with high LDL cholesterol levels. Fundam Toxicol Sci. 2020, 7: 25-31.
184. Nagata Y, Mizuta N, Kanasaki A et al. Rare sugars, d-allulose, d-tagatose and d-sorbose, differently modulate lipid metabolism in rats. J Sci Food Agric. 2018, 98: 2020-2026.
185. Kanasaki A, Niibo M, Iida T. Effect of D-allulose feeding on the hepatic metabolomics profile in male Wistar rats. Food Funct. 2021, 12: 3931-3938.
186. Hetz C. The unfolded protein response: controlling cell fate decisions under ER stress and beyond. Nat Rev Mol Cell Biol. 2012, 13: 89-102.

187. Qian YW, Schmidt RJ, Zhang Y et al. Secreted PCSK9 downregulates low density lipoprotein receptor through receptor-mediated endocytosis. J Lipid Res. 2007, 48: 1488-1498.
188. Jeong HJ, Lee HS, Kim KS et al. Sterol-dependent regulation of proprotein convertase subtilisin/kexin type 9 expression by sterol-regulatory element binding protein-2. J Lipid Res. 2008, 49: 399-409.
189. Lebeau PF, Byun JH, Platko K et al. Caffeine blocks SREBP2-induced hepatic PCSK9 expression to enhance LDLR-mediated cholesterol clearance. Nat Commun. 2022, 13: 770.
190. Lebeau P, Al-Hashimi A, Sood S et al. Endoplasmic Reticulum Stress and Ca2+ Depletion Differentially Modulate the Sterol Regulatory Protein PCSK9 to Control Lipid Metabolism. J Biol Chem. 2017, 292: 1510-1523.
191. Malhi H, Kaufman RJ. Endoplasmic reticulum stress in liver disease. J Hepatol. 2011, 54: 795-809.
192. Bobrovnikova-Marjon E, Hatzivassiliou G, Grigoriadou C et al. PERK-dependent regulation of lipogenesis during mouse mammary gland development and adipocyte differentiation. Proc Natl Acad Sci U S A. 2008, 105:16314-16319.
193. Pai JT, Brown MS, Goldstein JL et al. Purification and cDNA cloning of a second apoptosis-related cysteine protease that cleaves and activates sterol regulatory element binding proteins. Proc Natl Acad Sci U S A. 1996, 93: 5437-5442.
194. Kammoun HL, Chabanon H, Hainault I et al. GRP78 expression inhibits insulin and ER stress-induced SREBP-1c activation and reduces hepatic steatosis in mice. J Clin Invest. 2009, 119:1201-1215.
195. Simonen P, Kotronen A, Hallikainen M et al. Cholesterol synthesis is increased, and absorption is decreased in non-alcoholic fatty liver disease independent of obesity. J Hepatol. 2011, 54:153-159.
196. Silbernagel G, Lütjohann D, Machann J et al. Cholesterol Synthesis Is Associated with Hepatic Lipid Content and Dependent on Fructose/Glucose Intake in Healthy Humans. Exp Diabetes Res. 2012, 2012:361863.
197. Braun A, Trigatti BL, Post MJ et al. Loss of SR-BI expression leads to the early onset of occlusive atherosclerotic coronary artery disease, spontaneous

myocardial infarctions, severe cardiac dysfunction, and premature death in apolipoprotein E-deficient mice. Circ Res. 2002, 90: 270-276.
198. Braun A, Trigatti BL, Post MJ et al. Gene transfer and hepatic overexpression of the HDL receptor SR-BI reduces atherosclerosis in the cholesterol-fed LDL receptor-deficient mouse. Circ Res. 2002, 90:270-276.
199. Xin P, Han H, Gao D et al. Alleviative effects of resveratrol on nonalcoholic fatty liver disease are associated with up-regulation of hepatic low density lipoprotein receptor and scavenger receptor class B type I gene expressions in rats Food Chem Toxicol. 2013, 52: 12-18.
200. Jourdan T, Djaouti L, Demizieux L et al. CB1 antagonism exerts specific molecular effects on visceral and subcutaneous fat and reverses liver steatosis in diet-induced obese mice. Diabetes. 2010, 59: 926-934.
201. Zhao N, Tan H, Wang L et al. Palmitate induces fat accumulation via repressing FoxO1-mediated ATGL-dependent lipolysis in HepG2 hepatocytes. PLoS One. 2021, 16:e0243938.
202. Malerød L, Sporstøl M, Juvet LK et al. Hepatic scavenger receptor class B, type I is stimulated by peroxisome proliferator-activated receptor γ and hepatocyte nuclear factor 4α. Biochem Biophys Res Commun. 2003, 305: 557-565.
203. Kuo KK, Wu BN, Liu CP et al. Xanthine-based KMUP-1 improves HDL via PPARγ/SR-B1, LDL via LDLRs, and HSL via PKA/PKG for hepatic fat loss. J Lipid Res. 2015, 56: 2070-2084.
204. Attie AD. ABCA1: at the nexus of cholesterol, HDL and atherosclerosis. Trends Biochem Sci. 2007, 32:172-179.
205. Ogrodnik M, Miwa S, Tchkonia T et al. Cellular senescence drives age-dependent hepatic steatosis. Nat Commun. 2017, 8:15691.
206. Inoue C, Zhao C, Tsuduki Y et al. SMARCD1 regulates senescence-associated lipid accumulation in hepatocytes. NPJ Aging Mech Dis. 2017, 3:11.
207. Muñoz-Espín D, Serrano M. Cellular senescence: from physiology to pathology. Nat Rev Mol Cell Biol. 2014, 15:482-496.
208. Mittnacht S. Control of pRB phosphorylation. Curr Opin Genet Dev. 1998, 8:21-27.

209. Luo Y, Zou P, Zou J et al. ROS-induced cellular senescence via p21 in a p38 MAPKα dependent manner. Exp Gerontol. 2011, 46:860-867.
210. Li H, Wang W, Liu X. Transcriptional factor HBP1 targets P16(INK4A), upregulating its expression, and consequently is involved in Ras-induced premature senescence. Oncogene. 2010, 29:5083-5094.
211. Kurz DJ, Decary S, Hong Y et al. Senescence-associated (beta)-galactosidase reflects an increase in lysosomal mass during replicative ageing of human endothelial cells. J Cell Sci. 2000, 113:3613-22.
212. Yim WW, Mizushima N. Lysosome biology in autophagy. Cell Discov. 2020,6:6.
213. Haines DD, Juhasz B, Tosaki A. Management of multicellular senescence and oxidative stress. J Cell Mol Med. 2013,17:936-957.
214. Slobodnyuk K, Radic N, Ivanova S et al. Autophagy-induced senescence is regulated by p38α signaling. Cell Death Dis. 2019, 10:376.